

**QUANTIFYING BIDIRECTIONAL REFLECTANCE FACTORS FOR  
DELINEATING SHRUB-STEPPE VEGETATION FUNCTIONAL TYPES  
ACROSS SCALES FROM THE PLANT TO THE LANDSCAPE**

**A Dissertation**

**Presented in Partial Fulfillment and Requirements for the**

**Degree of Doctor of Philosophy**

**in**

**Natural Resources**

**in the**

**College of Graduate Studies**

**University of Idaho**

**By**

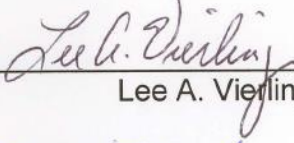
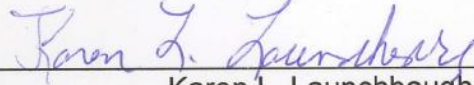
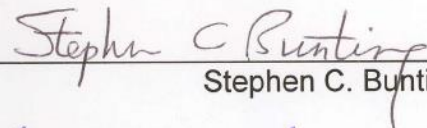
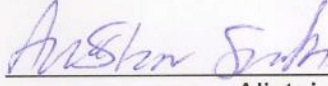
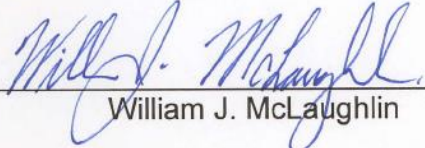
**Javier A. Ñaupari**

**June 2010**

**Major Professor: Lee A. Vierling, Ph.D.**

## AUTHORIZATION TO SUBMIT DISSERTATION

This dissertation of Javier A. Naupari, submitted for the degree of Doctor of Philosophy in Natural Resources and titled “**Quantifying bidirectional reflectance factors for delineating shrub-steppe vegetation functional types across scales from the plant to the landscape**” has been reviewed in final form. Permission, as indicated by the signatures and dates given below, is now granted to submit final copies to the College of Graduate Studies for approval.

Major Professor		Date	6/11/10
	Lee A. Vierling		
Committee Members		Date	16 Jun 10
	Karen L. Launchbaugh		
		Date	6/11/10
	Stephen C. Bunting		
		Date	6/14/10
	Alistair M.S. Smith		
Department Administrator		Date	6/18/10
	Jo Ellen Force		
Discipline's College Dean		Date	6/23/10
	William J. McLaughlin		

Final Approval and Acceptance by the College of Graduate Studies

Date \_\_\_\_\_

\_\_\_\_\_  
Margrit von Braun

## ABSTRACT

### **Quantifying bidirectional reflectance factors for delineating shrub-steppe vegetation functional types across scales from the plant to the landscape**

Annual invasive grasses increases in sagebrush steppe have degraded vast areas in the Western US reducing biodiversity and production of rangelands. Discriminating this plant functional type (PFT) from other vegetation types such as shrubs and perennial grasses at the landscape scale has been challenging because of background (soil and litter) reflectance and effects of shadows using nadir-only view angle passive remote sensors. However, changes in vegetation structure and anisotropic behavior in the middle and late stages of the growing season have enabled us to differentiate some of these PFTs using remote sensing measurements collected at different spatial scales within a shrub-steppe rangeland ecosystem in west-central Idaho. Changes from erectophile to planophile leaf orientation of annual invasive grasses, comprised in this area mostly by medusahead (*Taeniatherum caput-medusae* [L.] Nevski) produced a distinctive set of vegetation reflectance values for this PFT at ground level during the transition from green to senesce stages. However, measuring plant canopy reflectance depends on the geometry between sensor view angle and solar position. We therefore further demonstrated that medusahead can be detected from native perennial vegetation near solar noon, which could be useful when scheduling multispectral or hyperspectral aerial image surveys. Medusahead did not exhibit strong anisotropic reflectance behavior, quantified through the

measurement of bidirectional reflectance factors (BRF) and anisotropy index (ANIX), however the shrub PFT did exhibit high anisotropy in field measurements. We therefore tested whether we could classify areas dominated by shrubs, non-shrubs, and crops at the landscape scale to generate PFT-based productivity estimates using the MODIS Gross Primary Productivity product. Although accuracy classification at moderate scales was high ( $K_{\text{hat}}$  88-98%), GPP shrub partitioning was very poor ( $R^2 < 0.06$ ).

## ACKNOWLEDGEMENTS

The list of persons and institutions that deserve recognition for their support during my doctoral program is extensive, but top of the list are Dr. Lee Vierling and Dr. Karen Launchbaugh, major professor and head of the rangeland department, respectively. Thank you, Dr. Lee for guiding me and always encouraging me to look at new sights of research and analysis. Thank you, Dr. Karen for accepting me in your program and for always keeping me steady. Most of all thank you for your friendship and support. I would like to thank Dr. Steve Bunting and Dr. Alistair Smith for being great mentors as members of my committee. I also would like to thank all the field assistants and my friends and colleagues Steve Garrity, Jan Eitel, Sebastian Martinuzzi and the rest of the GLED Lab for their insights and technical support during my research. I would like to thank the faculty, administration of the College of Natural Resources and the Rangeland Ecology and Management Department for their academic and technical support. Special thanks to the owners of the Soulen Livestock Co., especially to Joe and Margaret for their unconditional support during my field work. Thank you to the Fulbright Commission (LASPAU), the Heady Professorship and the Foster Graduate Research Assistantship for financially assisting me during my program and research. Special thanks to Drs. Enrique Flores and Lucrecia Aguirre, who encouraged and supported me to achieve my Ph.D degree. And last but not least thank you to my love ones Tanya, Josue and Alejandra for living this adventure far from our family and friends in Peru. Thank you God for every second in our life and for this unique experience!

## DEDICATION

I dedicate this dissertation to our Lord God for letting us appreciate the beauty and complexity of the rangeland ecosystems around the World.

I especially dedicate this dissertation to my beloved wife and children

Tanya, Josue and Alejandra, and

to my parents Arturo and Adela.

## TABLE OF CONTENTS

Authorization to submit dissertation .....	ii
Abstract .....	iii
Acknowledgements .....	v
Dedication .....	vi
Table of contents .....	vii
List of tables .....	xii
List of figures .....	xiii
CHAPTER 1. Remote Sensing of Rangeland Ecosystem Structure and Function:	
A Review of Techniques .....	1
Introduction.....	1
Nadir view imagery for assessment of rangeland structure and function.....	4
Applications of spectral data to quantifying semi-arid ecosystem properties.....	5
Classification techniques.....	7
Multi-view angle imagery for assessment of structure and function .....	9
Multi-angular reflectance theory .....	10
Multiangle sensing systems .....	11
Algorithms and models used to interpret multi angle remote sensing data .....	13
Radiative transfer models .....	13
Geometric optical models.....	14

Applications of multi angular remote sensing data in rangelands and related ecosystems .....	15
Active remote sensing for assessment of structure and function .....	18
Applications of LIDAR in rangeland ecosystems .....	19
Linking observations and modeling to understand ecosystem structure and function at the landscape scale .....	20
Conclusions .....	21
References .....	23
Tables .....	34
Figures .....	35
CHAPTER 2. Bidirectional reflectance of shrub-steppe vegetation:	
delineating native and invasive functional groups .....	36
Abstract .....	36
Introduction and background .....	38
Multi-angular reflectance for rangeland ecosystem monitoring .....	41
Methods .....	43
Study area .....	43
Bidirectional reflectance factor (BRF) ground measurements .....	44
BRF data processing .....	48
Sampling design and statistical analysis .....	52
Results and Discussion .....	53
Reflectance at nadir view .....	53

Red and NIR BRF .....	54
Effects of leaf orientation in medusahead detection .....	55
Bidirectional vegetation indices of plant functional groups.....	58
Reflectance anisotropy of rangeland plant functional types .....	60
Red and NIR angular signatures in spectral space.....	63
Conclusions.....	64
References .....	66
Tables .....	73
Figures .....	74
CHAPTER 3. Effects of sun zenith angle and leaf orientation on detecting the invasive grass medusahead ( <i>Taeniatherum caput-medusae</i> [L.] Nevski) using narrow band canopy reflectance .....	87
Abstract .....	87
Introduction and background .....	89
Methods.....	93
Study area .....	93
Reflectance measurements.....	94
Data analysis .....	96
Results and Discussion .....	98
Diurnal reflectance variation at different phenological stages .....	98
Seasonal reflectance changes between native perennial grasses and medusahead .....	102

Conclusions.....	105
References .....	106
Tables .....	110
Figures .....	111
CHAPTER 4. Bidirectional reflectance of shrub-steppe vegetation: towards	
MISR-based GPP partitioning.....	118
Abstract .....	118
Introduction and background .....	120
Methods.....	123
Study area .....	123
Field data collection .....	123
Imagery acquisition .....	125
Imagery pre-processing .....	126
Data analysis .....	127
BRF calculation .....	127
Image classification .....	128
Scaling up from Landsat (30 m x 30 m) to MISR local mode (275 x 275 m) to MODIS GPP (1 Km).....	129
GPP Fractional cover .....	130
Results and Discussion .....	131
Vegetation type classification.....	131
MODIS GPP fractional cover.....	136

Conclusions .....	138
References .....	140
Tables .....	145
Figures .....	147
CHAPTER 5. Conclusions .....	154
Question 1 .....	154
Question 2 .....	155
Question 3 .....	156
References .....	158

## LIST OF TABLES

### CHAPTER 1

Table 1.1. Spectral vegetation indices commonly used in rangeland studies .....	34
---	----

### CHAPTER 2

Table 2-1. NDVI values derived from nadir measurements for five vegetation types sampled at different periods and SZA.....	73
--	----

### CHAPTER 3

Table 3-1. Canopy cover classification of vegetation under light sensor field of view (Footprint 1 m radius).....	110
---	-----

Table 3-2. Collection dates samples and sun zenith angles (SZA) for full day reflectance measurement at four different phenological stages .....	110
--	-----

Table 3-3. p-values for T-test between perennial grass and Medusahead for full day reflectance comparisons ( $p < 0.05$ ) .....	110
---	-----

### CHAPTER 4

Table 4-1. Orbit number, acquisition date and time for two MISR local mode over passing the study site.....	145
---	-----

Table 4-2. Scaling up Landsat pixels to MISR and MODIS pixels .....	145
---	-----

Table 4-3. Composition of MISR shrub and non-shrub vegetation 'pure' pixels located at different locations .....	146
--	-----

Table 4-4. Accuracy classification for shrub using Landsat and MISR nadir (An) images.....	146
--	-----

## LIST OF FIGURES

### CHAPTER 1

Figure 1.1. Directional reflectance of vegetation depicted by Schaepman-Strub et al (2006) .....	35
---	----

### CHAPTER 2

Figure 2-1. Anisotropy behavior along the solar plane recorded with the MMR spectroradiometer (Asner, 1998) .....	74
--	----

Figure 2-2. Study area and distribution of simulated MODIS GPP 1 Km Macroplots .....	75
---	----

Figure 2-3. Spectroradiometer footprint classifications .....	76
---	----

Figure 2.4 Angular signature in spectral space form by red and NIR BRF as a function of view zenith angles (Zhang et al., 2002a) .....	77
---	----

Figure 2-5 Variation of average spectra for 5 vegetation types at 4 different periods gathered at nadir view around solar noon .....	78
---	----

Figure 2-6. Red and NIR BRF variations for 5 different vegetation types at 2 different periods gathered around solar noon.....	79
---	----

Figure 2-7 Erectophile (left) versus planophile (right) leaf orientation for Medusahead annual grass.....	80
--	----

Figure 2-8 Simulated reflectance for planophile (senesced medusahead) versus erectophile (green medusahead) leaf orientation .....	81
--	----

Figure 2-9 Invasive NIR BRF variations for 2007-2008 .....	82
--	----

Figure 2-10 NDVI average variations for 5 different vegetation types at 4 different periods gathered around solar noon .....	83
---	----

Figure 2-11 ANIX average variations for 5 different vegetation types at 4 different periods .....	84
--	----

Fig 2-12 NADX and NDVI average variations for 5 different vegetation types at 4 different periods .....	85
--	----

Figure 2-13 Angular signatures on the red and NIR plane for the third week of July .....	86
 CHAPTER 3	
Figure 3-1. Near infrared (NIR) and Red bidirectional reflectance factor (BRF) for annual grasses for two different phenology periods .....	111
Figure 3-2. Correction factor for reflectance measurements at different sun zenith angles .....	112
Figure 3-3. Green NDVI (NDVI <sub>g</sub> ) of perennial and medusahead at four phenological stages .....	113
Figure 3-4. Photosynthetically active radiation (PAR) reflectance of perennial grass and medusahead for four phenology periods .....	114
Figure 3-5. Green (568 and 532 nm) and NIR (800 nm) reflectance of perennial grass and medusahead at four different phenological stages .....	115
Figure 3-6. Green NDVI (NDVI <sub>g</sub> ) and PAR reflectance variation of perennial grass and medusahead throughout the observational period.....	116
Figure 3-7. Green and NIR reflectance variation of perennial grasses and medusahead throughout the observational period .....	117
 CHAPTER 4	
Figure 4-1 Line transect (225 m) over Landsat pixels. Red dots represent stakes set at every 45 m .....	147
Figure 4-2 MISR paths over CraneCreekID, Local Mode Site # 313 (44.300, -116.600). Path 042 and block 55 are shown with a dot .....	148
Figure 4-3 (a) Landsat and (b) MISR An image classification.....	149

Figure 4-4 NDVI variation for MISR 9-view cameras .....	150
Figure 4-5 BRF variation for each band and each MISR viewing camera.....	151
Figure 4-6 Comparison between ANIX at coarse scale (MISR local mode, left panels) and fine scale (field data, right panels) .....	152
Figure 4- 7 MODIS GPP and EVI variation at different levels of shrub and crop cover in the study area .....	153

## CHAPTER 1. Remote sensing of rangeland ecosystem structure and function: A review of techniques

### 1. Introduction

Vast expanses of grasslands, shrublands, and savannas comprise the semi-arid rangelands of western North America. While these ecosystems constitute a large fraction of the Western landscape, it has been difficult to establish quantitative methods for objective and repeatable assess rangeland vegetation status across broad scales. Rangeland ecosystem health has been assessed at the ground level using a wide variety of indicators, but these techniques are often limited in the spatial extent of the area assessed.

A relatively fast and cost effective protocol to assess rangeland health that uses site-specific data derived from 17 indicators has been adopted by federal organizations (Pellant et al. 2000, Havstad and Herrick 2003). Rangeland ecosystem health is defined as “*The degree to which the integrity of the soil, vegetation, water, and air as well as the ecological processes of the rangeland ecosystem are balanced and sustained*”, where integrity is defined as “*maintenance of the functional attributes characteristics of a locale, including normal variability*” (USDA 1997). Assessments of individual sites may limit interpretation of vegetation dynamics within landscapes and minimize the confounding effects of landscape heterogeneity (Stafford-Smith 1996, Briske et al. 2005). In addition, the rate and magnitude of vegetation change studies based on individual ecological sites may have been overemphasized compared with

changes at large scales (Briske et al. 2003). Thus, assessment and monitoring of the rangeland functionality related to structural attributes across broad scales represent the major approach of rangeland health (Tongway and Ludwig 1997, Hunt et al. 2003, Briske et al. 2005)

Vegetation structure affects light use efficiency (Ross 1981, Ryel et al. 1994, Widlowski et al. 2004), water uptake (Smith and Nobel 1977, Ryel et al. 2004, Loik 2007), and wildlife habitat (McNaughton 1979, Bradford et al. 1996, Stewart et al. 2006). At the plant canopy level, vegetation characteristics such as cover, leaf position and leaf area index affect reflectance, absorption and transmittance of the incoming radiation or irradiance (Asner 1998a, Larcher 2003). In addition, community and ecosystem structure affect how incoming irradiance is utilized by the plants as a result of variations in soil characteristics, slope and aspect of the terrain, vegetation cover, biomass and physiognomy, foliage density and layering, canopy openness and gap proportions (West 1993).

Monitoring changes in vegetation structure due to natural or human disturbances is needed to maintain ecological services of rangelands (Walker 1992, West 1993). Although the value of these ecological services is difficult to conceptualize and quantify (Walker 1992, West 1993), maintenance of the gaseous composition of the atmosphere; genesis, fertility and stability of soils; energy flow; cycling of nutrients; and natural control of pathogenic and parasitic organisms are some examples of ecological services provided by rangelands (West 1993, Holecheck et al. 1995).

Plant functional types bridge the gap between plant physiology and community and ecosystem processes (Diaz et al. 2002). For instance, the estimation of the amount of plant production (Pellant et al. 2000), the fraction of invasive species present (D'Antonio and Vitousek 1992), and the amount of woody vegetation occurring across the landscape (Hibbard et al. 2001, Hughes et al. 2006) present promising opportunities for rangeland monitoring using remote sensing (Hunt et al. 2003, Lass et al. 2005, Strand et al. 2006).

Computer-based technological advances have allowed scientists to develop deep insights about the structure and function of ecological systems around the globe. In particular, analyses of vegetation spectral patterns in remotely sensed imagery have revealed unprecedented information about ecosystem dynamics occurring across almost every major biome (Skole and Tucker 1993, Myneni et al. 1997, Nemani et al. 2003).

Research of rangeland ecosystems using remote sensing techniques have mainly focused on ecological structural pattern through image interpretation (processing), image classification, and validation of remote sensing products using field collected data (Tueller 1989, Hunt et al 2003). For example, classification techniques have been used to detect invasive species, distinguish different vegetation types and estimate cover fractions of bare ground and vegetation. Spectral vegetation indices such as the normalized difference vegetation index (NDVI) have been used in models to derive information about rangeland ecosystem function such as net primary production and to monitor changes in vegetation greenness over time (Tueller 1989, Turner et al. 2004).

However, studies that examine the interplay between rangeland ecosystem structure and function are relatively few. Thus, the objective of this paper is to review new techniques in remote sensing such as multi-view angle spectrometry that can enhance delineation of plant functional types as well as potential to complement existing rangeland ecosystem health monitoring techniques. In addition, a review of studies of structural and functional ecosystem attributes related with remote sensing techniques is presented.

## **2. Nadir view imagery for assessment of rangeland structure and function**

The vast majority of remote sensing-based vegetation studies share the common measurement technique such that the sensor is pointed vertically down at the ground (also called the *nadir* position). For instance, multispectral remote sensors such as Landsat collect the reflected radiance of the surface in a defined range of wavebands at the nadir position. Moreover, the first hyperspectral (more than ~30 spectral wavebands) airborne sensors also collect measures of reflected light along lines of flight pointed vertically to the ground. These reflectance values recorded at nadir view have been extensively used to extract spectral indices, generate vegetation type cover and develop and test ecological models (Tueller 1989, Hunt et al. 2003).

## 2.1 Applications of Spectral Data to Quantifying Semi-Arid Ecosystem

### Properties

Structural and functional components of the vegetation such as LAI, biomass, fraction of absorbed photosynthetically active radiation (fPAR) and plant cover have been extracted using spectral indices (Tueller 1989, Hunt et al. 2003). Vegetation spectral characteristics in the red (R) and near infrared (NIR) wavebands have been used to generate different vegetation indices like the Normalized Difference Vegetation Index (NDVI; Rouse et al. 1974), the Soil Adjustment Vegetation Index (SAVI; Huete 1988) and the Enhanced Vegetation Index (EVI; Huete and Justice 1999) (Table 1-1).

Multispectral remote sensors using red and NIR wavebands provide data for estimating vegetation indices and developing spectrally-based ecological modeling products. For example, the Moderate Resolution Imaging Spectroradiometer (MODIS) and the Advanced Very High Resolution Radiometer (AVHRR) NDVI values have been related to gross primary productivity (GPP) (Tucker et al. 1985, Running et al. 1994). Hunt et al. (2003) used Advanced Very High Resolution Radiometer (AVHRR, 1000-m spatial resolution) NDVI as a surrogate of fPAR to estimate gross primary production using the following equation (1) (after Monteith 1972, Running et al. 1994):

$$GPP = \varepsilon \times fPAR \times PAR \approx \varepsilon \times NDVI \times PAR \quad (1)$$

Where:

GPP = Gross primary production

$\varepsilon$  = light use efficiency

fPAR= fraction of absorbed photosynthetically active radiation

PAR = photosynthetic active radiation

NDVI = Normalized Difference Vegetation Index

Broad scale GPP estimates resulting from these analyses have enabled numerous studies of carbon cycle dynamics, vegetation phenology, and vegetation productivity over the past two decades.

Vegetation indices have also been used to detect invasive plants because of differences in phenology between invasive and native vegetation (Lass et al. 2005). Bradley and Mustard (2005) established that satellite scenes must be chosen to capture peak productivity of cheatgrass. Bradley and Mustard (2005) showed that NDVI values derived from Landsat TM (30-m spatial resolution) and Advanced Very High Resolution Radiometer (AVHRR, 1000-m spatial resolution) detect interannual variation in productivity in ecosystems dominated by cheatgrass. In addition, Bradley and Mustard (2005) utilized similar phenological differences among grasses of the Great Basin to differentiate areas dominated by cheatgrass from those dominated by bunchgrasses. Lass et al. (2005) reviewed remote sensing techniques and algorithms used in different invasive plants that including multispectral and hyperspectral imagery at very high spatial resolution. However, similar spectral reflectance to other vegetation and coexistence with other vegetation remain challenging in annual invasive plant detection (Shafii et al. 2004)

Other analyses using different spectral bands are related with soil erosion in semi-arid regions. For instance, Pickup and Nelson (1984) developed an empirical model that transforms Landsat MSS data into an approximate measure of erosion and deposition. It uses the MSS 4/6 and 5/6 band ratios that when plotted against each other for each pixel, occupy a space between two parallel lines. Values close to the upper line are usually associated with areas of severe erosion. Points midway between the lines tended to depict areas of apparent stability. The lower part of the data space is occupied by depositional sites with the intensity of deposition. Measurements of ground cover are correlated with soil stability, watershed function and grazing management (Booth and Tueller 2003). Thus, measuring ground cover using remote sensing imagery enhances the ability to detect soil degradation and erosion (Pick up and Nelson 1984, Wang et al. 2002, Vrieling 2006).

## **2.2 Classification techniques**

Rangeland cover-type classification using remotely sensed imagery has been mainly based on pixel classification. At coarse scales this represents a big challenge because traditional rangeland ecosystem monitoring requires quantifying trends in assemblages of vegetation species. However, many of these species assemblages do not exhibit spectral reflectance patterns distinctive enough for remote detection/delineation throughout most of the year (Hunt et al. 2003). Although hyperspectral imagery can help distinguish among different vegetation types, it cannot distinguish spectral differences among

species due to similar spectral reflectance characteristics at the nadir view (Asner et al. 1998c). Nonetheless, because only remote sensing can provide cost effective data to evaluate ecosystems across broad extents at frequent return intervals (twice daily, in some cases), creative approaches are warranted to better relate these observations to rangeland ecosystem health.

A variety of classification techniques have been used in rangelands. Supervised and unsupervised classification techniques depend on having separable spectral signatures of different vegetation types and spatial resolution. Therefore, similar spectral responses within vegetation communities would potentially cause pixel misclassification, leading to omission and commission errors (Tueller 1989). Other approaches such as discrete Fourier transform, tasseled cap components and spatial wavelet analysis have been assessed to classify rangelands. Annual NDVI cycle and discrete Fourier transform were used to determine pixel class membership for different shrub types as characterized by differences in length of their growing period (Evans and Geerken 2006). Discrete Fourier transform has been used to minimize noise in NDVI time series and enhance key vegetation features. On the other hand, classified Landsat-7 ETM (+) imagery using mean values in tasseled cap brightness, greenness, and wetness components had 98% overall accuracy in identifying locations with normal or anomalous productivity within ecological site descriptions (Maynard et al. 2007).

In addition, location of individual shrubs was assessed using spatial wavelet analysis (SWA) and high spatial resolution (0.25 and 1 m) aerial

photography (Garrity et al. 2008). SWA convolves ever-increasing size (dilation scales) of the wavelet shape, called the basis function, with the imagery (Strand et al. 2006, 2008). The basis function to detect shrubs location was set between 0.2 and 0.4 m with a step interval of 0.1 m (Garrity et al. 2008)

### **3. Multi-view angle imagery for assessment of structure and function**

The nadir measurement method has been used out of necessity, because until recently a large fraction of satellite and aircraft imagery has been collected at or near nadir to minimize problems relating to image distortion and differing atmospheric path length. However, nadir measurements in rangeland systems can suffer from several potential pitfalls. First, nadir measurements include the highest fraction of background (i.e. soil, senesced vegetation litter) vs. green plant material; relative to measurements at the same location taken at oblique angles. As a result, the spectral data collected at nadir can be confounded by background reflectance properties, making interpretation of green plant material difficult (Huete et al. 1985), particularly in semi-arid rangeland landscapes. Second, because shadows play a large role in dictating the direction and amount of light being reflected off of vegetated rangeland surfaces, it is difficult to constrain the amount of shadow being included in a nadir measurement at different times of the day (Vierling et al. 1997).

### 3.1 Multi-angular reflectance theory

Angular spectral information has been shown to improve nadir view surface cover classification in some instances (Martonchik et al. 1998, Schaepman-Strub et al. 2006). Rangeland surfaces, like many other land surfaces, show complex structure that reflects the incoming light in many different directions, a phenomenon described as *anisotropy*. Middleton et al. (1987) were among the first researchers to quantify the anisotropy of rangeland reflectance. Walthall et al. (1985) showed that most bidirectional information of vegetated and soil surfaces is found in the principal solar plane within viewing angles approximately 50° either side of nadir. The relationship between the directional radiance reflected from a target and the sun's irradiance (incident flux) illuminating the target at a single incidence angle is called the bi-directional reflectance distribution function (BRDF) (Nicodemus et al. 1977, Diner et al. 1999, Schaepman-Strub et al. 2006). However, the BRDF cannot be directly measured (Nicodemus et al. 1977).

Nine possible relations between incoming and reflected radiance can result from combinations of three beam geometries; directional, conical and hemispherical (Nicodemus et al. 1977, Martonchik et al. 1998, Schaepman-Strub et al. 2006). Four of these combinations have been mostly used in ecological applications. The hemispherical directional reflectance factor (HDRF) is defined as the ratio of the view-angle-dependent surface-reflected radiance at location  $x,y$  to the reflected radiance from an ideal Lambertian target for the same incident radiance field at the same location (Figure 1-1). The bihemispherical

(BHR) reflectance or albedo is defined as the ratio of the reflected surface flux to the incident surface flux (Figure 1-1). Both the HDRF and BHR include diffuse and direct irradiance. From the definition of HDRF, the bidirectional reflectance factor (BRF) and the directional hemispherical reflectance (DHR) are determined. BRF and DHR are equivalent surface properties to HDRF and BHR but are defined for direct irradiance only. BRF can be obtained from HDRF only if the effects of diffuse irradiance are removed using BRF models (Martonchik et al. 1998, Schaepman-Strub et al. 2006).

### **3.2 Multiangle sensing systems**

Sensors that acquire simultaneous multi-angular radiance data have been used in aircraft and, more recently, launched on satellites. Airborne multi-angle sensors include the Advanced Solid-State Array Spectroradiometer (ASAS) and AirMISR. ASAS is an airborne, off-nadir pointing imaging spectroradiometer used to acquire bidirectional radiance data in 29 spectral bands in the visible and NIR portions of the spectrum (Irons 1991). AirMISR acquires imagery at nine different angles. Multi-view sensors launched to the space include the Compact High Resolution Imaging Spectrometer (CHRIS), the Polarization and Directionality of the Earth's Reflectance (POLDER-1 and 2), the Advanced Spaceborne Thermal Emission and Reflectance radiometer (ASTER) and the Multi-angle Imaging Spectroradiometer (MISR), with specifications listed below.

The *CHRIS* sensor onboard of the Belgian PROBA platform and operated by ESA (European Space Agency) was launched in 2001. It provides data for 62

spectral channels in the range of 415-1050 nm with a spectral resolution of 5-12 nm from five viewing angles (Chopping et al. 2004). The *POLDER* sensor onboard the Japanese platform ADEOS has 15 spectral bands which range from 443-910 nm and pixel size at nadir of 6 by 7 Km.

The *ASTER* sensor onboard the NASA's Terra spacecraft provides visible and near infrared a nadir view and additional backward telescope for stereo (15 x 15-m pixel size) as well as thermal infrared data at 90-m spatial resolution (Yamaguchi 1998, Diner et al. 2005).

The *MISR* sensor also onboard the NASA's Terra spacecraft acquires off-nadir imagery from 9 data acquisition cameras pointed in different directions in 4 spectral bands (446, 558, 673 and 866 nm) with a 275- or 1.1-Km spatial resolution depending on the channel (Diner et al. 1998, 2002) and whether the sensor is operated in local mode or general mode.

Other sensors include the Moderate resolution imaging spectroradiometer (MODIS – onboard both NASA's Terra and Aqua spacecraft), which acquires one view per overpass but obtains multiangle information based on its broad swath every 16 days (Diner et al. 2005). Moreover, SPOT (Systeme Pour l'Observation de la Terre) orbital characteristics allow the same area to be temporally visited every 9 and 18 days but some selected sites can be covered more often because the scanning instrument can be pointed off-nadir. All these sensors but CHRIS are multispectral, meaning that they can be used to detect spectral

characteristics long known to be characteristic of photosynthetically active vegetation (Gates et al. 1965, Tucker 1979).

### **3.3 Algorithms and models used to interpret multi angle remote sensing data**

Algorithms to detect vegetation structure include spectral vegetation indices such as those listed in Table 1-1. Vegetation structural characteristics have been extracted using land surface radiation models. These models can be grouped into three general classes: radiative transfer models, geometric-optical models, and computer simulations (Liang 2007).

#### **Radiative Transfer models**

Radiative transfer models simulate radiation transfer processes in a specific media, such as the interaction between solar radiation and plants. For instance, recent efforts in vegetation studies are focused on determining the three-dimension (3D) structure of the canopy using one-dimensional (1D) models (Liang, 2007). The Rahman-Pinty-Verstraete (RPV) model performs a functional decomposition of any reflectance field into an amplitude and a shape function. Among the parameters related with the shape function the modified Minnaert function parameter,  $k$ , which quantifies the degree by which the angular variations in the BRF values resemble a bowl-shaped (i.e. dense quasi-homogeneous vegetation layer in the red spectral domain) or bell-shaped pattern (i.e. relative sparse ensemble of vertically elongated foliage structure) (Widlowski

et al. 2004). Pinty et al. (2002) confirmed that bell-shaped anisotropy pattern exhibited some significant degree of heterogeneity at the scale of a few tens of meters in a study using the MISR airborne simulator, AirMISR, in the Konza prairie in Kansas.

### **Geometric optical models**

Geometric optical (GO) models assume that the canopy consists of a series of regular geometric shapes, placed on the ground surface in a prescribed manner that interacts with direct solar radiation. Li and Strahler (1992) include ellipsoidal crown shapes and the effects of mutual shadowing into this model. Franklin and Turner (1992) tested geometric optical models using SPOT multispectral imagery to estimate crown size, shrub size and density for three different shrubs (*Flourensia cernua*, *Prosopis glandulosa*, *Larrea tridentata*) located in the Chihuahuan desert. Predictions of shrub size and density were reasonably accurate when grouped by shrub classes but not for individual sites (Franklin and Turner 1992).

Hybrid radiative transfer and geometric optical models, which include the diffuse radiation into GO models, have been developed recently (Liang 2007). Chopping et al. (2008) described a hybrid geometric-optical model (simple geometric model) to retrieve understory background reflectance of large woody plants (shrubs) using MISR (275-m spatial resolution).

### **3.4 Applications of multi angular remote sensing data in rangelands and similar ecosystems**

Early studies during the late 1980's and early 1990's showed that multiangle measurements improved accuracies of depicting vegetation characteristics relative to single view angle measurements of plant geometric and radiometric variation (Deering and Eck 1987, Deering et al. 1990). These studies gave rise to a series of subsequent work demonstrating that observations collected using multiple sensor view angles can improve the classification of rangeland vegetation type and canopy structure (Vierling et al. 1997), ecosystem function (e.g. fPAR; Braswell et al. 1996) and soil surface texture identification (Asner et al. 1998a). Asner et al. (1998a) and Diner et al. (1999) summarize how multi-angle remote sensing might be applied to quantify a variety of ecological parameters across a wide range of ecosystems.

#### *CHRIS studies*

Chopping et al. (2006) attempted to determine fractional cover at the landscape scale of woody shrubs in dessert grasslands in the Jornada Experimental Rangeland (JER) using CHRIS multiangle data and modeling techniques. Separation of background and upper canopy contributions was determined with GO modeling and kernel weights of a Li-Ross model to obtain the background soil reflectance contribution to the overall signal. The results showed that the CHRIS directional signal can be explained in terms of the soil-

understory background response and woody shrub cover (Chopping et al. 2004, 2006).

#### *POLDER studies*

Because of its coarse spatial resolution, POLDER imagery has been used to assess vegetation structure at global scales (Chen et al. 2003). For example, the foliage clumping index and LAI were derived to separate sunlit and shaded leaves in uniform pixels of grassland, deciduous forest and conifer forest in Canada (Chen et al. 2003, 2005). The clumping index quantified the level of foliage grouping within different canopy structure types providing new structural information such as tree crowns, shrubs and row crops (Chen et al. 2005). In addition, POLDER observation provides measurements near the principal plane where BRDF effects are most pronounced, such as the hotspot. The hotspot is observed when the illumination and view directions coincide (principal plane), resulting in the absence of visible shadows (Hapke et al. 1996). Thus, to characterize the anisotropic behavior Chen et al. (2003) proposed the Normalized Difference between Hotspot and Darkspot (NDHD) which is linearly related to the clumping index.

#### *ASTER studies*

French et al. (2000) used aerial multiband thermal infrared (8-12  $\mu\text{m}$ ) imagery combined with Landsat TM and ground observations to discriminate senesced vegetation and bare soil to simulate ASTER performance prior that

sensor's launch. They showed that senescent vegetation can be distinguished from bare surfaces using thermal infrared emissivity differences. Later, French et al. (2008) using ASTER images between 2001 and 2003 assess the relationship between spectral emissivities (8.5-9.5  $\mu\text{m}$ ) and density of sparsely covered surface in the Jornada Experimental Range. They found that the thermal infrared data in combination with visible and NIR (NDVI) data can delineate bare soil, senesce and green vegetation.

Other ASTER land surface assessment that can be applied to rangeland classification are classifying land cover surfaces (Marcal et al. 2005, Yan et al. 2006, Gamanya et al. 2007), estimating fuel combustible in forested areas (Falkowski et al. 2005) and validating coarser spatial resolution sensors (Stefanov and Netzband 2005)

#### *MISR studies*

Chopping et al. (2003) used multi-angle aerial photography combined with physical light transfer models to derive shrubland structural canopy attributes (shrub density, width and canopy height). They found that variation between desert grassland and grass-shrub transition was related with structural canopy attributes. Later, Chopping et al. (2008) used the moderate resolution of MISR sensor (275 m) and bidirectional reflectance factors (BRFs) for the nadir blue, green and NIR cameras combined with light transfer and geometric optical models to separate shrubs canopy reflectance from their background (litter and

senesced grass) in the Jornada Experimental Range. They found good agreement between BRFs and the background.

Other assessments relating to MISR used the AirMISR simulator to delineate different landscape characteristics in the Konza prairie in Kansas. Using a radiative transfer model (RPV model described previously), differences among pasture and agricultural areas were detected (Pinty et al. 2002). Other applications of MISR surface analysis included the detection of three different cover types in the Brazilian Amazon region using a principal component analysis of the MISR spectra (Xavier and Galvao 2005). Off-nadir viewing data acquisition may improve discrimination of close and open lowland forest, open submontane forest and green/emerging pastures (Xavier and Galvao 2005).

Furthermore, multi-angle data acquired from different satellite and aircraft sensors can enhance understanding of rangeland ecosystem structure and functional components at regional scales. Discriminating land cover types (Xavier and Galvao 2005, Su et al. 2007), distinguishing upper canopy and background (Chopping et al. 2003, 2008), and estimating bidirectional reflectance distribution for different vegetation types (Lavergne et al. 2006) are some of the notable advances achieved recently using multi-angle reflectance data of rangelands.

#### **4. Active remote sensing for assessment of structure and function**

Active remote sensors create their own electromagnetic energy and do not depend on the Sun's electromagnetic energy. These sensors transmit laser

light and then record the amount of light backscattered from the terrain. Among the active remote sensors, Light Detection and Ranging (LIDAR) has shown great potential for vegetation classification (Ritchie et al 1992, Streutker and Glenn 2006, Bork and Su 2007) and for providing explicit three-dimensional structural information (Lefsky et al. 2002, Vierling et al. 2008). LIDAR sensors measure the horizontal distribution and vertical location of plant canopy elements using wavelengths in the infrared and near infrared.

#### **4.1 Applications of LIDAR in rangeland ecosystems.**

Few studies have addressed LIDAR applications in rangeland ecosystems. Weltz et al. 1994 have shown high correlation between lidar measurements of vegetation heights and cover with ground measurements. Streutker and Glenn (2006) used LIDAR to calculate vegetation heights and determine shrub presence and absence classification in a semi-arid sagebrush steppe. They found that the LIDAR heights were approximately 50% of the shrub heights because of the possibility that the pulse penetrates into the canopy to some extent before a detectable reflection occurs. They also found an overall 86% classification of sagebrush presence and absence with poor user accuracy because LIDAR missed low sagebrush (54 cm). Combination of LIDAR data and digital data improved the quality of land cover mapping. Bork and Su (2007) found that the accuracy classification improved 16 to 20% when integrate LIDAR and digital image classification compared to multispectral imagery classification (spatial resolution 0.5 m). Despite the potential of these sensors to detect

structural aspects of vegetation, they have not yet been used widely to characterize functional types (Ustin and Gamon 2010).

## **5. Linking observations and modeling to understand ecosystem structure and function at the landscape scale**

Strengthening our understanding of the linkage between structural and functional components in rangeland ecosystems needs to be addressed (Provenza 1991, West 1993, Briske et al. 2005). Rangeland health assessment and monitoring at landscape and regional scales using remote sensing tools may be more appropriate for rangeland management and conservation (Hunt et al. 2006). Thus, understanding the structure of species with similar physiological response to management and disturbance factors is relevant to determine rangeland health at broader scale.

Previous plant functional type (PFT) studies in rangeland ecosystems have focused on regional distribution of C3 and C4 plants, photosynthetic and nonphotosynthetic vegetation. Paruelo and Lauenroth (1996) evaluated the distribution of C3 and C4 plants in temperate grasslands and shrublands of North America as related with temperature, precipitation and geographic location. Breshears and Barnes (1999) developed models to predict proportions of plant functional types and soil moisture heterogeneity that can be applied to assess combine effects of climate and land use on semiarid plant communities within the grassland/forest continuum. Aguiar et al. (1996) used a model to predict

maximum biomass from mean annual precipitation to later partition this in the main PFTs for this location.

Few studies that link rangeland vegetation structure and function have been related to remote sensing. Asner et al. (1998b) used a combination of imaging spectrometry (AVIRIS) and radiative transfer inverse modeling to quantify structural and biophysical attributes of plant canopies and landcover types in a southern Texas savanna. A relationship between canopy structural attributes and fraction of photosynthetically active radiation absorbed by plant canopies and live and non-live foliage was found. Geerken et al. (2005), using MODIS and SPOT Vegetation NDVI time series, identified the distribution and fractional cover of species with an extended growing period in the Syrian steppe. Differences in the temporal spectral signature and length of growing period were related to other functional vegetation characteristics such as palatability and soil stabilization. However, no previous studies have combined remotely based productivity estimates with measurements of shrub, native grasses, and invasive grass abundance to derive productivity specific to vegetation functional groups. This stands as a research need to be filled in the future.

## **6. Conclusions**

Assessment and monitoring of the rangeland functionality related to structural attributes across broad scales represent a major approach used to understand rangeland health. A review of multi-angle remote sensing techniques shows the potential for these techniques to provide a better understanding of rangeland ecosystem structure components at regional scales. In addition,

combining spectrometry and plant functional types would strengthen the linkage between structural and functional components. Although not all aspects of rangeland ecosystem structure and function (including interrelations between these two qualities) are well understood, ecosystem responses to disturbances and their potential effects need to be addressed at regional and global scales (Aguilar et al. 1996).

This review of remote sensing techniques to delineate rangeland ecosystem and structure using multi-angle imagery will guide the next key questions addressed in the following chapters:

1. How does bidirectional reflectance factor (BRF) vary among the physiological and structural status of three different rangeland functional groups; shrubs, perennial native grasses, and annual invasive grasses?
2. What are the effects of sun zenith angle and view zenith angle on vegetation reflectance and vegetation indices?
3. Using the BRF response for these plant functional types, can we generate a fractional cover index using MISR BRF's values to partition MODIS gross primary production (GPP)?

## 7. References

- Aguilar, M.R., Paruelo, J.M., Sala, O.E., and Lauenroth, W.K. 1996. Ecosystem responses to changes in plant functional type composition: An example from the Patagonian steppe. *Journal of Vegetation Science* 7:381-390
- Asner, G.P., Braswell, B.H., Schimel, D.S., and Wessman, C.A. 1998a. Ecological research needs from multiangle remote sensing data. *Remote Sensing of Environment* 63:155-165
- Asner, G.P., Wessman, C.A., and Schimel, D.S. 1998b. Heterogeneity of savanna canopy structure and function from imaging spectrometry and inverse modeling. *Ecological Applications* 8:1002-1036
- Asner, G.P., Wessman, C.A., Schimel, D.S., and Archer, S. 1998c. Variability in leaf and litter optical properties: implications for BRDF model inversions using AVHRR, MODIS and MISR. *Remote Sensing of Environment* 63:243-257
- Booth, D.T., and Tueller, P.T. 2003. Rangeland monitoring using remote sensing. *Arid Land Research and Management* 17:455-467
- Bork, E.W., and Su, J.G. 2007. Integrating LIDAR data and multispectral imagery for enhanced classification of rangeland vegetation: A meta analysis. *Remote Sensing of Environment* 111:11-24
- Bradford, D.F., Franson, S.E., Neale, A.C., Heggem, D.T., Miller, G.R., and Canterbury, G.E. 1998. Bird species assemblages as indicators of biological integrity in great basin rangeland. *Environmental Monitoring and Assessment* 49:1-22
- Bradley, B.A., and Mustard, J.F. 2005. Identifying land cover variability distinct from land cover change: Cheatgrass in the Great Basin. *Remote Sensing of Environment* 94:204-213
- Braswell, B.H., Schimel, D.S., Privette, J.L., Moore, B., Emery, W.J., Sulzman, E.W., and Hudak, A.T. 1996. Extracting ecological and biophysical information from AVHRR optical data: An integrated algorithm based on inverse modeling. *Journal of Geophysical Research-Atmospheres* 101:23335-23348
- Breshears, D.D., and Barnes, F.J. 1999. Interrelationships between plant functional types and soil moisture heterogeneity for semiarid landscapes within the grassland/forest continuum: a unified conceptual model. *Landscape Ecology* 14:465-478

- Briske, D.D., Fuhlendorf, S.D. and Smeins, F.E. 2003. Vegetation dynamics on rangelands: a critique of the current paradigms. *Journal of Applied Ecology* 40:601-614
- Briske, D.D., Fuhlendorf, S.D. and Smeins, F.E. 2005. State-and-Transition models, Thresholds, and rangeland health: A synthesis of ecological concepts and perspectives. *Rangeland Ecology and Management* 58:1-10
- Chen, J.M., Liu, J., Leblanc, S.G., Lacaze, R., Roujean, J.L. 2003 Multi-angular optical remote sensing for assessing vegetation structure and carbon absorption. *Remote Sensing of Environment* 84:516-525
- Chen, J.M., Menges, C.H., and Leblanc, S.G. 2005. Global mapping of foliage clumping index using multi-angular satellite data. *Remote Sensing of Environment* 97:447-457
- Chopping, M.J., Rango, A., Havstad, K.M., Schiebe, F.R., Ritchie, J.C., Schmutge, T.J., French, A.N., Su L., Mckee L. and Davis M.R. 2003. Canopy attributes of desert grassland and transition communities derived from multiangle airborne imagery. *Remote Sensing of Environment* 85: 339-354
- Chopping, M.J., Laliberte, A., and Rango, A. 2004. Exploitation of multi-angle data from CHRIS on Proba: First results from the Jornada Experimental Range. *In: Lacoste H. [ED.]. Proceedings of the 2<sup>nd</sup> CHRIS/Proba Workshop; 28-30 April, 2004; ESRIN, Frascati, Italy: ESA Special Publication SP-578. p. 109-117*
- Chopping, M.J., Lihong, S., Laliberte, A., Rango, A., Peters, D.P.C and Martonchik, J.V. 2006. Mapping woody plant cover in desert grassland using canopy reflectance modeling and MISR data. *Geophysical Research Letters* 33:1-5
- Chopping, M.J., Lihong, S., Rango, A., Martonchik, J.V., Peters, D.P.C., and Laliberte, A. 2008. Remote sensing of woody shrub cover in desert grasslands using MISR with a geometric-optical canopy reflectance model. *Remote Sensing of Environment* 112:19-34
- D'Antonio, C.M., and Vitousek, P.M. 1992. Biological Invasions by exotic grasses, the grass fire cycle, and global change. *Annual Review of Ecology and Systematics* 23:63-87
- Deering, D.W., and Eck, T.F. 1987. Atmospheric optical depth effects on angular anisotropy of plant canopy reflectance. *International Journal of Remote Sensing* 8:893-916

- Deering, D.W., Eck, T.F., and Otterman, J. 1990. Bidirectional reflectances of selected desert surfaces and their 3-parameter soil characterization. *Agricultural and Forest Meteorology* 52:71-93
- Diaz, S, Briske, D.D., and McIntyre, S. 2002. Range management and plant functional types. In: Grice, A.C., and Hodgkinson, K.C. (Eds.). *Global rangelands: Progress and prospects*. Wallingford, Oxon, United Kingdom: CABI Publishing. p. 81-100
- Diner, D.J., Asner, G.P., Davies, R., Knyazikhin, Y., Muller, J.P., Nolin, A.W., Pinty, B., Schaaf C.B., and Stroeve, J. 1999. New directions in Earth observing: Scientific applications of multiangle remote sensing. *Bulletin of the American Meteorological Society* 80:2209 -2228
- Diner, D.J., Beckert, J.C., Bothwell, G.W., and Rodriguez, J.I. 2002. Performance of the MISR instrument during its first 20 months in Earth orbit. *IEEE Transactions on Geoscience and Remote Sensing* 40:1449-1466
- Diner, D.J., Beckert, J.C., Reilly, T.H., Bruegge, C.J., Conel, J.E., and Kahn R. 1998. Multiangle Imaging SpectroRadiometer (MISR) description and experimental overview. *IEEE Transactions on Geoscience and Remote Sensing* 36:1072-1087
- Diner, D.J., Braswell, B.H., Davies, R., Gobron, N., Hu, J., Jin, Y., Kahn R.A., Knyazikhin Y., Loeb N., Muller J., Nolin A.W., Pinty B., Schaaf C.B., Seiz B. and Stroeve, J. 2005. The value of multiangle measurements for retrieving structurally and radiatively consistent properties of clouds, aerosols and surfaces. *Remote Sensing of Environment* 97:495-518
- Duncan, J., Stow, D., Franklin, J. and Hope, A. 1993. Assessing the relationship between spectral vegetation indexes and shrub cover in the Jornada Basin, New-Mexico. *International Journal of Remote Sensing* 14:3395-3416
- Evans, J.P. and Geerken, R. 2006. Classifying rangeland vegetation type and coverage using a Fourier component based similarity measure. *Remote Sensing of Environment* 105:1-8
- Falkowski, M.J., Gessler, P.E., Morgan, P., Hudak, A.T., and Smith, A.M.S. 2005. Characterizing and mapping forest fire fuels using ASTER imagery and gradient modeling. *Forest Ecology and Management* 217:129-146
- Fensholt, R., and Sanholt, I. 2005. Evaluation of MODIS and NOAA AVHRR vegetation indices with in situ measurement in a semi-arid environment. *International Journal of Remote Sensing* 26:2561-2594

- Franklin, J., and Turner, D.L. 1992. The application of a geometric optical canopy reflectance model to semiarid shrub vegetation. *IEEE Transactions on Geoscience and Remote Sensing* 30:293-301
- French, A.N., Schmugge, T.J. and Kustas, W.P. 2000. Discrimination of senescent vegetation using thermal emissivity contrast. *Remote Sensing of Environment* 74:249-254
- French, A.N., Schmugge, T.J., Ritchie, J.C., Hsu, A., Jacob F. and Ogawa, K. 2008. Detecting land cover change at the Jornada Experimental Range, New Mexico with ASTER emissivities. *Remote Sensing of Environment* 112:1730-1748
- Gamanya, R., De Maeyer, P., De Dapper, M. 2007. An automated satellite image classification design using object-oriented segmentation algorithms: A move towards standardization. *Expert Systems with Application* 32:616-624
- Garrity, S.R., Vierling, L.A., Smith, A.M.S., Falkowski, M.J., and Hann, D.B. 2008 Automatic detection of shrub location, crown area, and cover using spatial wavelet analysis and aerial photography. *Canadian Journal of Remote Sensing* 34:S376-S384
- Gates, D.M., Keegan, H.J., Schleter, J.C., and Weidner, V.R. 1965. Spectral properties of plants. *Applied Optics* 4:11-20
- Geerken, R., Batikha, N., Celis, D., and Depauw, E. 2005. Differentiation of rangeland vegetation and assessment of its status: field investigations and MODIS and SPOT VEGETATION data analyses. *International Journal of Remote Sensing* 26:4499-4526
- Hapke, B., DiMucci, D., Nelson R., and Smythe, W. 1996. The cause of the hot spot in vegetation canopies and soil: shadow-hiding versus coherent backscatter. *Remote Sensing of Environment* 58:63-68
- Havstad, K.M., and Herrick, J.E. 2003. Long-term ecological monitoring. *Arid Land Research and Management* 17:389-400
- Hibbard, K.A., Archer, S., Schimel, D.S., and Valentine, D.W. 2001. Biogeochemical changes accompanying woody plant encroachment in a subtropical savanna. *Ecology* 82:1999-2011
- Holecheck, J.L., Pieper, R.D., and Herbel, C.H. 1995. *Range Management. Principles and Practices*. 2<sup>nd</sup> Edition. Prentice-Hall, Upper Saddle River, NJ pp 133-155

- Huete, A.R., Jackson, R.D., and Post, D.F. 1985. Spectral response of a plant canopy with different soil backgrounds. *Remote Sensing of Environment* 17:37-53
- Huete, A.R. 1988. A soil-adjusted vegetation index(SAVI). *Remote Sensing of Environment* 25:295-309
- Huete, A.R, and Justice, C. 1999. MODIS vegetation index (MOD 13) Algorithm Theoretical Basis Document, Greenbelt: NASA Goddard Space Flight Center. Available at <http://modarch.gsfc.nasa.gov/MODIS/LAND/#vegetation-indices>, Accessed 25 July 2008
- Huete, A.R., Liu, H.Q., Batchily, K., and van Leeuwen, W. 1997. A comparison of vegetation indices over a global set of TM images for EOS-MODIS. *Remote Sensing of Environment* 59:440-451
- Hughes, R.F., Archer, S.R., Asner, G.P., Wessman C.A., McMurtry, C., Nelson J. and Ansley, R.J. 2006. Changes in aboveground primary production and carbon and nitrogen pools accompanying woody plant encroachment in a temperate savanna. *Global Change Biology* 12:1733-1747
- Hunt, E.R., Jr., Everitt, J.H., Ritchie, J.C., Moran, M.S., Booth, D.T., Anderson, G.L., Clark, P.E., and Seyfried, M.S. 2003. Applications and Research Using Remote Sensing for Rangeland Management. *Photogrammetric Engineering and Remote Sensing* 69:675-693
- Hunt, E.R., and Miyake B.A. 2006. Comparison of stocking rates from remote sensing and geospatial data. *Rangeland Ecology and Management* 59:11-18
- Irons, J.R., Ranson, K.J., Williams, D.L., Irish, R.R. and Huegel, F.G. 1991. An Off-Nadir-Pointing imaging spectroradiometer for terrestrial ecosystem studies. *IEEE Transactions on Geoscience and Remote Sensing* 29:66-74
- Kawamura, K., Akiyama, T., Yokota, H.O, Tsutsumi, M., Yasuda, T., Watanabe, O., and Wang, S. 2005. Comparing MODIS vegetation indices with AVHRR NDVI for monitoring the forage quantity and quality in Inner Mongolia grassland, China. *Japanese Society of Grassland Science* 51:33-40
- Larcher, W. 2003. Physiological plant ecology. Ecophysiology and stress productivity of functional groups. Chapter 2. 4<sup>th</sup> Edition. Springer-Verlag, Berlin, Germany. p. 69-184
- Lass, L.W., Prather, T.S., Glenn, N.F., Weber, K.T., Mundt, J.T., and Pettingill, J. 2005. A review of remote sensing of invasive weeds and example of the early detection of spotted knapweed (*Centaurea maculosa*) and babysbreath

- (*Gypsophila paniculata*) with a hyperspectral sensor. *Weed Science* 53: 242-251
- Lavergne, T., Kaminski, T., Pinty, B., Taberner, M., Gobron, N., Verstraete, M., Vossbeck, M., Widlowski, J.L., and Giering, R. 2006. Application to MISR land products of an RPV model inversion package using adjoint and Hessian codes. *Remote Sensing of Environment* 107:362-375
- Lefsky, M.A., Cohen, W.B., Parker, G.G., and Harding, D.J. 2002. Lidar remote sensing for ecosystem studies. *BioScience* 52: 19-30
- Li, X., and Strahler, A.H. 1992. Geometric-optical bidirectional reflectance modeling of the discrete crown vegetation canopy: effect of crown shape and mutual shadowing. *IEEE Transactions on Geoscience and Remote Sensing* 30:276-291
- Liang, S. 2007. Recent developments in estimating land surface biogeophysical variables from optical remote sensing. *Progress in Physical Geography* 31: 501-516
- Loik, M.E. 2007. Sensitivity of water relations and photosynthesis to summer precipitation pulses for *Artemisia tridentate* and *Purshia tridentate*. *Plant Ecology* 191:95-108
- Marcal, A.R.S., Borges, J.S., Gomes, J.A., and Pinto Da Costa, J.F. 2005. Land cover update by supervised classification of segmented ASTER images. *International Journal of Remote Sensing* 26:1347-1362
- Martonchik, J.V., Diner, D.J., Pinty B., Verstraete, M.M., Myneni, R.B., Knyazikhin Y., and Gordon H.R. 1998. Determination of land and ocean reflective, radiative, and biophysical properties using multiangle imaging. *IEEE Transactions on Geoscience and Remote Sensing* 36:1266-1281
- Maynard, C.L., Lawrence, R.L., Nielsen, G.A. and Decker, G. 2007. Ecological site descriptions and remotely sensed imagery as a tool for rangeland evaluation. *Canadian Journal of Remote Sensing* 33:109-115
- McNaughton, S.J. 1979. Grazing as an optimization process: grass-ungulate relationships in the Serengeti. *The American Naturalist* 133:691-703
- Middleton, E.M., Deering, D.W., and Ahmad, S.P. 1987. Surface anisotropy and hemispheric reflectance for a semiarid ecosystem. *Remote Sensing of Environment* 23:193-212
- Monteith, J.L. 1972. Solar radiation and productivity in tropical ecosystems. *The Journal of Applied Ecology* 9:747-766

- Moran, M.S., Clarke, T.R., Kustas, W.P., Weltz, M. and Amer, S.A. 1994. Evaluation of hydrologic parameters in a semiarid rangeland using remotely-sensed spectral data. *Water Resources Research* 30:1287-1297
- Myneni, R.B., and Williams, D.L. 1994. On the relationship between fAPAR and NDVI. *Remote Sensing of Environment* 49:200-211
- Myneni, R.B., Maggion, S., Laquinta, J., Privette, J.L., Gobron, N., Pinty, B., Verstraete, M.M., Kimes, D.S. and Williams, D.L. 1995 Optical remote sensing of vegetation: Modeling, caveats and algorithms. *Remote Sensing of Environment* 51:169-188
- Myneni, R.B., Keeling, C.D., Tucker, C.J., Asrar, G., and Nemani, R.R. 1997. Increased plant growth in the northern high latitudes from 1981 to 1991. *Nature* 386:698-702
- Nemani, R.R., Keeling, C.D., Hashimoto, H., Jolly, W.M., Tucker, C.J., Myneni, R.B., and Running, S.W. 2003. Climate-driven increases in global terrestrial net primary production from 1982 to 1999. *Science* 300:1560-1563
- Nicodemus, F.E., Richmond, J.C., Hsia, J.J., Ginsberg, I.W. and Limperis, T. 1977. Geometrical considerations and nomenclature for reflectance. NBS Monograph 160. National Bureau of Standards. U.S. Department of Commerce, Washington D.C. 52 p
- Paruelo, J.M., and Lauenroth, W.K. 1996. Relative abundance of plant functional types in grasslands and shrublands of North America. *Ecological Applications* 6:1212-1224
- Pellant, M., Shaver, P., Pyke, D.A., and Herrick, J.E. 2000. Interpreting Indicators of Rangeland Health (Version 3). Technical Reference 1734-6, National Science and Technology Center, Bureau of Land Management, United States Department of Interior, Denver, Colorado. 130 p
- Pickup, G., and Nelson, J. 1984. Use of Landsat radiance parameters to distinguish soil erosion, stability, and deposition in arid Central Australia. *Remote Sensing of Environment* 16:195-209
- Pinty, B., Widlowski, J.L., Gobron, N., Verstraete, M.M., and Diner, D.J. 2002 Uniqueness of multiangular measurements- Part I: An indicator of subpixel surface heterogeneity from MISR. *IEEE Transactions on Geoscience and Remote Sensing* 40:1560-1573

- Provenza, F.D. 1991. Viewpoint: Range science and range management are complementary but distinct endeavors. *Journal of Range Management* 44:181-183
- Ritchie, J.C., Everitt, J.H., Escobar, D.E., Jackson, T.J., and Davis, M.R. 1992. Airborne laser measurements of rangeland canopy cover. *Journal of Range Management* 45:189-193
- Ross, J. 1981. The radiation regime and architecture of plant stands. The Hague, The Netherlands: Dr. W. Junk Publishers. 391 p
- Rouse, J.W., Hass, R.H., Schell, J.A. and Deering D.W. 1974. Monitoring vegetation systems in the Great Plains with ERTS. In Proceedings, Third Earth Resources Technology Satellite-1 Symposium, Greenbelt: NASA SP-351, 3010-3017
- Running, S.W., Justice, C.O., Salomonson, V., Hall, D., Barker, J., Kaufmann, Y.J., Strahler A.H., Huete, A.R., Muller, J.P., Vanderbilt, V. Wan, Z.M., Teillet, P. and Carneggie, D. 1994. Terrestrial remote sensing science and algorithms planned for EOS/MODIS. *International Journal of Remote Sensing* 15:3587-3620
- Ryel, R.J., Beyschlag, W., and Caldwell, M.M. 1994. Light field heterogeneity among tussock grasses: theoretical considerations of light harvesting and seedling establishment in tussocks and uniform tiller distributions. *Oecologia* 98:241-246
- Ryel, R.J., Leffler, A.J., Peek, M.S., Ivans, C.Y. and Caldwell, M.M. 2004. Water conservation in *Artemisia tridentata* through redistribution of precipitation. *Oecologia* 141:335-345
- Schaepman-Strub, G., Schaepman, M.E., Painter, T.H., Dangel, S., and Martonchik, J.V. 2006. Reflectance quantities in optical remote sensing – definitions and case studies. *Remote Sensing of Environment* 103:27-42
- Shafii, B, Price, W.J., Prather, T.S., Lass L.W., and Thill, D.C. 2004. Using landscape characteristics as prior information for Bayesian classification of yellow starthistle. *Weed Science* 52:948-953
- Skole, D., and Tucker, C. 1993. Tropical deforestation and habitat fragmentation in the Amazon – Satellite data from 1978 to 1988. *Science* 260:1905-1910
- Smith, W.K., and Nobel, P.S. 1977. Influences of seasonal changes in leaf morphology on water-use efficiency for three desert broadleaf shrubs. *Ecology* 58:1033-1043

- Stafford-Smith, M. 1996. Management of rangelands: paradigms at their limits. In: J. Hodgson and A.W. Illius. The ecology and management of grazing systems. Wallingford, UK: CAB International p 325-357
- Stefanov, W.L., and Netzband, N. 2005. Assessment of Aster land cover and MODIS NVDI data at multiple scales for ecological characterization of an arid urban center. *Remote Sensing of Environment* 99:31-43
- Stewart, K.M., Bowyer, R.T., Ruess, R.W., Dick, B.L., and Kie, J.G. 2006. Herbivore optimization by North American elk: Consequences for theory and management. *Wildlife Monographs* 167:1-24
- Strand, E.K., Smith, A.M.S., Bunting, S.C., Vierling, L.A., Hann, D.B., and Gessler, P.E. 2006. Wavelet estimation of plant spatial patterns in multi-temporal aerial photography. *International Journal of Remote Sensing* 27:2049-2054
- Strand, E.K., Vierling, L.A., Smith, A.M.S., and Bunting, S.C. 2008. Net changes in aboveground woody carbon stock in western juniper woodlands, 1946-1998. *Journal of Geophysical Research, Biogeosciences* 113: 1-13
- Streutker, D.R., and Glenn, N.F. 2006. LiDAR measurement of sagebrush steppe vegetation heights. *Remote Sensing of Environment* 102:135-145
- Su, L. Chopping, M.J., Rango, A., Martonchik, J.V., and Peters, D.P.C. 2007. Differentiation of semi-arid vegetation types based on multi-angular observations from MISR and MODIS. *International Journal of Remote Sensing* 28:1419-1424
- Tongway, D.J., and Ludwig, J.A. 1997. The nature of landscape dysfunction in rangelands. Chapter 5. In Ludwig, J., Tongway, D., Freudenberger, D., Nobel, J., and Hodgkinson, K. (Eds). *Landscape Ecology: Function and Management. Principles from Australia's Rangelands*. Melbourne, Australia: CSIRO Publishing. p. 49-61
- Tucker, C.J. 1979. Red and photographic infrared linear combinations for monitoring vegetation. *Remote Sensing of Environment* 8:127-150
- Tucker, C.J., Vanpraet, C.L., Sharman, M.J., and Vanittersum, G. 1985. Satellite remote-sensing of total herbaceous biomass production in the Senegalese Sahel 1980-1984. *Remote Sensing of Environment* 17:233-249
- Tueller, P.T. 1989. Remote sensing technology for rangeland management applications. *Journal of Range Management* 42:442-453

- Turner, D.P., Ollinger, S., Smith, M.L., Krankina, O. and Gregory, M. 2004. Scaling net primary production to a MODIS footprint in support of Earth observing system product validation. *International Journal of Remote Sensing* 24:1961-1979
- USDA, NRCS. 1997. National range and pasture handbook. Chapter 4. USDA, NRCS, Grazing Lands Technol. Inst. 190-vi-NRPH, Washington, D.C. p 73
- Ustin, S.L., and Gamon, J.A. 2010. Remote sensing of plant functional types. *New Phytologist* 186:795-816
- Vierling, L.A., Deering, D.W., and Eck, T.F. 1997. Differences in arctic tundra vegetation type and phenology as seen using bidirectional radiometry in the early growing season. *Remote Sensing of Environment* 60:71-82
- Vierling, K.T., Vierling, L.A., Gould, W.A., Martinuzzi, S., and Clawges, R.M. 2008. Lidar: shedding light on habitat characterization and modeling. *Frontiers in Ecology and the Environment* 6: 90-98
- Vrieling, A. 2006. Satellite remote sensing for water erosion assessment: A review. *Catena* 65:2-18
- Walker, B.H. 1992. Biodiversity and ecological redundancy. *Conservation Biology* 6:18-23
- Walthall, C.L., Norman, J.M., Welles, J.M., Campbell, G., and Bland, B.L. 1985. Simple equation to approximate the bidirectional reflectance from vegetative canopies and bare soil surfaces. *Applied Optics* 24:383-387
- Wang, G., Wente, S., Gertner, Z.G. and Anderson, A.B. 2002. Improvement in mapping vegetation cover factor for universal soil loss equation by geo-statistical methods with Landsat TM images. *International Journal of Remote Sensing* 23:3649-3667
- Washington-Allen, R.A., West, N.E., and Ramsey, R.D. 2003. Remote sensing-based dynamical systems analysis of sagebrush steppe vegetation in rangelands. *Proceedings of the VII<sup>th</sup> International Rangelands Congress* Alssopp N., Palmer A.R., Milton S.J., Kirkman K.P., Kerley G.I.H., Hurt C.R. and Brown C.J. (Eds). p. 416-418
- Weltz, M.A., Ritchie, J.C., and Fox, H.D. 1994. Comparison of laser and field measurements of vegetation height and canopy cover. *Water Resources Research* 30:1311-1319
- West, N.E. 1993. Biodiversity of Rangelands. *Journal of Range Management* 46:2-13

- Widlowski, J.L., Pinty, B., Gobron, N., Verstraete, M.M., Diner, D.J. and Davis, A.B. 2004. Canopy structure parameters derived from multi-angular remote sensing data for terrestrial carbon studies. *Climatic Change* 67:403-415
- Xavier, A.S., and Galvao, L. S. 2005. View angle effects on the discrimination of selected Amazonian land cover types from a principal-component analysis of MISR spectra. *International Journal of Remote Sensing* 26:3797-3811
- Yamaguchi, Y., Kahle, A., Tsu, H., Kawakami, T. and Pniel, M. 1998. Overview of Advanced Spaceborne Thermal Emission and Reflection Radiometer (ASTER). *IEEE Transactions on Geoscience and Remote Sensing* 36:1062-1071
- Yan, G., Mas, J.F., Maathuis, B.H.P., Xiangmin Z. and Van Dijk P.M. 2006. Comparison of pixel-based and object-oriented image classification approaches-a case study in a coal fire area, Wuda, Inner Mongolia China. *International Journal of Remote Sensing* 27:4039-4055

**Table 1.1** Spectral vegetation indices commonly used in rangeland studies

Index	Acronym	Formula	Applications	Author(s)
Normalized difference vegetation index	NDVI	$\frac{\rho_{nir} - \rho_{red}}{\rho_{nir} + \rho_{red}}$	Leaf area index (LAI) Biomass Plant cover Fraction of absorbed photosynthetic active radiation (fPAR)	Myneni et al. 1995 Running et al. 1994 Hunt et al. 2003 Myneni 1994
Enhanced vegetation index	EVI	$G \frac{\rho_{nir} - \rho_{red}}{\rho_{nir} + C_1 \rho_{red} - C_2 \rho_{blue} + L} (1 + L)$	fPAR Canopy background Biomass and forage quality	Huete et al. 1997 Fensholt and Sandholt 2005 Kawamura et al. 2005
Soil adjusted vegetation index	SAVI	$\frac{(1+L)(\rho_{nir} - \rho_{red})}{\rho_{nir} + \rho_{red} + L}$	Soil background effects Shrub cover Hydrologic parameters	Washington-Allen et al. 2003 Duncan et al. 1993 Moran et al. 1994

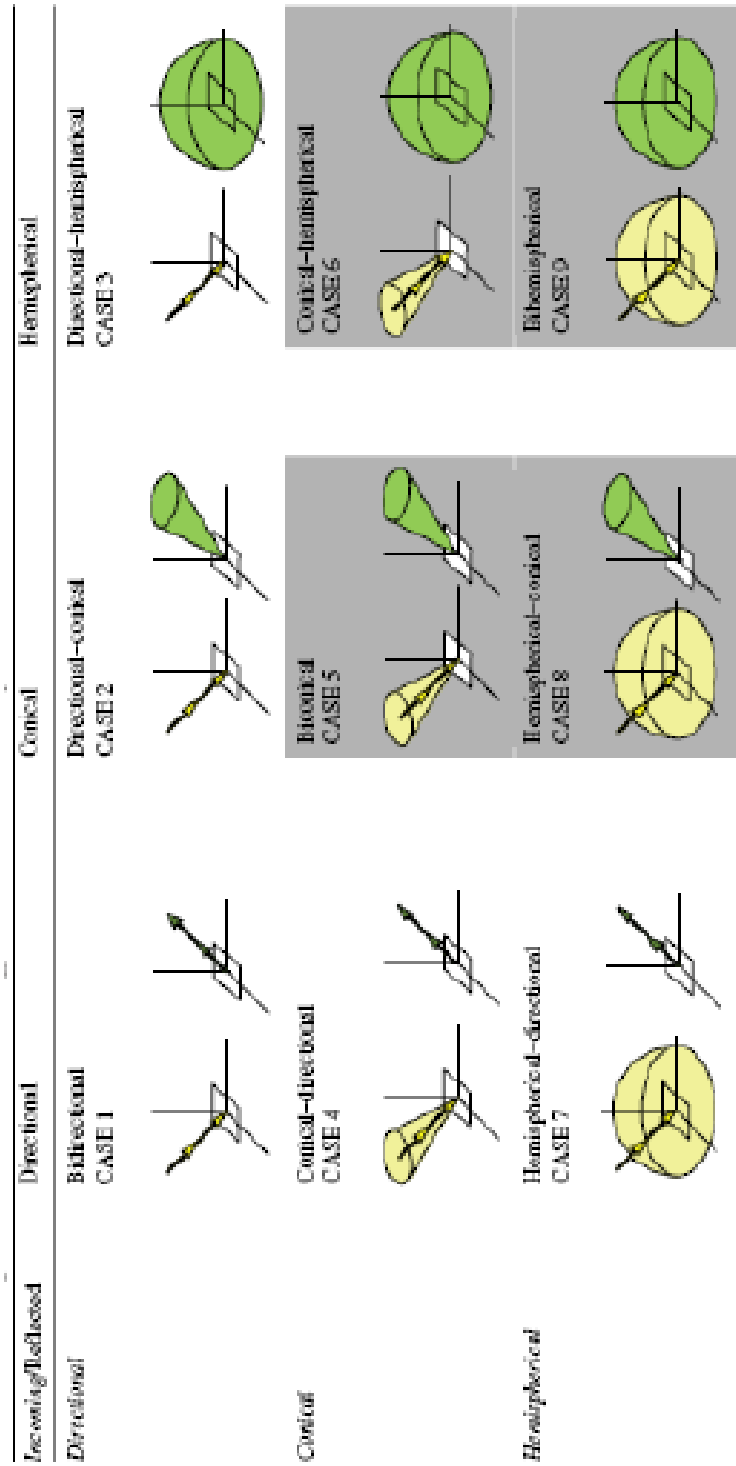


**Figure 1-1** Directional reflectance of vegetation depicted by Schaeppman-Strub et al. (2006). 'Case' labels correspond to definitions established by Nicodemus et al. (1977)

## **CHAPTER 2. Bidirectional reflectance of shrub-steppe vegetation: delineating native and invasive functional groups**

### **Abstract**

The application of remote sensing for delineating invasive grasses from native plant assemblages is important for improved understanding of rangeland ecology and management. When characterizing native and invasive rangeland vegetation across broad scales, the vast majority of remote sensing-based studies utilize the nadir-only view angle. However, nadir measurements in rangeland systems can suffer from several potential shortcomings, such as effects of background (soil and litter) reflectance and the effects of shadows. Ground-based and off-nadir radiometric measurements were collected on a shrub-steppe vegetated landscape located in west-central Idaho throughout the mid- to late-growing season to: 1) quantify the bidirectional reflectance factors of four rangeland vegetation functional groups (shrub, native grasses, invasive annual grasses, and forbs), and 2) examine ways in which these bidirectional reflectance values can help to delineate the various native vegetation types from invasive plants relative to nadir-only viewing angles. The multiple spectro-radiometric measurements were acquired within two hours of solar noon to facilitate comparison of these ground datasets with orbiting sensors such as the Multi-Angle Imaging Spectroradiometer (MISR). In addition, MISR bidirectional reflectance factor (BRF) was simulated using the PROSPECT and Scattering by Arbitrarily Inclined Leaves (SAIL) vegetation reflectance models for medusahead

rye (*Taeniatherum caput-medusae* [L.] Nevski) invasive grass at green and senesced stages because of influence of leaf orientation on red and near infrared bidirectional reflectance signal. Because of changes in leaf orientation, medusahead could be discriminated from other vegetation types at nadir and across four forward viewing zenith angles. For instance, the normalized difference vegetation index (NDVI) difference between medusahead and other vegetation types was significant during the transition of green to senesced stages ( $p < 0.05$ ). In addition, the NDVI of invasive grasses, on the other hand, was flatter and lower than the other plant functional types across all view angles, and similar to bareground NDVI. We also confirmed that shrubs exhibited the highest amount of anisotropy in all wavebands, as the relatively complex structure of the shrub canopy and concomitant shadowing greatly affected values of NDVI across all view angles. The anisotropy index (ANIX) helped to quantify these shifts, and provided additional information that allowed us to differentiate shrubs from other plant functional groups. In order to delineate rangeland vegetation types at coarser scales (i.e. across the landscape) further study is needed to quantify the spectral angular signatures of these plant groups using satellite-based multiangle imagers.

## 1. Introduction and background

Invasive plant species are changing the ecosystem structure and function of rangelands worldwide. In particular, increased prevalence of annual grasses in shrub-steppe communities has had several detrimental effects. For example, medusahead (*Taeniatherum caput-medusae* [L.] Nevski) and cheatgrass (*Bromus tectorum* L.), invasive Eurasian annual plants that have proliferated in the Great Basin of the western United States, germinate and establish their root systems prior to native species (Harris 1977, Sharp et al. 1957) and therefore alter the seasonal soil moisture and nutrient regimes available to all plants (Dahl and Tisdale 1975, Evans and Young 1972). In addition, invasive annuals have altered historic fire regimes and permanently modified Great Basin plant communities because they produce a large amount of litter that decomposes slowly, further competing with native plant regeneration (Young 1992). Beyond these effects on interspecific competition, invasive grasses may affect carbon storage through volatilization of carbon and nitrogen during fires, and exhibit relatively low carbon storage below ground (Bradley et al. 2006). In the Great Basin, cheatgrass shows high inter-annual variability in response to precipitation and exhibits five times more inter-annual live cover than perennial communities with 20-cm variance in rainfall (Elmore et al. 2003, Bradley and Mustard 2005).

The ecological impacts of invasive grasses, coupled with their widespread distribution, have spurred a variety of investigations to detect the presence, abundance, and ecological characteristics of these plants. These studies underscore the importance of developing remote sensing tools to identify and

characterize invasive grass outbreaks. For example, Bradley and Mustard (2005) found that phenological differences between cheatgrass and bunch grasses in the Great Basin could be detected using Landsat TM (30-m spatial resolution) and Advanced Very High Resolution Radiometer (AVHRR, 1000-m spatial resolution) data, thereby allowing wide scale mapping of these species. In addition, Bradley and Mustard (2005) showed that the variation in interannual productivity could be quantified using these remote measurements. Lass et al. (2005) reviewed characteristics of different remote sensing instruments and algorithms used to detect a wide variety of invasive species and found that weed detection depends on unique growth patterns (such as those found in leafy spurge (*Euphorbia esula* L.); formation of large dense patches (such as is the case with broom snakeweed (*Gutierrezia sarothrae* [Pursh] Britt & Rusby), and, in some cases, the availability of hyperspectral instruments (i.e., which are needed to detect some species such as yellow starthistle (*Centaurea solstitialis* L.).

Several remote sensing techniques and algorithms have been recently developed to detect invasive grass species using multispectral and hyperspectral imagery at very high spatial resolution. As with cheatgrass, the different phenology between invasive plants and the native species allow for the invasives to be identified. For instance, Andrew and Ustin (2008) showed that hyperspectral imagery taken in different phenological states of perennial peppergrass (*Lepidium latifolium* L.) can improve its detection in uniform sites. Noujdina and Ustin (2008) showed that it is more likely to detect cheatgrass

using hyperspectral data acquired in different seasons rather than when using single-date datasets. Hunt et al. (2007), using a canopy reflectance model, predicted that leafy spurge can be detected when leaf area index is greater than 1.0 and flower-bract cover is greater than 10%. Despite the ability to detect phenological differences, however, the spectral reflectance of invasive species can often be similar to native vegetation and it is often challenging to detect invasives when they are well mixed with native species (Shafii et al. 2004). The application of remote sensing in delineating some major invasive grasses, such as medusahead is still developing.

When characterizing native and invasive rangeland vegetation across broad scales, the vast majority of remote sensing-based studies utilize the nadir-only view angle. Reflectance values recorded at nadir view have been extensively used to generate vegetation type cover and develop and test ecological models in rangelands (Tueller 1989, Hunt et al. 2003). The nadir measurement method has been used out of necessity, because until recently most satellite and aircraft imagery has been collected at or near nadir to minimize image distortion problems. However, nadir measurements in rangeland systems can suffer from several potential shortcomings. First, nadir measurements include the highest fraction of background (e.g. soil, senesced vegetation litter) vs. green plant material relative to measurements at the same location taken at oblique angles. As a result, the spectral data collected at nadir can be confounded by background reflectance properties, making interpretation of green plant material difficult (Huete et al. 1985), particularly in semi-arid rangeland

landscapes. Second, because shadows play a large role in dictating the direction and amount of light being reflected off of vegetated rangeland surfaces, it is difficult to constrain the amount of shadow being included in a nadir measurement at different times of the day (Vierling et al. 1997).

### **1.1 Multi-angular reflectance for rangeland ecosystem monitoring**

Multi-angular reflectance information can improve surface vegetation cover classification relative to nadir-based assessment (Martonchik et al. 1998, Schaepman-Strub et al. 2006). As with most land surfaces, rangelands possess complex structures that result in highly anisotropic reflectance characteristics (Figure 2-1). The relationship between the directional radiance of a target and the sun's irradiance illuminating the target at a single incidence angle is called the bi-directional reflectance distribution function (BRDF) (Nicodemus et al. 1977, Diner et al. 1999, Schaepman-Strub et al. 2006). While the BRDF cannot be directly measured (Nicodemus et al. 1977), the anisotropic nature of vegetation canopies can be quantified in various ways for use in ecological applications. One of these ways is through the measurement of the bidirectional reflectance factor (BRF). The BRF is the ratio of the reflected radiant flux from a sample surface to the radiant flux reflected from an ideal and diffuse standard surface under identical view geometry and single direction illumination.

Early studies during the late 1980's and early 1990's showed that multiangle measurements added substantial information to those using single view angles alone (Walthall et al. 1985, Middleton et al. 1987, Deering and Eck 1987, Deering et al. 1990). These studies gave rise to a series of subsequent

work demonstrating that observations collected using multiple sensor view angles can improve the classification of rangeland vegetation type and canopy structure (e.g. Vierling et al. 1997), ecosystem function (e.g. the fraction of absorbed photosynthetically active radiation; fPAR, Braswell et al. 1996) and soil surface texture identification (e.g. Asner et al. 1998b). Asner et al. (1998b) and Diner et al. (1999) summarized how multi-angle remote sensing might be applied to quantify a variety of ecological parameters across a wide range of ecosystems. More recently, studies incorporating the bidirectional reflectance of rangeland vegetation using aircraft and satellite data have improved our understanding of rangeland ecosystem structure and functional components at regional scales. Notable recent work in rangeland systems includes discrimination of land cover types (Su et al. 2007, Xavier and Galvao 2005), distinguishing upper canopy from background (Chopping et al. 2003, 2008), and estimating bidirectional reflectance distribution functions for different vegetation types (Lavergne et al. 2006).

Because invasive annual grass species often exhibit different structure and phenology as compared with other rangeland plant functional groups, characterizing the temporal and angular reflectance characteristics of rangelands may assist in making important distinctions among these plant types. The objectives for this study are therefore: 1) to measure and report the bidirectional reflectance factors of four rangeland vegetation functional groups (shrub, native grasses, invasive annual grasses, and forbs) throughout the mid- to late-growing season, and 2) to examine ways in which these bidirectional reflectance values

can help to delineate vegetation types dominated by native species from those dominated by invasive plants relative to nadir-only viewing angles. In achieving these objectives, we hope to improve techniques for mapping various rangeland plant functional groups over broad areas.

## 2. Methods

### 2.1 Study area

The study area comprises 38,000 ha of sagebrush steppe and grassland vegetation managed by the Soulen Livestock Co., near Weiser, Idaho. The area includes private and public grazing lands, and is mostly grazed by livestock. The land is fenced and cross-fenced to facilitate livestock grazing management. In addition, the company's private lands are leased for big game and bird hunting during the fall season. The annual precipitation at the site measures 300 mm, with elevation ranging from 950 to 1300 m above sea level. Garrity et al. (2008) provide additional information about the study area.

Study sites were selected with respect to ecological site classes (USDA – NRCS; <http://websoilsurvey.nrcs.usda.gov/>). Four study sites, each measuring 5 by 5 km, were selected because of the uniformity in soil types, vegetation and topography (Figure 2-2). These ecological sites included mostly the Loamy 12-16 (ARTRX-PSSP6; 28.4%), which represents loamy soil type, 12-16 inches (304-406 mm) of precipitation, and vegetation dominated by foothill big sagebrush (*Artemisia tridentata* Nutt ssp. *xericensis* Winward ex R. Rosentreter & R. Kelsey), and bluebunch wheatgrass (*Pseudoroegneria spicata* (Pursh) A. Love).

Other ecological sites occurring within the study sites were the very shallow (12-20 ARRI2-POSE; 20.8%), dominated by scabland sagebrush (*Artemisia rigida* (Nutt.) A. Gray) and Sandberg bluegrass (*Poa secunda* J.Presl), and the South slope loamy (12-16 ARTRX-PSSP6; 12.1%). In addition, over the past five decades two exotic species, cheatgrass and medusahead, have spread throughout this landscape (Novak 2004).

## 2.2 Bidirectional reflectance factor (BRF) ground measurements

Reflectance values of four different vegetation types at nine different angles were acquired with an Ocean Optics spectroradiometer (USB2000+; Ocean Optics, Dunedin, FL, USA) and a GER 1500 spectroradiometer (SpectroTech Inc., Clemson, SC). In 2008, the Ocean Optics spectroradiometer was used to acquire spectral data of the target vegetation surfaces, a dark reference, and a Spectralon white reference panel to calculate the reflectance ( $R_\lambda$ ) for each 0.4 nm bandwidth within the range of 350 - 1000 nm spectral range using the formula (1):

$$\rho_\lambda = \frac{S_\lambda - D_\lambda}{I_\lambda - D_\lambda} \quad (1)$$

Where:

- $\rho_\lambda$  = reflectance at wavelength  $\lambda$
- $S_\lambda$  = sample intensity at wavelength  $\lambda$
- $D_\lambda$  = dark intensity at wavelength  $\lambda$
- $I_\lambda$  = Spectralon panel intensity at wavelength  $\lambda$

To ensure the quality of the data collected with the Ocean Optic spectroradiometer, the sensor integration time was optimized prior to each measurement of the dark and reference spectra (Ocean Optics, Walsh et al. 2000). The integration time of the spectrometer is similar to the shutter speed of a camera and was set to between 1 and 3 seconds. In addition, to decrease the likelihood of spurious readings, we specified the number of discrete spectral acquisitions that should be averaged for each measurement to be five scans. A personal computer recorded the radiometric data.

The GER 1500 spectroradiometer was used in 2007 to acquire spectral data of invasive annual grasses and a Spectralon white reference panel to calculate reflectance ( $R_\lambda$ ) for each 1.5 nm bandwidth within the spectral range of 300-1050 nm using the mathematical relationship described in equation (2).

$$\rho_\lambda = \frac{r_\lambda}{I_\lambda} \quad (2)$$

Where:

$\rho_\lambda$  = reflectance at wavelength  $\lambda$

$r_\lambda$  = radiance from target at wavelength  $\lambda$  ((W/cm<sup>2</sup>/nm/sr) x 10<sup>-10</sup>)

$I_\lambda$  = Reference irradiance at wavelength  $\lambda$ ((W/cm<sup>2</sup>/nm/sr) x 10<sup>-10</sup>)

In addition to the invasive annual grasses, we characterized the spectral response of perennial forbs, native grasses (sparse and bunch types), and shrubs present at each of the sites. These four plant functional groups

represented a range of canopy structure, phenology, biomass and soil background reflectivity. The perennial forbs group included lupine (*Lupinus spp.*), curlycup gumweed (*Grindelia squarrosa* [Pursh] Dunal) and western yarrow (*Achillea millefolium* L.). Curlycup gumweed was usually mixed with sparse grass vegetation. The sparse grass group included bulbous bluegrass (*Poa bulbosa* L.), which exhibits different structure and phenology than the bunch type perennial grasses. Bunchgrasses were mainly comprised of bluebunch wheatgrass and squirreltail (*Elymus elymoides* [Raf.] Swezey). The shrub group was comprised of big sagebrush and bitterbrush (*Purshia tridentata* [Pursh] DC.). Invasive annual grasses were represented mainly by medusahead and some scattered samples of cheatgrass. Medusahead was more abundant in the area and found in open areas, whereas cheatgrass was mainly found in closed communities of sagebrush.

We measured the bidirectional reflectance factor of each of the vegetation groups using different sensor view angles and sun zenith angles. The multiple spectroradiometric measurements were acquired within two hours of solar noon to facilitate comparison of these ground datasets with orbiting sensors such as the Multi-angle imaging spectroradiometer (MISR; Diner et al. 1998). We also measured the BRF at the same nine view zenith angles (nadir, plus 26.1°, 45.6°, 60.0° and 70.5° in both the forward and back viewing directions) as measured by MISR. Reflectance measurements were acquired during clear days in four different weeks between the period of July 5<sup>th</sup> and August 18<sup>th</sup>, 2008 with sun zenith angles (SZA) ranging from 25 to 35 degrees around noon. Reflectance

data was also acquired for invasive annual grasses for three different weeks between the period May 30<sup>th</sup> and July 27<sup>th</sup> of 2007 with SZA ranging from 25 to 35 degrees around noon.

To enable multi-angle measurement, the spectrometer was attached to a 2m-tall T-bar. The field of view Ocean Optics spectrometer was 14 degrees, resulting in a ground instantaneous field of view (GIFOV) diameter of 0.30 m at nadir, while the GIFOV of the GER 1500 was 0.25 m in diameter. In order to quantify the composition of the spectrometer footprint, an 8-megapixel digital camera was attached to the T-bar and remotely triggered for every reflectance measurement (after Seefeldt and Booth 2006). Each picture was resized to the footprint area of the spectrometer and classified in vegetation (forbs, grass, invasive, shrub), litter, shadow, rock and bare ground components. We used a 100-pixel grid overlaid on the picture to classify each image (Figure 2-3). Footprints with more than 70% uniformity in any vegetation component were selected to calculate BRF. However, it should be noted that particularly at forward scatter viewing angles, shadowed vegetation was common and included in the analysis (Figure 2-3).

BRF ground measurements can be difficult to acquire because the spectroradiometer captures small parts of plants (Chopping et al. 2003). To address this issue, measurements of shrubs having different heights and diameters were collected and averaged. Invasive grasses and native grasses (bunchgrasses and sparse grasses) were usually uniform in cover. Four different species of forbs were dominant in the area but these were mostly surrounded

with grasses; thus, footprints of pictures with 50% or more of the pixel representing forbs were selected for further analyses.

### **2.3 BRF data processing**

Bidirectional reflectance factors were estimated for the blue, red and near infrared wavebands using bandwidths similar to those used by the MISR sensor: blue (404-488 nm), red (660-682 nm) and near infrared (846-886nm). Because spectroradiometer measurements were collected mostly on clear days, the BRF was assumed to be the same as the reflectance value acquired with the spectroradiometer, and the diffuse component of the reflectance value was assumed to be negligible (Deering and Eck 1987, Martonchik 1994). In addition, MISR BRF was simulated for medusahead at green and senesced stages because of influence of leaf orientation on BRF signal. The simulation was run using the Prospect model and Scattering by Arbitrarily Inclined Leaves (SAIL) model. Prospect is a radiative transfer model that represents leaf optical properties spectra from 400 to 2500 nm with a limited number of input parameters: leaf biochemistry like chlorophyll content and a structure parameter such as leaf mesophyll structure index (Jacquemoud and Baret 1990, Jacquemoud et al. 1996). Once we set the parameters at the leaf scale we then ran the SAIL model that uses transmittance and reflectance spectra of leaves to simulate the directional spectral reflectance of a canopy (Verhoef 1984). The chlorophyll content ranges to simulate the spectral reflectance of medusahead at green (erectophile) and dead (planophile) stages were derived from Bokari

(1983) and Gaborcik (1985). The leaf mesophyll structure index was set based on Jacquemoud and Baret (1990).

Although temperature and precipitation regimes were different between 2007 and 2008, we adjusted the dates of BRF collections by calculating the growing degree days (GDD) for these two years using an averaging method. The GDD approach is based upon the principle that development of a plant occurs when temperature exceeds a specific base temperature for a certain period of time (Frank and Hofmann 1989). The averaging method was calculated as  $GDD = (\text{average daily temperature}) - (\text{base temperature})$ . A base temperature of 4.4 °C was used for all vegetation groups. The starting date for accumulation of GDD was set at January 1<sup>st</sup>. For example, the accumulated GDD for May 30<sup>th</sup>, 2007 was similar to Jun 19<sup>th</sup> 2008. Therefore, we then calculated the Julian day that corresponded with each date in order to compare BRF from these two years.

We calculated the commonly-used normalized difference vegetation index (NDVI; Rouse et al. 1974) and enhanced vegetation index (EVI; Miura et al. 1998, Huete et al. 1997) using data values of the MISR-convolved bandwidths. These spectral vegetation indices can minimize the reflectance effects relating to the soil background and within-canopy shading, and therefore can provide information that can complement single-band reflectance values. The vegetation spectral characteristics in the red (R) and near infrared (NIR) wavebands were used to generate the NDVI (equation 3).

$$NDVI_g = \frac{\rho(\lambda_{NIRg}) - \rho(\lambda_{redg})}{\rho(\lambda_{NIRg}) + \rho(\lambda_{redg})} \quad (3)$$

Where:

$NDVI_{\theta}$  = Normalized Difference Vegetation Index at  $\theta$  zenith angle

$\rho(\lambda_{NIR_{\theta}})$  = Near infrared waveband at  $\theta$  zenith angle

$\rho(\lambda_{red_{\theta}})$  = Red waveband at  $\theta$  zenith angle

The EVI, which is less sensitive to soil and atmospheric effects, was calculated using the following formula (Huete et al. 1997) (equation 4).

$$EVI = G \frac{\rho(\lambda_{NIR_{\theta}}) - \rho(\lambda_{red_{\theta}})}{\rho(\lambda_{NIR_{\theta}}) + C1\rho(\lambda_{red_{\theta}}) - C2\rho(\lambda_{blue_{\theta}}) + L} \quad (4)$$

Where

G = gain factor

C1 and C2 = adjustment factor for atmospheric aerosol scattering

L = soil adjustment factor

Values used for G, C1, C2 and L were 2.5, 6, 7.5 and 1 respectively (after Huete et al. 1997).

In addition, we calculated two anisotropic indices that incorporate the variation in target reflectance that can occur as the target is viewed from multiple angles along the solar principle plane. The reflectance on the forward scattering direction, called the “dark spot”, registered the minimum reflectance, while the reflectance of the retrosolar position, called the “hot spot”, registered the maximum reflectance (Figure 2-1; Hapke et al. 1996, Sandmeier and Itten 1999). The anisotropy index (ANIX) represents the ratio between the hotspot and dark spot BRF for a spectral band (Sandmeier and Itten 1999). Using the ANIX values

for the red and NIR wavebands, the normalized difference anisotropic index (NDAX) was calculated (Sandmeier and Deering 1999) following equation 5:

$$NADX = \frac{ANIX_{red} - ANIX_{NIR}}{ANIX_{red} + ANIX_{NIR}} \quad (5)$$

We also explored the use of an approach to depict canopy characteristics based on the correlation between red and NIR BRFs with view zenith angles (Zhang et al. 2002 a,b, Hu et al. 2007). Three metrics developed by Zhang et al. (2002 a, b) characterized the angular signature in spectral space (Figure 2-4; Hu et al. 2007). Two of the metrics are the location in the spectral space determined by each plant functional group, and the inclination determined by the slope and intercept of the signature of the red and NIR BRF. These angular signatures are affected by the structure of the canopy as well as by soil and leaf optical properties. The third metric is the length of the signature that describes variations in the shape of BRF due to heterogeneity in vegetation canopies such as orientation of foliage, mutual shadowing and spatial discontinuities. For example, for isotropic surfaces the length is zero because in spectral space the angular signature is a point (Zhang et al. 2002 a, b). We calculated the inclination metric using linear regression for each vegetation type in order to get the slope and the intercept (Figure 2-4, Hu et al. 2007). However, Zhang et al. (2002 a, b) described other methods to calculate the inclination and length metrics.

## 2.4 Sampling design and statistical analysis

To evaluate differences among BRF values for each of the vegetation types we randomly selected two representative areas in each of the four study sites. In each of these areas we selected 6 plant individuals that were not grazed and exhibited a representative plant height from which to collect spectral measurements. These areas were located at least 50 m away from fence lines or roads.

We acquired a large enough dataset to run a randomized complete block design analysis with 3 x 3 factors where each of the two study sites, in addition to the time of sampling, were defined as a separate block. However, because we also wanted to explore vegetation type and view angle as factors, we had to change the analysis to a non-parametric statistical analysis to compare mean reflectance values among plant functional groups and between periods of spectrometer collection. We had many spurious data that were due to dropouts in the spectroradiometer signal that could not be detected at the moment of the measurement. The other reason we had low number of data is that we constrained our database to singular SZA values described in Table 2-1. Hence, we used the Kruskal-Wallis test as a nonparametric ANOVA. We also compared means between vegetation groups using Wilcoxon rank sum test. We assumed results to significantly differ from random chance when the p-value was less than 0.05.

### 3. Results and Discussion

#### 3.1 Reflectance at nadir view

Nadir reflectance spectra of senesced invasive annual grasses, which were mainly composed of medusahead, differed substantially from the other vegetation types during the third week of July (Figure 2-5). Although sparsegrass showed the same pattern (July, week 1), it is difficult to draw a conclusive pattern because of the small number of samples considered for this analysis ( $n=1$ ). In contrast, the reflectance spectra of shrubs in all periods show the chlorophyll absorption in the red region and the strong near-infrared reflectance related to the internal structure of living leaves. The same spectral pattern might happen with green forbs and bunchgrasses during the first and third week of July despite the low number of samples. In addition, it was difficult to separate the spectral reflectance patterns of any of the vegetation types from the bareground reflectance spectra especially when vegetation types were senesced (Figure 2-5; Gates 1965, Tueller 1987, Asner 1998a). However, the spectral reflectance exhibited by medusahead during senescence showed surprising results, as described in the next two sections. Spectral differences among forbs, native grasses and shrubs were difficult to distinguish at the nadir viewing angle (Figure 2-5). The same differences and similarities are quantified by the NDVI values (Table 2-1). Even though we selected a small number of samples for some of the vegetation types during parts of the study period, we could still establish that the invasive annual NDVI was significantly lower than the other vegetation types ( $p<0.05$ ). However, significant differences between invasive annual grasses and

bareground NDVI were only found between weeks 1 and 3 of July (We did not include values for the first week of August because of the number of samples  $n=1$ ). In other words, during the transition from green to senescence, invasive annual grasses could be distinguished from bareground based on NDVI values. Moreover, although we would expect significant differences between shrubs and bunchgrasses especially when the latter are senesced (August, week 3), it was not possible to clearly distinguish these two groups in any but the red waveband (Table 2-1). Further separation among the other vegetation types NDVI was not possible (Table 2-1). Thus, nadir spectral measurements did not allow forbs, native grasses and shrubs to be clearly differentiated during the measurement period.

### **3.2 Red and NIR BRF**

Invasive annual grass red and NIR BRF differed substantially from that of the other plant functional groups across all forward view angles (Figure 2-6). This differentiation was greater during the late July-early August period when invasive grasses were senesced yet most native plants still contained some green foliage. The higher red BRF signal was likely due to the decreased foliar starch, chlorophyll, and protein that occur during senescence (Gausman 1985). This differentiation was also possible due to the strong effects of high chlorophyll absorptance on the BRF of red wavelengths (Sandmeier and Itten 1999). The near infrared BRF of invasive annual grasses also exhibited significant differences from NIR BRF of the other functional groups in late July and early

August, but this differentiation did not always occur across all view zenith angles (Figure 2-6). Although sagebrush is considered evergreen vegetation, shrub red and NIR BRFs was not substantially different from the other vegetation types (Figure 2-6).

### **3.3 Effects of leaf orientation in medusahead detection**

We found that the NIR reflectance at nadir and multiview angle of the invasive medusahead substantially increased during the onset of senescence in late July and early August relative to pre-senesced values (Figures 2-5 and 2-6). This finding seems to be unique to medusahead canopies, as the NIR reflectance of all other vegetation canopies (of which we are aware) generally decreases, rather than increase, as the canopy senesces (Gates 1965, Tueller 1987, Elvidge 1990, Asner 1998a). The long-held explanation for this phenomenon is that, as interior mesophyll cells degrade during senescence, the intercellular pore spaces that so effectively reflect NIR radiation also break down, creating a marked decrease in NIR reflectance. Indeed, this phenomenon, combined with the higher reflectance that occurs in the red portion of the spectrum, is the basis of using the NDVI as an indicator of plant greenness (Rouse et al. 1974).

Two lines of reasoning may help to explain the temporal differences in red and NIR BRF of senesced medusahead versus other functional groups (including senesced sparse grass, which has similar canopy characteristics to medusahead). One possible explanation is that the high content of silica present

in medusahead may affect these reflectance properties. Upon burning, medusahead contains 10% more ashes than other grass species, where 75% of the ash includes silica deposit mainly on the barbs of awns and the epidermis of leaves (Bovey et al. 1961, Swenson et al. 1964). Leaf optical properties are primarily determined by leaf structure and chemistry, including water content, the concentration of structural carbon constituents (e.g. cellulose, lignin), chlorophyll and other biologically active pigments (Gausman 1985). However, since refractive indices are similar among silica (1.45; Swenson et al. 1964), cellulose (1.4-1.5; Wooley 1975) and lignin (1.604; Donaldson et al. 2001), it cannot be possible that the high content of silica in medusahead would have an effect on red and NIR BRFs (Dr. Peter Griffiths, personal communication). In addition, because the high silica content occurs within medusahead leaves both before and after senescence, it would be unlikely that the silica content would affect reflectance characteristics during this phenological shift.

Another possible explanation for the enhanced NIR reflectance of medusahead canopies relates to its changed canopy morphology as medusahead makes the transition from green to senesced. Medusahead produces tillers that reach a maximum height of 15 cm to 60 cm high and exhibit very few leaves. The seedhead of medusahead becomes twisted as the seed matures, but it does not break apart completely after dehiscence (Sharp et al. 1957). As a result, while prior to senescence medusahead canopies are comprised of mostly narrow, upright plants, after senescence the still-heavy seedhead causes the plants to lay down, creating a matted plant canopy with a

near-planophile leaf orientation (Figure 2-7). Canopies with horizontal-leaves tend to have higher canopy reflectance, especially in the NIR because multiple scattering dominates the reflected radiation field (Myneni and Williams 1994).

Changes in leaf inclination angle can drive changes in spectral reflectance similar to those caused by variation in leaf area index (LAI) or tissue chemical content (Asner 2004, Myneni and Williams 1994). We simulated changes in canopy reflectance using the Scattering by Arbitrarily Inclined Leaves (SAIL) model. Two different leaf orientations were used in this model, erectophile and planophile, to simulate the change in medusahead canopy structure (Figure 2-7). Figure 2-8 shows that NIR reflectance (730-1000 nm) is more sensitive to changes in leaf orientation than is red reflectance (600-700 nm), a result that agrees with previous findings (Asner 2004, Myneni and Williams 1994). This increase in NIR reflectance after senescence also affected the NDVI of this canopy such that differences in the NDVI of the medusahead canopy vs. other plant functional groups were not as stark as differences seen in the individual red and NIR bands (Figures 2-6 and 2-10). Leaf orientation in medusahead grass can also explain differences in NIR BRF between green and senesced vegetation measured in the two growing seasons characterized in this study (Figure 2-9). In 2007, invasive annual grasses senesced earlier in the summer because of different precipitation and temperature regime compared to 2008.

### 3.4 Bidirectional vegetation indices of plant functional groups

The NDVI of senesce invasive annual grasses was significant lower than that of the other vegetation groups over a range of view angles (from 70° forward scatter to nadir view) in the solar principal plane (Figure 2-10). These low values of invasive grasses' NDVI are significant lower than that of the shrub ( $p < 0.05$ ). However, because of the number of samples, we could not establish statistical differences between shrubs and either forbs or grasses and between invasive annuals and either forbs or grasses. In addition, when invasive grasses started to senesce, the NDVI angular signatures showed a flatter shape than that of other functional groups (Figure 2-10). The flat shape could be related to the high reflectance in both red and NIR wavebands. Because the 'hotspot' effect increases reflectance in the red band, the reflectance contrast between NIR and red is reduced (Myneni and Williams 1994). Another reason could be related to confounding effects of bare ground BRDF values.

Although there is a clear separation of red and NIR BRDF values for invasive annual grasses from those of the other vegetation types, this differentiation was not clear when comparing medusahead and bare ground bidirectional NDVI values (Figures 2-6 and 2-10). Bare ground or soil also exhibits an anisotropic behavior that would depend on soil texture, roughness and moisture (Deering et al. 1992, Jacquemoud et al. 1992). For instance, a rough soil surface shows a 'hotspot' effect (Jacquemoud et al. 1992). Moreover, Myneni and Williams (1994) reported that the reflectance contrast between NIR and red is reduced for top of the canopy (TOC) NDVI as a function of view

zenith angle gathered in the principal plane. TOC peat NDVI exhibits similar flat spectral patterns to the medusahead NDVI when it is senesced. Although senesced medusahead leaf orientation changed, dark litter reflectance, accumulated in the understory from previous years, would affect the medusahead bidirectional signal (Figure 2-7; Young 1992).

NDVI was affected by view zenith angle at all time periods measured (Figure 2-10). The degree of change varied as a function of the phenological stage and the vegetation functional group. For instance, the presence of a 'hotspot' in bunchgrasses changed from 60° forward scatter when this functional group was green (July, week 1 and week 3), to 45° and 26° forward scatter when these plants started to senesce (August, week 1 and August week 3, respectively). This result coincides with Goodin et al. (2004), who reported greater NDVI values at large off-nadir view than values near nadir for green tallgrass prairie. Middleton (1991) reported that tallgrass prairie NDVI was significantly affected by differences in view zenith angle and SZA. We tried to avoid effects of changing SZA by constraining our measurements to the period around solar noon. Middleton (1991) also suggested that vegetation indices measured at solar noon (high sun elevation angles or low SZA) could generate good indicators of percent cover but not canopy attributes. For instance, we could distinguish a shrub NDVI "hotspot" that is mostly located at 26° forward scatter. The presence of these hotspots must be due to the large presence of bright green leaves in the footprint of the handheld spectroradiometer (Figure 2-10). In addition, decreases in NDVI values occurred at larger backscatter view

zenith angles as a result of gaps between leaves allowing within-canopy shadows to be viewed by the sensor. Despite the fact that measurements of shrubs were taken in mostly open communities with few shadows, at large zenith angles, within-canopy shadowing from other surrounding vegetation becomes an important factor constraining canopy reflectance (Li and Strahler 1992).

Class differentiation based on bidirectional NDVI for forbs, sparse grass and bunchgrasses was not possible at any of the view zenith angles. EVI angular signatures showed the same pattern as the NDVI signatures but slightly enhanced the differences among invasive grasses, shrubs, and the other native plant functional groups (data not shown). Although EVI values are generally less sensitive to soil and atmospheric effects (Huete et al 2002), shadowing effects in the vegetation did not allow us to get new information to differentiate other plant functional types different from shrubs and invasive plants.

### **3.5 Reflectance anisotropy of rangeland plant functional groups**

All plant functional groups exhibited anisotropic reflectance in the red and NIR BRF (Figures 2-6). The location of greatest reflectance, or 'hotspot', was mostly present in the backscatter direction, while low reflectance 'darkspots' were present in the forward scatter direction depending on the canopy of the plant functional group. These observations agree with previous studies of plant BRF which have shown that the locations of the 'hotspot' and 'darkspot' correspond with a low shadow fraction in the backscatter view direction and a high shadow fraction in the forward scatter direction (Hapke et al. 1996, Sandmeier and Itten

1999). Shrubs had the highest anisotropy behavior, most likely because of their relatively complex canopy dimensions and canopy understory characteristics. The height of shrubs determined the amount of shadow viewed by the instruments, which in turn affects values of reflectance in the forward scatter direction (Li and Strahler 1992). The diameter of sagebrush and bitterbrush samples range from 1.06 to 1.89 m. Thus, depending on the dimension of the shrubs, the footprint of the reflectance measurement at very high view zenith angle ( $>45^\circ$ ) varied from shrub leaves and wood, to understory vegetation (forbs and grasses), and to litter (Li and Strahler 1992).

The anisotropy of invasive annual plants was different from other plant functional groups during the first days of senescence (July, week 3). Its concave shape (two hotspots occurring at the limbs of the angular observation range) is likely due to the change in position of seed heads and lack of shadows (see Figures 2-7 and 2-8). The view footprint of senesced medusahead was mostly comprised of seed-heads and stems, compared to the footprints when plants were green. While the reflectance of the green invasive canopy included not only the erect plants, but also background litter and within-canopy shadowing, the senescent canopies had reduced litter and shadow fractions due to the planophile orientation of the grass (Figure 2-7).

The anisotropy index (ANIX) confirmed that shrubs exhibit high anisotropy behavior compared to other plant functional groups (Figure 2-11; Sandmeier and Deering 1999, Pocewicz et al. 2007). Forbs also exhibited a slight anisotropy index that is clearly different from the other vegetation types (July, week 1 and

August, week 3). However, measurements taken on forbs were not consistent throughout the season. During the first weeks, we took measurements for lupine, curlycup gumweed and western yarrow because these species were abundant, and had almost the same height. However, their canopy reflectance is not similar because lupine ANIX was completely different from the others when measured alone (August, week 3). To our knowledge there is not information related to this species reflectance. Further research is needed to better understand the reflectance anisotropy of forb species in this location.

Although ANIX showed distinctive patterns between shrubs and the other vegetation types, NADX values did not contain the same trend at all periods (Figure 2-12). Moreover, when we compared NADX with NDVI at the nadir viewing angle, we could detect almost the same pattern for NDVI along the season for each vegetation type. This NDVI pattern still could be detected even though NDVI values decreased due to changes in phenology (Figure 2-12). The only ANIX-related pattern that might be distinguished occurred during the third week of July.

Shrubs, vertically elongated foliage, exhibit a bell-shaped angular signature, while compact vegetation canopies, such as native and invasive grasses, exhibit bowl-shaped reflectance patterns (Pinty et al. 2002, Wildowski et al. 2004). For example, in boreal land cover types NDAX allowed discrimination between planophile and erectophile canopy structures (Sandmeier and Deering 1999). However, high NADX for shrubs could not be detected at all periods. NDAX may be influenced by canopy characteristics (Sandmeier and Deering

1999). However, at the scale of our study variations in the spectral response of some components of shrubs, such as gray leaves, senesced leaves, gray bark, gray wood and brown wood, might have affected ANIX values in the red waveband (Tueller 1989).

### **3.6 Red and NIR angular signatures in spectral space**

We depicted the angular spectral signature of each plant functional group building a curve shaped by the entire range of view zenith angles measured in this study. Figure 2-13 shows angular signatures plotted on the red and NIR plane for the third week of July. The location of invasive annual grasses in spectral space can be differentiated from the other plant functional types. Sparse grasses and bunchgrasses have different slope values (1.63 vs 1.89) because of differences in canopy structure. In addition, the slope generated from shrub reflectance values (2.41) was steeper than the rest of plant functional types because of its canopy structure and leaf optical properties (high absorption in the red bandwidth).

The length of signature for all the vegetation groups was similar, indicating that these canopies are heterogeneous. For example, the length of the invasive grasses revealed that this heterogeneity occurred due to changes in leaf orientation. Hu et al. (2007) indicated that forest biomes exhibit large length magnitudes because of their high degree of vertical heterogeneity. This method highlights the high level of differentiation that could be achieved when examining

the BRF of invasive grasses relative to the native plant functional groups during the onset of senescence (Hu et al. 2007).

#### **4. Conclusions**

We conclude that the red BRF and NIR BRF at nadir and four forward view zenith angles allowed spectral differentiation between the invasive annual grass medusahead from other plant functional groups. This differentiation was most possible when the invasive grass was in the transition period from green to senescent phenology status (July, week 3 and August, week 1). The relationship of red and NIR BRF in the spectral plane clearly depicted this differentiation. Vegetation indices such as the NDVI were not as useful for differentiating medusahead when senesced because of the unprecedented observation that medusahead canopies increased their reflectance in the NIR even after senescence (Elvidge 1990). Medusahead canopy structure changed in that while green stems were erect, and senesced stems exhibited a drooped planophile orientation. We also conclude that shrubs exhibited the highest amount of anisotropy in all wavebands, as the relatively complex structure of the shrub canopy and concomitant shadowing greatly affected values of NDVI across all view angles. The NDVI of invasive grasses, on the other hand, was flatter and lower than the other plant functional types across all view angles. The anisotropy index (ANIX) helped to quantify these shifts, and provided additional information that allowed us to differentiate shrubs from other plant functional groups.

Further study is needed to quantify the spectral angular signatures of these plant groups at coarser scales (i.e. across the landscape) in order to delineate rangeland vegetation types. Red BRF from the MISR local mode satellite product (pixel size: 275 x 275m) might be useful for detecting invasive plant distributions. In addition, BRF values for earlier spring (April), when annual invasive grasses are still dormant, may also allow perennial grasses to be discriminated from other groups because BRF values for this plant functional type proved to be different from shrubs but not from annual invasive grasses. Finally, because changes in leaf orientation for annual grasses allowed this plant functional group to be detected at nadir, intermediate spatial resolution imagery (e.g. Landsat, with-30 m pixel size) could be used to map medusahead patches during its transition from green to senesced phenology.

## 5. References

- Andrew, M.E., and Ustin, S.L. 2008 The role of environmental context in mapping invasive plants with hyperspectral image data. *Remote Sensing of Environment* 112: 4301-4317
- Asner, G.P. 1998a. Biophysical and biochemical sources of variability in canopy reflectance. *Remote Sensing of Environment* 64:234-253
- Asner, G.P., Braswell, B.H., Schimel, D.S., and Wessman, C.A. 1998b. Ecological research needs from multiangle remote sensing data. *Remote Sensing of Environment* 63:155-165
- Asner, G.P. 2004. Biophysical remote sensing signatures of Arid and Semiarid ecosystems. In: Susan Ustin (Ed). *Remote Sensing for Natural Resource Management and Environmental Monitoring: Manual of Remote Sensing*. Vol 4. 3 Ed.: John Wiley & Sons, Hoboken, New Jersey. p 53-109
- Bokari, U.G. 1983. Chlorophyll, dry matter, and photosynthetic conversion-efficiency relationships in warm-season grasses. *Journal of Range Management* 36:431-434
- Bovey, R.W., Le Tourneau, D., Erickson, L.C. 1961. The chemical composition of medusahead and downy brome. *Weeds* 9:307-311
- Bradley, B.A., and Mustard, J.F. 2005. Identifying land cover variability distinct from land cover change: Cheatgrass in the Great Basin. *Remote Sensing of Environment* 94:204-213
- Bradley, B.A., and Mustard, J.F. 2006. Characterizing the landscape dynamics of an invasive plant and risk of invasion using remote sensing. *Ecological Applications* 16:1132-1147
- Braswell, B.H., Schimel, D.S., Privette, J.L., Moore, B., Emery, W.J., Sulzman, E.W., and Hudak, A.T. 1996. Extracting ecological and biophysical information from AVHRR optical data: An integrated algorithm based on inverse modeling. *Journal of Geophysical Research-Atmospheres* 101:23335-23348
- Chopping, M.J., Rango, A., Havstad, K.M., Schiebe, F.R., Ritchie, J.C., Schmutz, T.J., French, A.N., Su L., Mckee L. and Davis M.R. 2003. Canopy attributes of desert grassland and transition communities derived from multiangle airborne imagery. *Remote Sensing of Environment* 85: 339-354

- Chopping, M.J., Lihong, S., Rango, A., Martonchik, J.V., Peters, D.P.C., and Laliberte, A. 2008. Remote sensing of woody shrub cover in desert grasslands using MISR with a geometric-optical canopy reflectance model. *Remote Sensing of Environment* 112:19-34
- Dahl, B.E., and Tisdale, E.W. 1975. Environmental factors related to medusa-head distribution. *Journal of Range Management* 28:463-468
- Deering, D.W., and Eck, T.F. 1987. Atmospheric optical depth effects on angular anisotropy of plant canopy reflectance. *International Journal of Remote Sensing* 8:893-916
- Deering, D.W., Eck, T.F., and Otterman, J. 1990. Bidirectional reflectances of selected desert surfaces and their 3-parameter soil characterization. *Agricultural and Forest Meteorology* 52:71-93
- Deering, D.W., Middleton, E.M., Irons, J.R., Blad, B.L., Walter-Shea, E.A., Hays C.J., Walthall, C., Eck, T.F., Ahmad, S.P., and Banerjee, B.P. 1992. Prairie grassland bidirectional reflectances measured by different instruments at the FIFE site. *Journal of Geophysical Research* 97:18887-18903.
- Diner, D.J., Asner, G.P., Davies, R., Knyazikhin, Y., Muller, J.P., Nolin, A.W., Pinty, B., Schaaf C.B., and Stroeve, J. 1999. New directions in Earth observing: Scientific applications of multiangle remote sensing. *Bulletin of the American Meteorological Society* 80:2209 -2228
- Diner, D.J., Beckert, J.C., Reilly, T.H., Bruegge, C.J., Conel, J.E., and Kahn R. 1998. Multiangle Imaging SpectroRadiometer (MISR) description and experimental overview. *IEEE Transactions on Geoscience and Remote Sensing* 36:1072-1087
- Donaldson, L., Hague, J., and Snell, R. 2001. Lignin distribution in Coppice Poplar, Linseed and Wheat Straw. *Holzforschung* 55: 379-385
- Elmore, A.J., Mustard, J.F., Manning S.J. 2003. Regional patterns of plant community response to changes in water: Owens valley, California. *Ecological Applications* 13:443-460
- Elvidge, C.D. 1990. Visible and near infrared reflectance characteristics of dry plant materials. *International Journal of Remote Sensing* 11:1775-1795
- Evans, R.A. and Young, J.A. 1972. Microsite requirements for establishment of annual rangeland weeds. *Weed Science* 20: 350-356
- Frank, A.B., and Hofmann, L. 1989. Relationships among grazing management, growing degree-days, and morphological development for native grasses on

- the Northern Great Plains. *Journal of Range Management* 42:199-202
- Gaborcik, N. 1985. Variability of chlorophyll content in grasses. *Rostlinna Vyroba* 31:401-408
- Garrity, S.R., Vierling, L.A., Smith, A.M.S., Falkowski, M.J. and Hann, D.B. 2008. Automatic detection of shrub location, crown area, and cover using spatial wavelet analysis and aerial photography. *Canadian Journal of Remote Sensing* 34:S376-S384
- Gates, D.M., Keegan, H.J., Schleter, J.C., and Weidner, V.R. 1965. Spectral properties of plants. *Applied Optics* 4:11-20
- Gausman, H.W. 1985. Plant leaf optical properties in visible and near-infrared light. Graduate studies (Texas Tech University) No 29. 78 p.
- Goodin, D.G., Gao, J., and Henebry, G.M. 2004. The effect of solar illumination angle and sensor view angle on observed patterns of spatial structure in tallgrass prairie *IEEE Transactions on Geoscience and Remote Sensing* 42:154-165
- Hapke, B., DiMucci, D., Nelson R., and Smythe, W. 1996. The cause of the hot spot in vegetation canopies and soil: shadow-hiding versus coherent backscatter. *Remote Sensing of Environment* 58:63-68
- Harris, G.A. 1977. Root phenology as a factor of competition among grass seedlings. *Journal of Range Management* 30:172-177
- Hu, J., Su, Y., Tan, B., Huang, D., Yang, W., Schull, M., Bull M.A., Martonchik, J.V., Diner, D.J., Knyazikhin, Y., and Myneni, R.B. 2007. Analysis of the MISR LAI/FPAR product for spatial and temporal coverage, accuracy and consistency. *Remote Sensing of Environment* 107:334-347
- Huete, A.R., Didan, K., Miura, T., Rodriguez, E.P., Gao X., and Ferreira, L.G. 2002. Overview of the radiometric and biophysical performance of the MODIS vegetation indices. *Remote Sensing of Environment* 83:195-213
- Huete, A.R., Jackson, R.D., and Post, D.F. 1985. Spectral response of a plant canopy with different soil backgrounds. *Remote Sensing of Environment* 17:37-53
- Huete, A.R., Liu, H.Q., Batchily, K., and van Leeuwen, W. 1997. A comparison of vegetation indices over a global set of TM images for EOS-MODIS. *Remote Sensing of Environment* 59:440-451

- Hunt, E.R., Jr., Everitt, J.H., Ritchie, J.C., Moran, M.S., Booth, D.T., Anderson, G.L., Clark, P.E., and Seyfried, M.S. 2003. Applications and Research Using Remote Sensing for Rangeland Management. *Photogrammetric Engineering and Remote Sensing* 69:675-693
- Hunt, E.R. Jr., Daughtry, C.S.T., Moon, S.K., and Parker Williams, A.E. 2007. Using canopy reflectance models and spectral angles to assess potential of remote sensing to detect invasive weeds. *Journal of Applied Remote Sensing* 1: 1-19
- Jacquemoud, S., and Baret, F. 1990. Prospect: A model of leaf optical properties spectra. *Remote Sensing of the Environment* 34:75-91
- Jacquemoud, S., Baret, F. and Hanocq, J.F. 1992. Modeling spectral and bidirectional soil reflectance. *Remote Sensing of the Environment* 41:123-132
- Jacquemoud, S., Ustin, S.L., Verdebout, J., Schmuck, G., Andreoli, G., and Hosgood, B. 1996. Estimating leaf biochemistry using the PROSPECT leaf optical properties model. *Remote Sensing of the Environment* 56:194-202
- Lass, L.W., Prather, T.S., Glenn, N.F., Weber, K.T., Mundt, J.T., and Pettingill, J. 2005. A review of remote sensing of invasive weeds and example of the early detection of spotted knapweed (*Centaurea maculosa*) and babysbreath (*Gypsophila paniculata*) with a hyperspectral sensor. *Weed Science* 53: 242-251
- Lavergne, T, Kaminski T., Pinty, B., Taberner, M., Gobron, N., Verstraete M., Vossbeck, M., Widlowski, J-L, Giering R. 2006. Application to MISR land products of an RPV model inversion package using adjoint and Hessian codes. *Remote Sensing of Environment* 107:362-375
- Li, X., and Strahler, A.H. 1992. Geometric-optical bidirectional reflectance modeling of the discrete crown vegetation canopy: effect of crown shape and mutual shadowing *IEEE Transactions on Geoscience and Remote Sensing* 30:276-291
- Martonchik, J.V. 1994. Retrieval of surface directional reflectance properties using ground level multiangle measurements. *Remote Sensing of the Environment* 50 303-316
- Martonchik, J.V., Diner, D.J., Pinty B., Verstraete, M.M., Myneni, R.B., Knyazikhin Y., and Gordon H.R. 1998. Determination of land and ocean reflective, radiative, and biophysical properties using multiangle imaging. *IEEE Transactions on Geoscience and Remote Sensing* 36:1266-1281

- Middleton, E.M., Deering, D.W., and Ahmad, S.P. 1987. Surface anisotropy and hemispheric reflectance for a semiarid ecosystem. *Remote Sensing of Environment* 23:193-212
- Middleton, E.M. 1991. Solar zenith angle effects on vegetation indexes in tallgrass prairie. *Remote Sensing of Environment* 38:45-62
- Miura, T., Huete, A.R., van Leeuwen, W.J.D., and Didan, K. 1998. Vegetation detection through smoke-filled AVIRIS images: An assessment using MODIS band passes. *Journal of Geophysical Research* 103:32001-32011
- Myneni, R.B., and Williams, D.L. 1994. On the relationship between fAPAR and NDVI. *Remote Sensing of Environment* 49:200-211
- Nicodemus, F.E., Richmond, J.C., Hsia, J.J., Ginsberg, I.W. and Limperis, T. 1977. Geometrical considerations and nomenclature for reflectance. NBS Monograph 160. National Bureau of Standards. U.S. Department of Commerce, Washington D.C. 52 p
- Noujdina, N.V., and Ustin, S.L. 2008. Mapping downy brome (*Bromus tectorum*) using multivariate AVIRIS data. *Weed Science* 56:173-179
- Novak, S.J. 2004. Genetic analysis of Downy Brome (*Bromus tectorum*) and Medusahead (*Taeniatherum caput-medusae*): Management implications. *Weed Technology* 18:1417-1421
- Pinty, B., Widlowski, J.L, Gobron, N., Verstraete, M.M., and Diner, D.J. 2002. Uniqueness of multiangular measurements- Part I: An indicator of subpixel surface heterogeneity from MISR. *IEEE Transactions on Geoscience and Remote Sensing* 40:1560-1573.
- Pocewicz, A., Vierling, L.A., Lentile, L.B. and Smith, R. 2007. View angle effects on relationships between MISR vegetation indices and leaf area index in a recently burned ponderosa pine forest. *Remote Sensing of Environment* 107:322-333
- Rouse, J.W., Hass, R.H., Schell, J.A. and Deering D.W. 1974. Monitoring vegetation systems in the Great Plains with ERTS. In *Proceedings, Third Earth Resources Technology Satellite-1 Symposium, Greenbelt: NASA SP-351*, 3010-3017
- Sandmeier, S.R. and Deering, D.W. 1999. A new approach to derive canopy structure information for boreal forests using BRDF data. *IEEE IGARSS 1999 Proceedings, Germany: Hamburg*. 1: 410-412

- Sandmeier, S.R. and Itten, K.I. 1999. A field goniometer system (FIGOS) for acquisition of hyperspectral BRDF data IEEE Transactions on Geoscience and Remote Sensing 37:978-986
- Schaepman-Strub, G., Schaepman, M.E., Painter, T.H., Dangel, S., and Martonchik, J.V. 2006. Reflectance quantities in optical remote sensing – definitions and case studies. Remote Sensing of Environment 103:27-42
- Seefeldt, S.S., and Booth, D.T. 2006. Measuring plant cover in sagebrush steppe rangelands: A comparison of methods. Environmental Management 37:703-711
- Shafii, B, Price, W.J., Prather, T.S., Lass L.W., and Thill, D.C. 2004. Using landscape characteristics as prior information for Bayesian classification of yellow starthistle. Weed Science 52:948-953
- Sharp, L.A., Hironaka, M., and Tisdale, E.W. 1957. Viability of medusahead seed collected in Idaho. Journal of Range Management 10:123-126
- Swenson, C.F., Le Tourneau, D. and Erickson, L.C. 1964. Silica in medusa-head. Weeds 12:16-18
- Su, L. Chopping, M.J., Rango, A., Martonchik, J.V., and Peters, D.P.C. 2007. Differentiation of semi-arid vegetation types based on multi-angular observations from MISR and MODIS. International Journal of Remote Sensing 28:1419-1424
- Tueller, P.T. 1987. Remote sensing science applications in arid environment. Remote Sensing of Environment 23:143-154
- Tueller, P.T. 1989. Remote sensing technology for rangeland management applications. Journal of Range Management 42:442-453
- USDA, NRCS. 2007. Web Soil Survey. Available online at <http://websoilsurvey.nrcs.usda.gov/>. Accessed March/03/2007
- Verhoef, W. 1984. Light scattering by leaf layers with application to canopy reflectance modeling: The SAIL model. Remote Sensing of Environment 16: 125-141
- Vierling, L.A., Deering, D.W., and Eck, T.F. 1997. Differences in arctic tundra vegetation type and phenology as seen using bidirectional radiometry in the early growing season. Remote Sensing of Environment 60:71-82
- Walsh, K.B., Guthrie J.A., and Burney, J.W. 2000. Application of commercially available, low-cost, miniaturized NIR spectrometers to the assessment of the

- sugar content of intact fruit. Australian Journal of Plant Physiology 27: 1175-1186
- Walthall, C.L., Norman, J.M., Welles, J.M., Campbell, G., and Bland, B.L. 1985. Simple equation to approximate the bidirectional reflectance from vegetative canopies and bare soil surfaces. Applied Optics 24:383-387
- Widlowski, J.L, Pinty, B., Gobron, N., Verstraete, M.M., Diner, D.J. and Davis A.B. 2004. Canopy structure parameters derived from multi-angular remote sensing data for terrestrial carbon studies. Climatic Change 67:403-415
- Wolley, J.T. 1975 Refractive index of soybean leaf cell-walls. Plant Physiology 55:172-174
- Xavier, A.S., and Galvao, L. S. 2005. View angle effects on the discrimination of selected Amazonian land cover types from a principal-component analysis of MISR spectra. International Journal of Remote Sensing 26:3797-3811
- Young, J.A. 1992. Ecology and management of medusahead (*Taeniatherum caput-medusae* ssp. *Asperum*[Simk] Melderis) Great Basin 52: 245-252
- Zhang, Y., Tian, Y., Myneni, R.B., Knyazikhin, Y., and Woodcock, C.E. 2002a. Assessing the information content of multiangle satellite data for mapping biomes I. Statistical analysis. Remote Sensing of Environment 80:418-434
- Zhang, Y., Shabanov, N., Knyazikhin, Y., and Myneni, R.B. 2002b. Assessing the information content of multiangle satellite data for mapping biomes II. Theory. Remote Sensing of Environment 80:435-446

Table 2-1. NDVI values derived from nadir measurements for five vegetation types sampled at different periods and SZA (different letters mean significant differences between vegetation types ( $p < 0.05$ ))

Veg. type	July, week 1			July, week 3			August, week 1			August, week 3			
	sza	n	NDVI	sza	n	NDVI	sza	n	NDVI	sza	n	NDVI	
Forbs	25-26	1	0.49	36	1	0.39	30-31	3	0.24	0.04	31-32	5	0.27 <sup>a</sup>
Sparsgrass	25-26	1	0.23	33-35	3	0.25	30-35	4	0.24 <sup>a</sup>	0.02	31-32	1	0.22
Bunchgrass	25-27	1	0.45	32-34	2	0.34	36-39	4	0.26 <sup>a</sup>	0.04	31-32	4	0.24 <sup>b</sup>
Shrubs	25-27	4	0.57 <sup>a</sup>	30-35	9	0.47 <sup>a</sup>	30-35	7	0.38 <sup>a</sup>	0.10	31-32	12	0.38 <sup>b</sup>
Invasive	25-28	4	0.28 <sup>b</sup>	25-26	9	0.20 <sup>b</sup>	36-37	1	0.14		31-32	5	0.17 <sup>b</sup>
Bareground	33-41	7	0.16 <sup>c</sup>	33-41	7	0.16 <sup>c</sup>	33-41	7	0.16 <sup>b</sup>	0.04	33-41	7	0.16 <sup>b</sup>

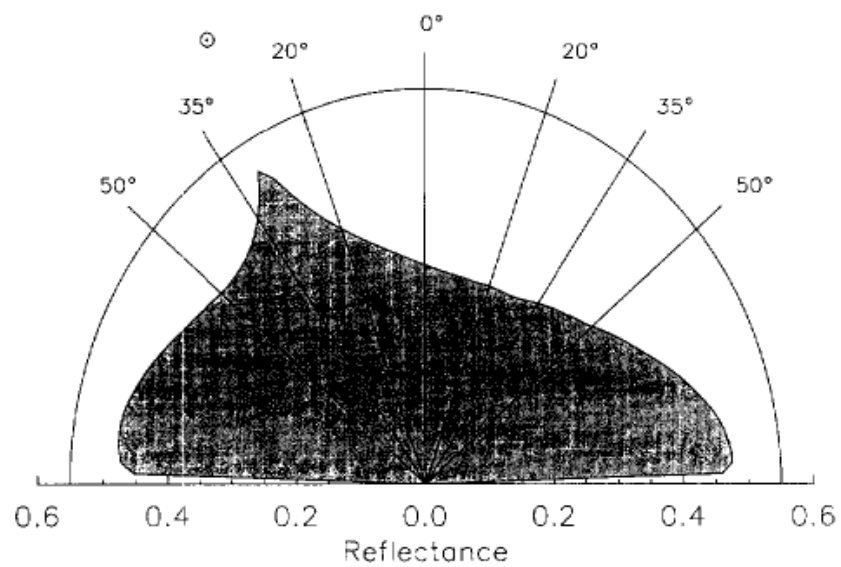


Figure 2-1. Anisotropy behavior along the solar plane recorded with the MMR spectroradiometer (Asner 1998). Strong backward scatter is brighter and the location of a hotspot is at 25° from nadir. Forward scatter is affected by shadowing (darkspot). BRF is determined by canopy structural characteristics.

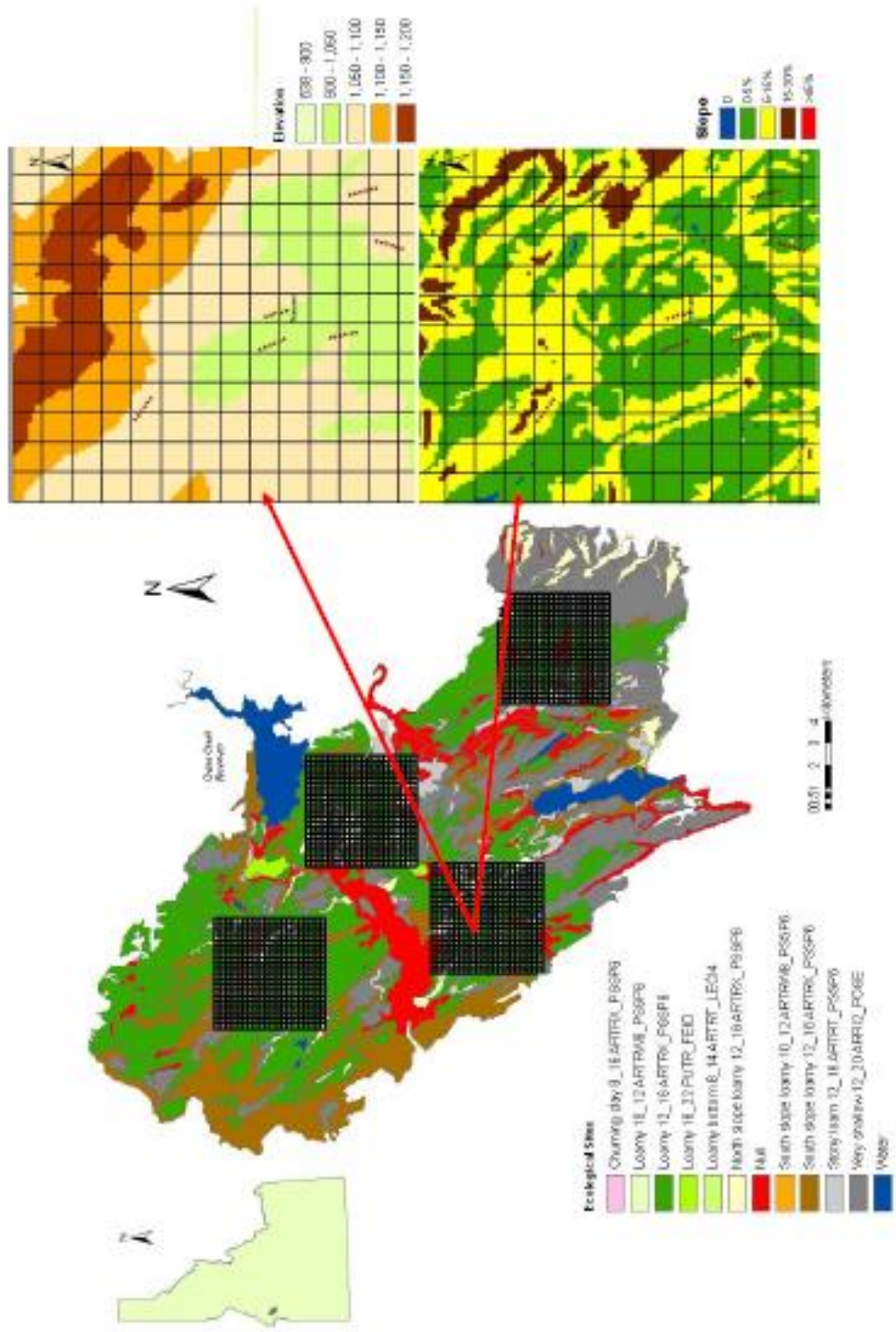


Figure 2-2. Study area and distribution of simulated MODIS GPP 1-Km Macroplots. Spectroradiometer readings and line-transsects were set on areas dominated by the Loamy 12-16 ARTRX-PSSP6 ecological site and areas with less than 15% slope.

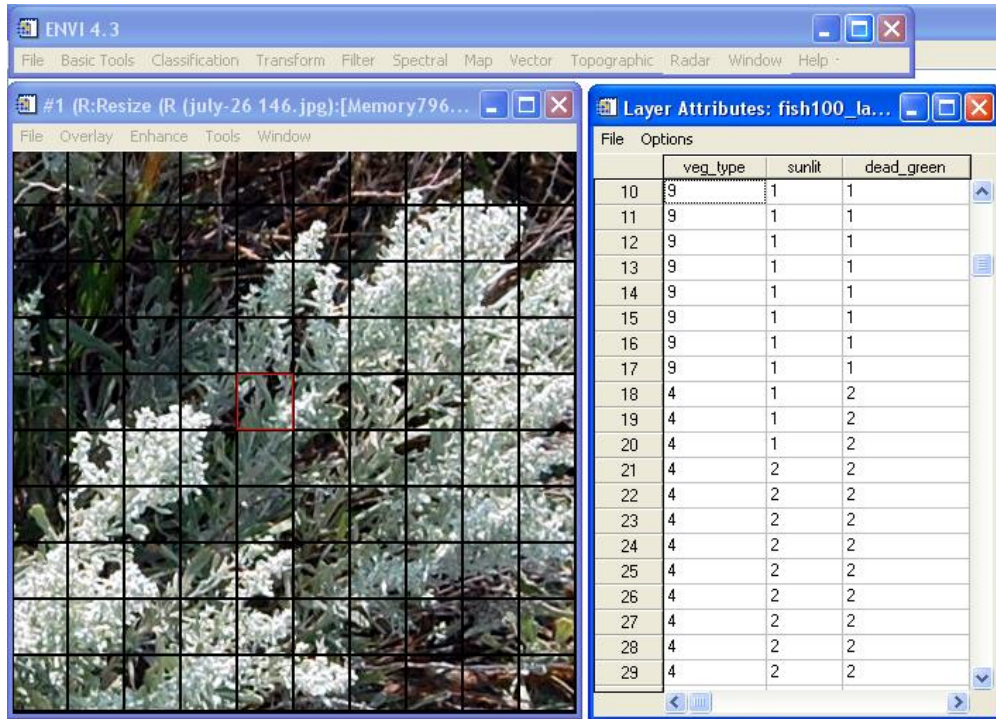


Figure 2-3. Spectroradiometer footprint classifications. A one-hundred grid cell overlay on the picture in ENVI 4.3 to classify vegetation type, sunlit and dead/green vegetation for each pixel.

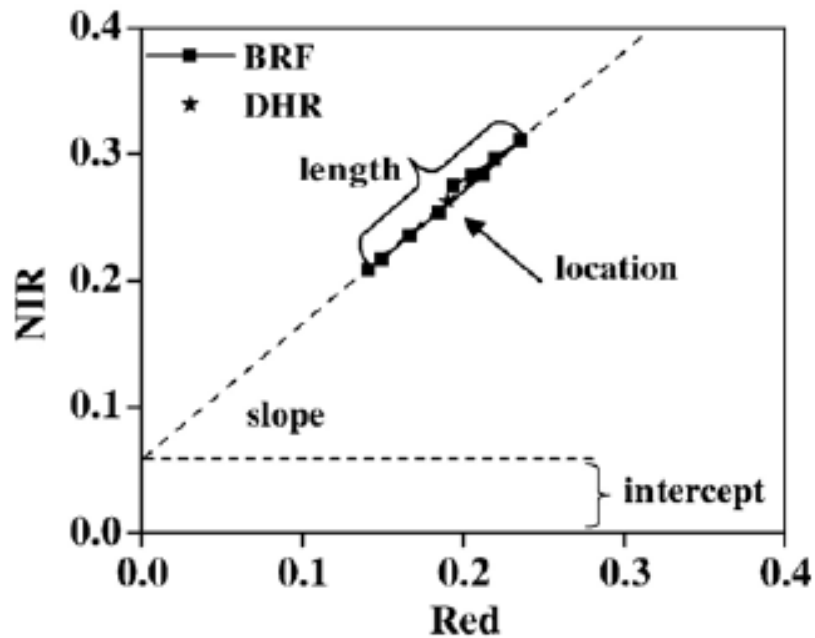


Figure 2.4. Angular signature in spectral space form by red and NIR BRF as a function of view zenith angles (Zhang et al. 2002a). The signature is characterized by (a) its location in the spectral space, determined by the directional hemispherical reflectance (HDR), (b) inclination (intercept and slope) of the signature, and (c) the length of the signature. (Taken from Hu et al. 2007)

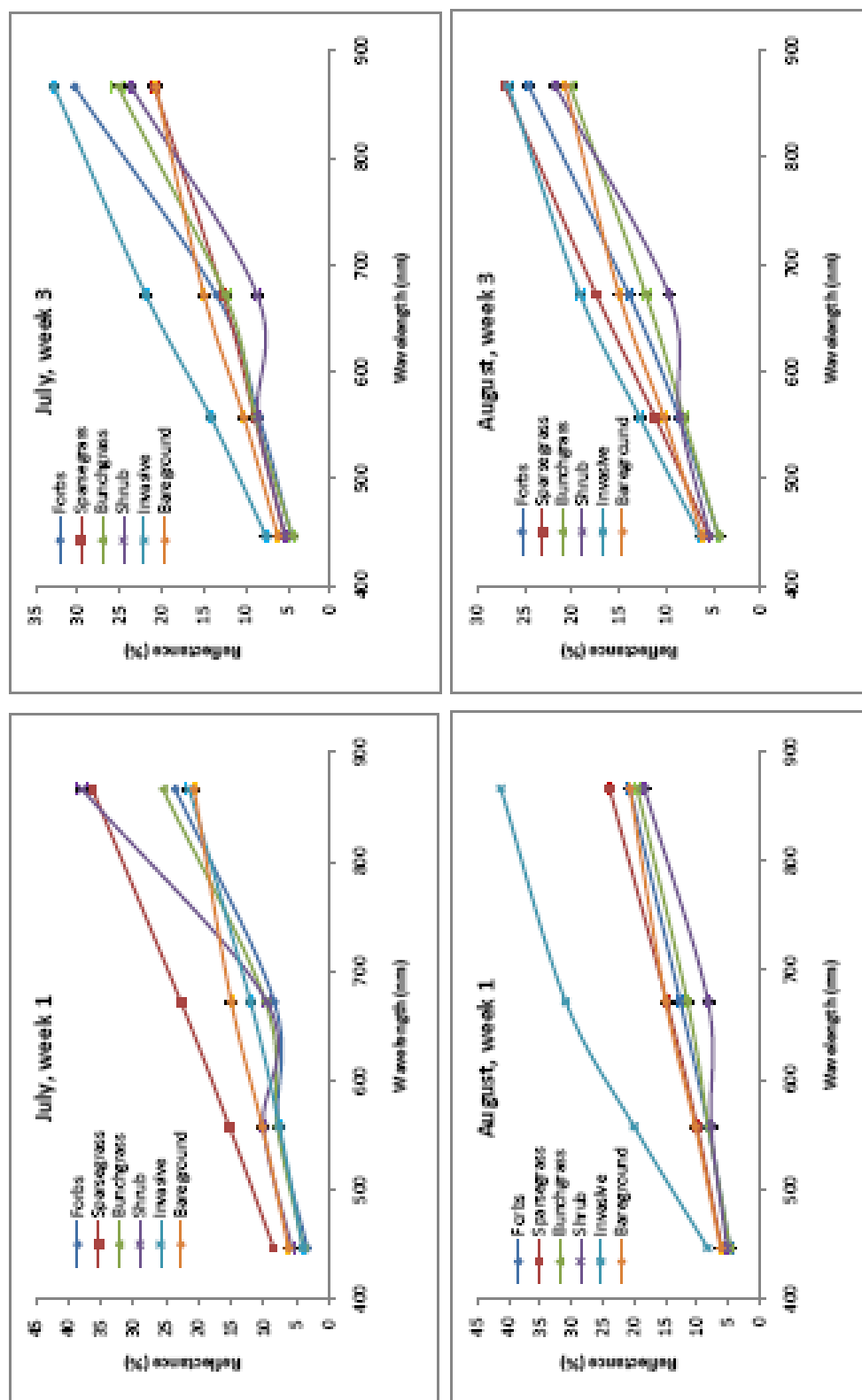
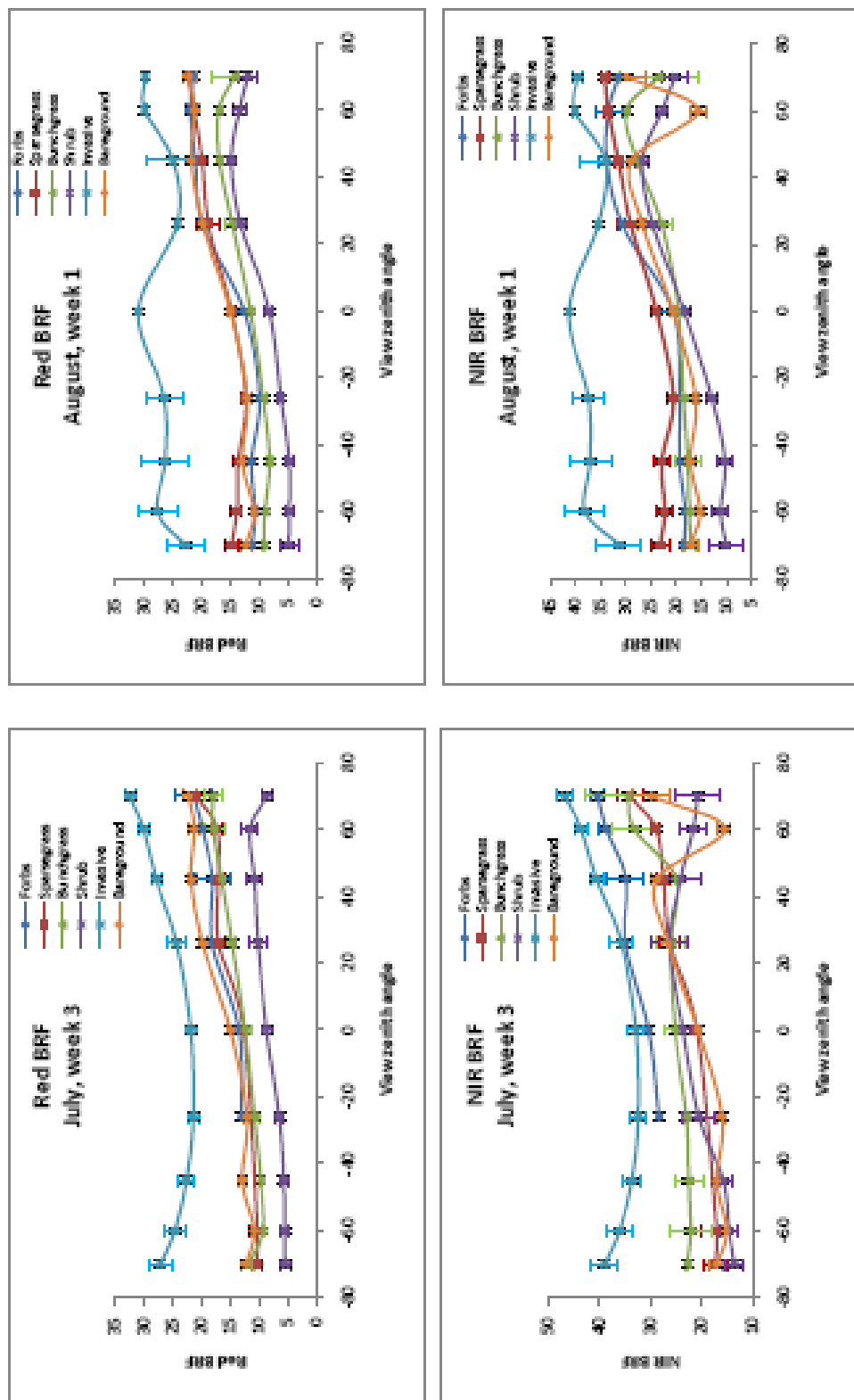


Figure 2-5. Variation of average spectra for 5 vegetation types at 4 different periods gathered at nadir view around solar noon. Standard errors are depicted with vertical bars.



← Forward → Backward →

Figure 2-6. Red and NIR BRDF variations for 5 different vegetation types at 2 different periods gathered around solar noon. Anisotropy behaviors and presence of hotspots are observed for all functional groups. Invasive grasses are distinguished when these start to senesce. Standard errors are depicted with vertical bars.



Figure 2-7. Erectophile (left) versus planophile (right) leaf orientation for medusahead annual grass. The large fraction of shadow was only present when the vegetation was green.

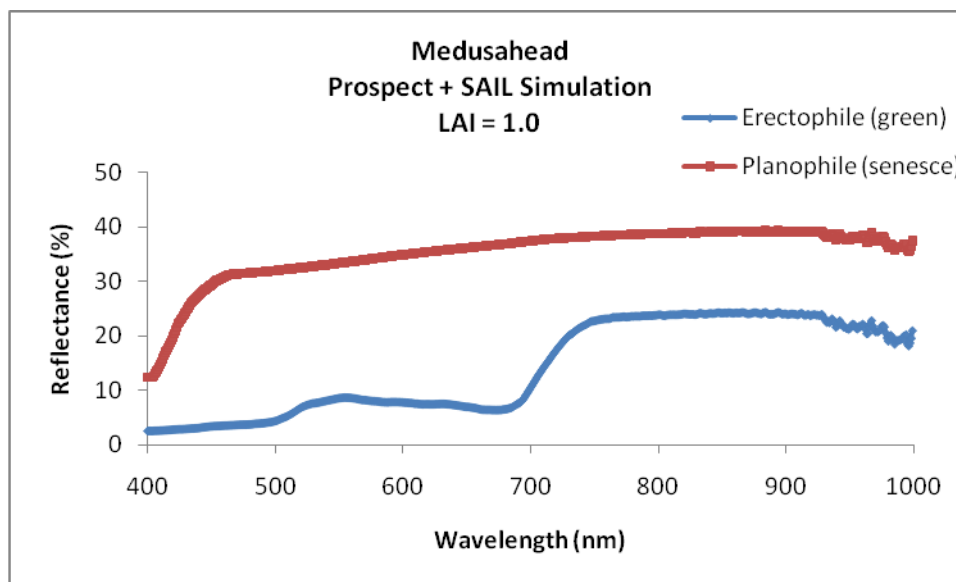


Figure 2-8 Simulated reflectance for planophile (senesced medusahead) versus erectophile (green medusahead) leaf orientation. Leaf inclination angle drives changes in spectral reflectance especially in the near infrared bandwidth. Chlorophyll content ranges from  $30 \mu\text{g}/\text{cm}^2$  to  $0 \mu\text{g}/\text{cm}^2$  for green and senesce medusahead, respectively (Bokari 1983, Gaborcik 1985). Leaf mesophyll structure index ranges from 1.3 (green) to 2.5 (senesce) (Jacquemoud and Baret 1990). Water content values vary from  $0.02 \text{ g}/\text{cm}^2$  to  $0 \text{ g}/\text{cm}^2$  and dry matter values vary from  $0.005 \text{ g}/\text{cm}^2$  to  $0.003 \text{ g}/\text{cm}^2$  for green and senesce medusahead, respectively.

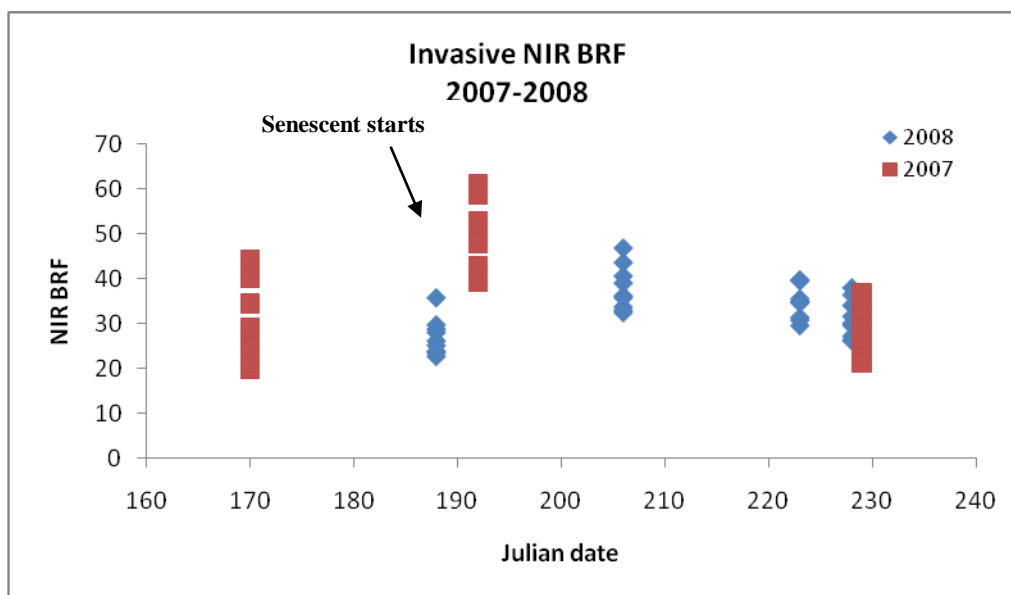


Figure 2-9. Invasive NIR BRF variations for 2007-2008. Growing degree days were calculated for 2007 and 2008 so we could compare data from 2007 with 2008. NIR BRF is affected by leaf orientation.

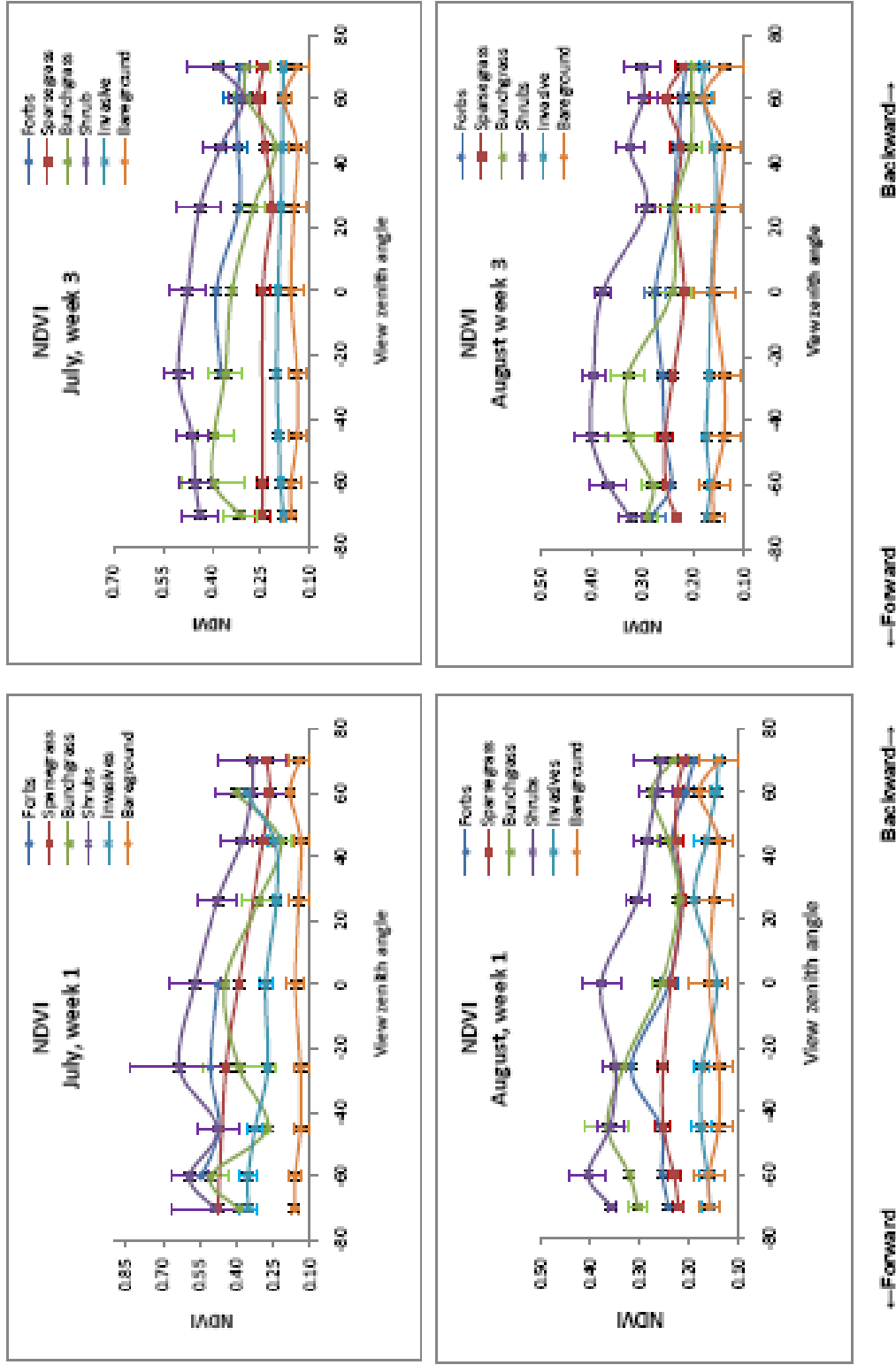


Figure 2-10. NDVI average variations for 5 different vegetation types at 4 different periods gathered around solar noon. Invasive grasses' NDVI have the lowest values for all periods. Standard errors are depicted with vertical bars.

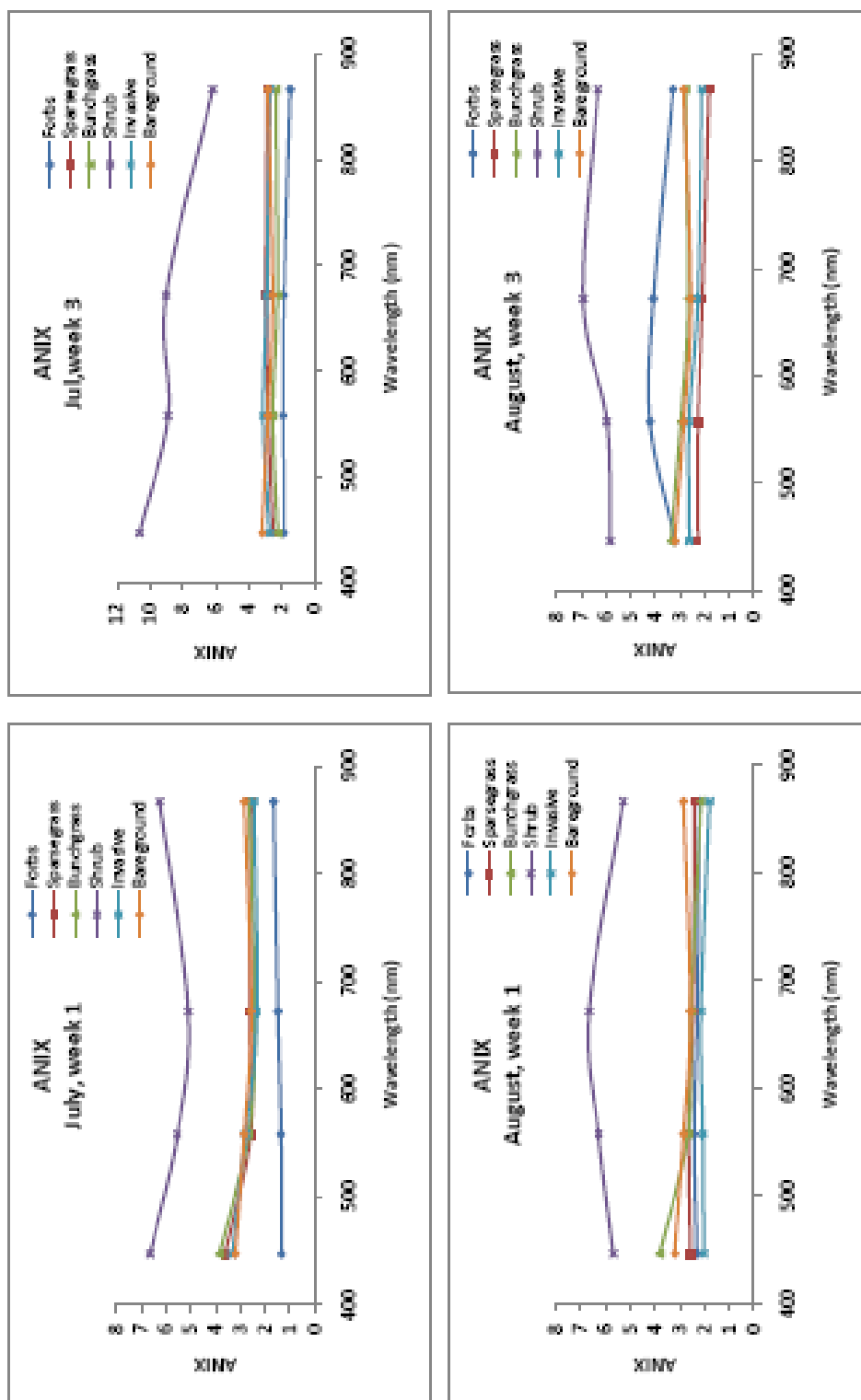


Figure 2-11. ANIX average variations for 5 different vegetation types at 4 different periods. ANIX values differentiate shrubs from other plant functional groups at all periods. Forbs ANIX in August, week 3 correspond only to lupine.

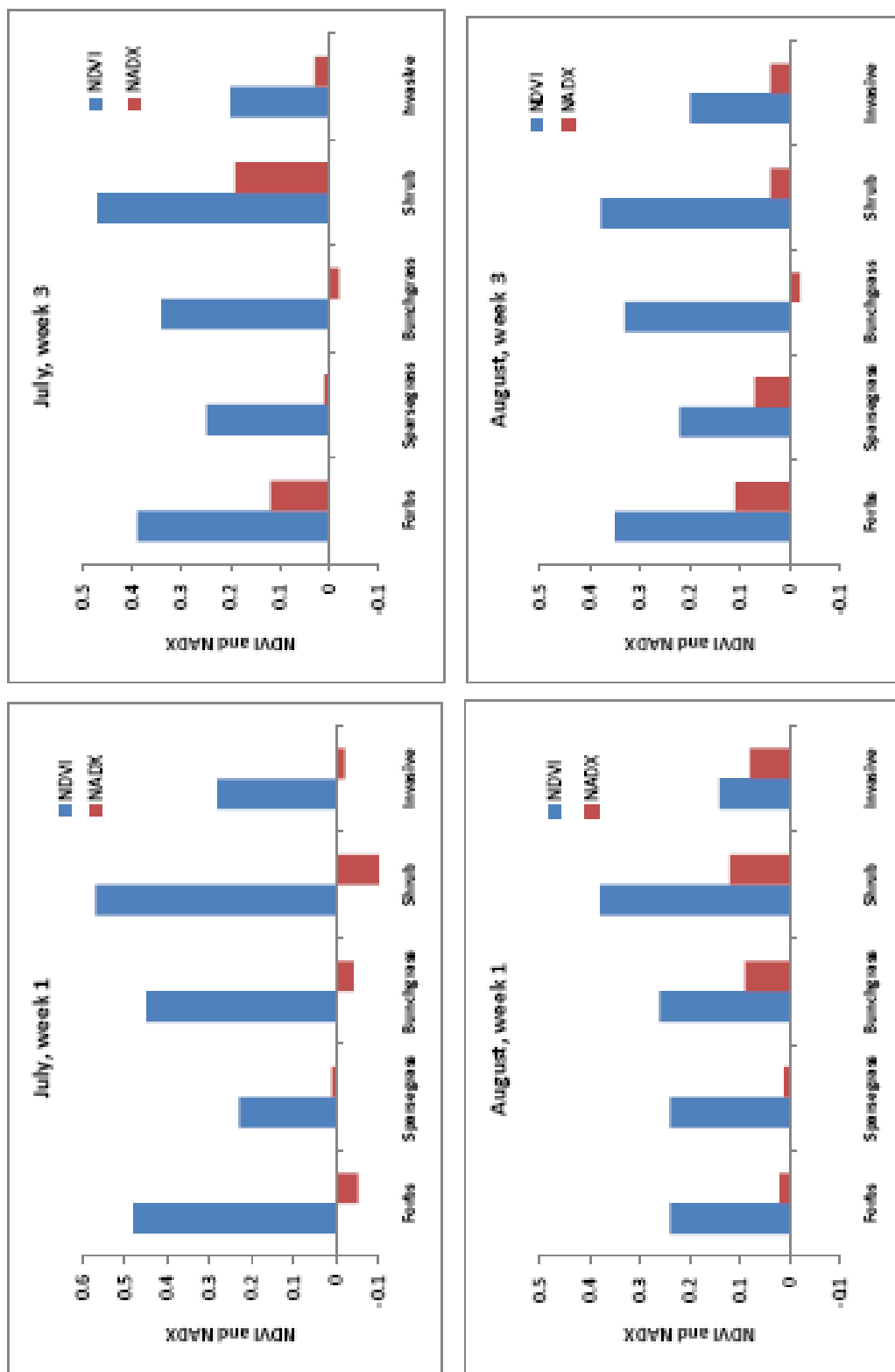


Fig 2-12. NADX and NDVI average variations for 5 different vegetation types at 4 different periods .

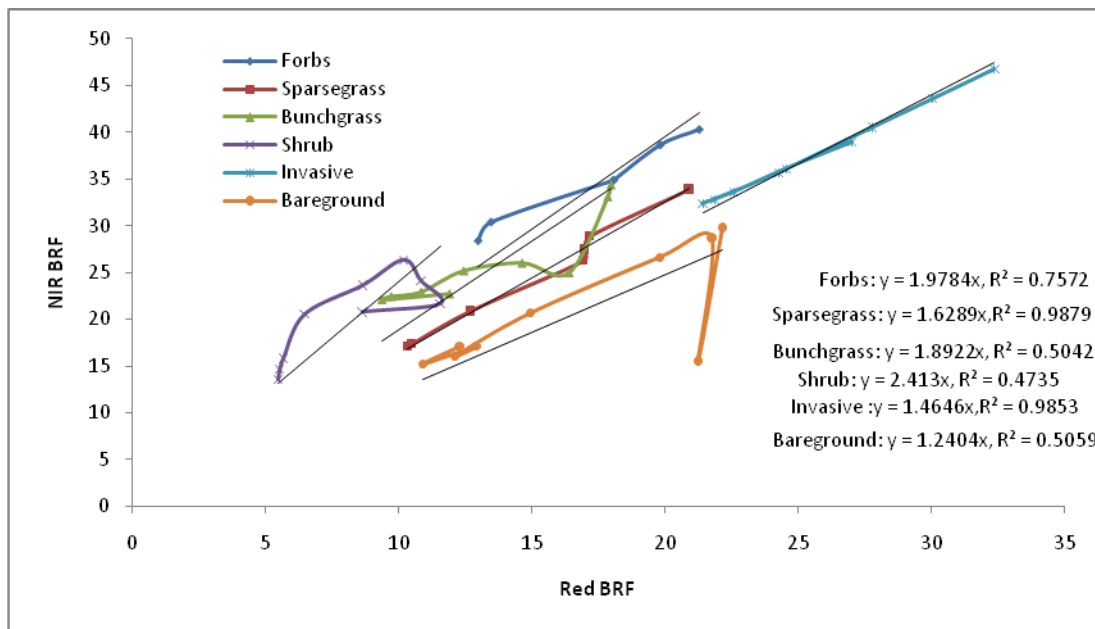


Figure 2-13. Angular signatures on the red and NIR plane for the third week of July. Invasive annual grasses location in spectral space can be differentiated from the other plant functional types. Shrub slope (2.41) is different from other plant functional types because of the structure of its canopy.

**CHAPTER 3. Effects of sun zenith angle and leaf orientation on detecting the invasive grass medusahead (*Taeniatherum caput-medusae* [L.] Nevski) using narrow band canopy reflectance.**

**Abstract**

Extensive areas of shrublands have been invaded in the western US by annual grasses such as medusahead (*Taeniatherum caput-medusae* [L.] Nevski) and cheatgrass (*Bromus tectorum* L.). Although vast areas have been degraded, the high cost of mapping and monitoring these invasive annual grasses lead to great challenges in monitoring and protecting affected areas at the ground level. However, it has been shown that medusahead reflectance values can be discriminated from other vegetation groups based on changes in the leaf angle orientation of medusahead plants when they senesce. Because measuring plant canopy reflectance is dependent on the geometry between the sensor view angle and solar position, variations in this geometry can also assist in delineating vegetation types over time. This study was conducted to detect the effects of changes in solar geometry on vegetation indices, visible and near infrared (NIR) reflectance of perennial grasses and medusahead, as well as to evaluate seasonal changes in spectral reflectance between these two functional groups. We used twenty four lightweight, low power spectral radiometers (after Garrity et al. 2010) in sixteen enclosures to monitor reflectance of perennial grasses and medusahead. Analog measurements were recorded every twenty minutes to measure diurnal variation of photosynthetic active radiation (PAR), green, and NIR reflectance during four different phenological periods. In addition, we

quantified seasonal spectral reflectance patterns. High sun zenith angles (early in the morning and late in the afternoon) affect NIR more and the contrary (sun zenith angles close to solar noon) affects the visible light wavebands. In addition, the reflectance of medusahead in the NIR and green bands (28.9% and 15.57%, respectively) was considerably higher than that of perennial grasses (19.48% and 9.74%) at the latest stages of senescence due to changes in leaf orientation. Medusahead can also be distinguished from perennial grasses throughout the season because of differences in its green and NIR reflectance near solar noon. These differences could be useful to detect medusahead from perennial grasses when scheduling multispectral or hyperspectral aerial image surveys.

## 1. Introduction and background

Detection and mapping of invasive annual grasses is important in rangelands of the western United States. Annual grasses such as medusahead (*Taeniatherum caput-medusae* [L.] Nevski) and cheatgrass (*Bromus tectorum* L.) have become dominant across many semiarid landscapes, and have led to the degradation of several ecosystem properties associated with changing disturbance regimes and biodiversity loss across a wide range of trophic levels (Davies 2008). Areas previously occupied by annuals are more likely to be invaded by medusahead than areas occupied by perennial vegetation (Dahl and Tisdale 1975, Davies 2008). Characteristics of medusahead invasion include rapid spread (Dahl and Tisdale 1975), reduction of grazing capacity by 50 – 90% (Hironaka 1961, Davies and Svejcar 2008), slow litter decomposition (Harris 1965), and low diversity. Davies and Svejcar (2008) compared medusahead -invaded and non-invaded sagebrush communities and found that medusahead invasion substantially altered vegetation cover, density, biomass, species richness and diversity. For example, medusahead -invaded communities produced only 13% of the biomass produced by non-invaded communities (Davies and Svejcar 2008). In addition, medusahead invasion appeared to reduce the cover and density of Sandberg bluegrass (*Poa secunda* J.Presl) as much as or more than the large perennial bunchgrasses. Accumulation of medusahead litter could shade the photosynthetically active tissue of the relatively short-stature Sandberg bluegrass (Davies and Svejcar 2008).

Although extensive areas within shrublands have been invaded by medusahead and other annual grasses, the high cost of mapping and monitoring these invasive annual grasses lead to great challenges in monitoring and protecting affected areas at the ground level. However, recent advances in utilizing passive multispectral and hyperspectral remote sensing technology have enabled improved detection of invasive annual grasses across the western US. A large fraction of these studies have focused on detecting and quantifying cheatgrass cover and productivity. Most of these studies include multitemporal imaging because the phenology of invasive annual grasses often differs substantially from native vegetation. For example, Bradley and Mustard (2005) used multitemporal Landsat TM and Advanced Very High Resolution Radiometer (AVHRR) data to detect interannual productivity variation in Great Basin ecosystems, and analyzed phenological differences among grasses to differentiate areas dominated by cheatgrass from those dominated by native bunchgrasses. These results were corroborated by studies by Noujdina and Ustin (2008), which showed that it is more likely to detect cheatgrass using hyperspectral data acquired in different seasons rather than single-date datasets.

A primary reason that multitemporal studies assist in invasive annual grass detection is that the radiation regime of a plant canopy results from an integrated outcome of photon scattering by leaves, stems, and soils (Asner et al. 1998a). As a result, plant canopy reflectance will be modified by leaf area index (LAI), leaf angle distribution (LAD), and foliage clumping that accompanies changes in vegetation phenology (Ross 1981). In semiarid rangelands, it has

been shown that changes in leaf angle resulting from maturity of some invasive grasses can increase the reflectance values in the visible and near infrared regions relative to green vegetation (Chapter 2; Figure 3-1). Changes in medusahead leaf angle occur because the plant seedhead becomes twisted as the seed matures, but it does not break apart completely once the seeds mature (Sharp et al. 1957). In contrast, stands of native grasses such as bluebunch wheatgrass (*Pseudoroegneria spicata* (Pursh) A. Love) maintain a more upright (erectophile) canopy structure throughout their phenological development, which results in a different balance of sunlit and shaded foliage and canopy radiation regime relative to medusahead (Chapter 2; Gold and Caldwell 1990). Many grasses maintain this erectophile canopy structure so that they can maintain higher levels of canopy light penetration even in dense canopies, which can lead to higher production (Gold and Caldwell 1990), net photosynthetic rates, and water use efficiency (Ryel and Beyschlag 1995) relative to those with more prostrate foliage.

Because measuring plant canopy reflectance is dependent on the geometry between the sensor view angle and solar position, (Vierling et al. 1997, Asner et al. 1998c, Goodin et al. 2004, Middleton 1991) variations in this geometry can also assist in delineating vegetation types over time. The sun-target-sensor geometry can be characterized by the illumination or incidence angle and the view angle that are determined by the solar elevation angle (counterpart of the solar zenith angle) and off-nadir sensor position, respectively. The reflectance resulted from these sun-target-sensor geometry is governed by

the bidirectional reflectance distribution function (BRDF) or its quantified expression BRF (Asner et al. 1998c).

We found in Chapter 2 that by using multiple off-nadir sensor viewing angles, differences between the bidirectional reflectance factors (BRFs) of various rangeland canopy types allowed distinct delineation of annual grasses and sagebrush relative to native bunch grasses during much of the growing season. Vierling et al. (1997), using off-nadir radiometric measurements, were able to discriminate two tussock tundra sites (woody vs non-woody) that could not be distinguished at nadir view. Chopping et al. (2003) reported variations in canopy structure within two transition communities in the Jornada Experimental Range using aerial photography at different view angles and model inversion of BRDF parameters. These studies indicate that additional study using various sun-sensor geometries, when coupled with variation in plant canopy phenology, may lead to improved understanding in the detection of invasive grasses using remote sensing data. Hunt et al. (2007) using spectral angles from SAIL model simulation predicted that flowering leafy spurge (*Euphorbia esula* L.) (LAI >1.0) may be detected from co-occurring vegetation at a threshold spectral angle of 3.5°. However, Hunt et al. (2007) had to include flower-bract cover (>10%) of leafy spurge to increase the overall accuracies (from 50 to 60%) of classifying leafy spurge with Landsat ETM+ and SPOT data with the Spectral Angle Mapper (SAM) algorithm. Similar studies to classify hyperspectral images using the SAM algorithm (but without an assessment of the sun-viewing geometry) have been reported in detecting spotted knapweed (*Centaurea maculosa* Lam. Syn. *C.*

*biebersteinii* DC. or *C. stoebe* L. subsp. *microanthos* (Gugler) Hayek) and babysbreath (*Gypsophila paniculata* L.) infestations, where overall accuracies of 57% and 97% were achieved (Lass et al. 2005).

We conducted this study to measure: 1) the effects of changes in solar geometry on vegetation indices and visible and NIR reflectance of perennial grasses and medusahead over the course of a growing season, and to evaluate 2) seasonal reflectance changes between these two functional groups. Our accompanying hypotheses are therefore that: 1) illumination angle affects values of spectral vegetation indices and broadband reflectance in pre-senesced and senesced perennial grasses and medusahead, and 2) perennial grass can be distinguished from medusahead at different phenological stages based on differences in vegetation indices and broadband reflectance.

## **2. Methods**

### **2.1 Study area**

The study area comprises 38,000 ha of sagebrush steppe and grassland vegetation managed by the Soulen Livestock Co., near Weiser, Idaho. The area includes private and public grazing lands that are mostly grazed by cattle and sheep in addition to native ungulates, small mammals and insects. The land is fenced to facilitate livestock grazing management. The average daily maximum temperature ranges from -7.3 °C in January to 33.6 °C in July and average total annual precipitation is 298.4 mm. The elevation of the study sites ranges from 950 to 1300 m above sea level.

Sixteen 3 x 3-m enclosures were established in pairs along the Loamy 12-16 ARTRX-PSSP6 ecological site which covers 28.4% of the study area (USDA – NRCS, <http://websoilsurvey.nrcs.usda.gov/>). Each pair of enclosures was located on relatively flat terrain and was separated by approximately 200 m, with one enclosure situated in a native perennial grass canopy and one situated in medusahead canopy. Perennial grasses bluebunch wheatgrass (*Pseudoroegneria spicata* (Pursh) A. Love), squirreltail (*Elymus elymoides* [Raf.] Swezey) and bulbous bluegrass (*Poa bulbosa* L.) and the annual invasive grasses like medusahead (*Taeniatherum caput-medusae* [L.]Nevski) and cheatgrass (*Bromus tectorum* L.) were the primary species in each type of enclosure, respectively. In one corner of each enclosure, an L-shaped boom pole was installed to mount a box containing a radiometer that recorded nadir spectral reflectance.

## 2.2 Reflectance measurements

Twenty four lightweight, low power spectral radiometers were constructed following a modified version of Garrity et al. (2010) and used to monitor the reflectance of perennial grasses and medusahead. Each radiometer consisted of three filtered photodiodes with band centers at 532, 568, and 800 nm, each with a 10 nm full width half maximum bandwidth (Garrity et al. 2010) and one unfiltered GaAsP photodiode to record photosynthetically active radiation (PAR; 400-700 nm; Gutschick et al. 1985). Analog measurements were recorded using a Hobo data logger (Onset Computer Corp., Natick, MA). The data loggers

recorded voltage signals every 20 minutes from June 25<sup>th</sup> to September 8<sup>th</sup> 2008 but only values from 7 a.m. to 5 p.m. (local daylight savings time) were used for the analysis. The field of view of the sensor was approximately 60° and the footprint was 2 m in diameter at 1.60 m height. Canopy cover for each light sensor field of view is described in Table 3-1. Eight radiometers included two sets of detectors, with one set to measure solar irradiance (to serve as a standard for calculating reflectance) and one set to measure upwelling radiance. The other 8 radiometers measured only radiance, and used their paired counterparts as irradiance reference measurements.

Reflectance was calculated using ratios between down- and up- dwelling readings recorded by the light sensors in each of the measured bandwidths. This “raw” reflectance was calibrated using correction factors obtained by cross-calibration between the irradiance (upward pointing) sensors and radiance of downward pointing sensors positioned over a white Lambertian panel (Gamon et al. 2006). This procedure is summarized in equation 1.

$$R_{\text{corrected}} = (V_{\text{target}}/V_{\text{upwelling}}) * (V_{\text{upwelling}}/V_{\text{panel}}) \quad (1)$$

Where:

$R_{\text{corrected}}$ : corrected reflectance

$(V_{\text{target}}/V_{\text{upwelling}})$ : raw reflectance

$(V_{\text{upwelling}}/V_{\text{panel}})$ : correction factor based on cross validation

Correction factors were calculated for 5 different sun zenith angle classes under clear sky conditions similar to clear sky conditions over the study period (after Middleton 1991). Linear or polynomial equations were then used to

estimate correction factors for sun zenith angles that ranged from 21 to 75 degrees (Figure 3-2). The solar elevation angles during the data collection and light sensor reflectance calibration was calculated with an online program provided by the US Naval Oceanography, Astronomical Applications Department (<http://aa.usno.navy.mil/data/docs/AltAz.php>). Measurements under cloudy sky conditions were discarded to minimize influences of high diffuse sky irradiance, and because clear sky conditions are necessary for subsequent comparison with aircraft and satellite data.

### 2.3 Data analysis

Green normalized difference vegetation index (NDVI<sub>g</sub>; Gitelson et al. 1996) was calculated using spectral characteristics in the green (G) and near infrared (NIR) wavebands in equation 2.

$$NDVI_g = \frac{\rho(\lambda_{NIR}) - \rho(\lambda_{green})}{\rho(\lambda_{NIR}) + \rho(\lambda_{green})} \quad (2)$$

Where:

$NDVI_g$  = Green NDVI

$\rho(\lambda_{NIR})$  = 800 nm or near infrared waveband

$\rho(\lambda_{green})$  = Green waveband

To measure diurnal variation of both broadband PAR and NDVI<sub>g</sub> reflectance, comparisons between perennial grasses and medusahead were analyzed during four different phenological periods: pre-senescent, early senescent, mid senescent and late senescent (Table 3-2). Because of the reflectance variation along the day, especially at noon, and in order to compare

seasonal changes in reflectance, PAR and NDVIg between perennial and medusahead, we set the seasonal analysis at 40° sun zenith angle per each clear day (after Middleton 1991).

T-student for means with equal variance was also calculated to compare diurnal reflectance means between perennial grass and medusahead at different phenological stages (Table 3-3).

### 3. Results and Discussion

#### 3.1 Diurnal reflectance variation at different phenological stages

NDVIg shows higher values for medusahead at the four different phenological stages (Figure 3-3, Table 3-3). These differences are highly significant ( $p < 0.01$ ) at the pre-senescent and late-senescent phenological stages. Although the phenological stages were collected at different dates (Table 3-2), the NDVIg of medusahead and perennial grasses showed similar trends, with higher values at the pre-senescent stage and lower values during the early-, mid- and late-senescent stages. However, perennial grasses did not show significant differences in NDVIg between pre-senescent and senescent stages. The small amount of variation in NDVIg for perennial grasses could be related to the presence of bulbous bluegrass (which was senescent throughout the course of the measurements and comprised approximately 25% of the plot coverage) and litter (3% plot coverage), and the proportion of green/standing dead biomass in the footprint of the sensor (Table 3-1). In addition, because of the early senescence of bulbous bluegrass, only six radiometers of the sixteen were used for reflectance analysis (Table 3-1). NDVIg was affected by interactions between sun angle and structure of the vegetation. Although with a nadir-sensing view angle the least amount of shaded material occurred in the field of view at solar noon, lower values of NDVIg occurred mostly around solar noon. Caldwell et al. (1983) demonstrated that over half of the foliage of a typical desert wheatgrass (*Agropyron desertorum* (Fisch. Ex Link) Schult) is shaded at midday in the spring. Thus, photosynthetic rates of shaded desert wheatgrass foliage are

considerably less than fully illuminated foliage (Caldwell et al. 1983). Similar results in diurnal effects on NDVI were found by Gamon et al. (2006) and Sims et al. (2006). In addition, Sellers (1985) and Huete (1992) showed that NDVI values increase as solar zenith angles increase. However, diurnal variation of the NDVI<sub>g</sub> of perennial grass was not as great as the values for medusahead (Figure 3-3).

Full day PAR reflectance followed an inverse pattern relative to NDVI<sub>g</sub>. PAR was more highly absorbed when plants were pre-senescent, relative to plants in other stages of senescence (Figure 3-4). In addition, the PAR reflectance of medusahead was significantly higher for all phenological stages than that from perennial grasses (Table 3-3). Similarly to NDVI<sub>g</sub>, PAR was affected by sun angle and plant structure, but to a lesser degree. However, this decrease did not occur in a linear fashion relative to NDVI (Walter-Shea et al. 1992). Variations in PAR reflectance can likely be attributed to the changing proportion of shaded area, leaf litter and soil (Walter-Shea et al. 1992). For example, standing grass litter canopies can absorb almost as much PAR as green grass canopies (Asner 1998b). Nonphotosynthetic materials such as twigs, branches, stems, senescent foliage and soils can also be strong absorbers of PAR (Asner and Wessman 1997), which may partially explain the trends seen in our data.

Green and near infrared reflectance of medusahead were higher than the reflectance of perennial grasses along different phenological stages (Figure 3-5). In addition, green reflectance at 568 nm was higher than reflectance at 532 nm. These two wavelengths were chosen initially to calculate the photochemical

reflectance index (PRI). PRI is highly correlated with light use efficiency (LUE) in growing plants (Gamon et al. 1997) and it can be used as a surrogate of LUE in the gross primary productivity algorithm developed by Monteith (Rahman et al. 2004). However, during the period of evaluation there was not significant vegetation growth that could have been detected by clipping and weighing biomass method (Bonham 1989). Nevertheless green reflectance was used for the calculation of NDVIg. Perennial grass green reflectance showed anisotropic behavior at the four different stages especially at solar noon. However, there were not significant differences among the green reflectance values of perennial grass at different phenological stages.

The NIR and green reflectance of medusahead were higher at the latest stages of senescence than the early-senescence and pre-senescence (green) stages (Figure 3-5). This reflectance response is more closely related with changes in leaf orientation than with physiological changes. The seedhead of medusahead becomes twisted as the seed matures but it does not break apart completely once the seeds mature (Sharp et al. 1957). Thus, when medusahead is green, the orientation of the leaves is usually erectophile, changing to planophile when the plants start to senesce. Leaf inclination angles drives changes in spectral reflectance similar to those driven by variation in LAI or tissue content (Asner 2004). Generally the NIR waveband (730-1300 nm) is more sensitive to changes in leaf orientation than the visible region (400-700 nm) (Asner 2004). Furthermore, medusahead cover was sparser at early green stages where litter from previous years was more abundant, but this component

plays a less significant role in overall canopy reflectance when the plant matures and covers up the litter component.

Changes in NIR canopy reflectance were sensitive not only to leaf orientation, but also to sun illumination angles. As seen in the results of our study (Figures 3-4 and 3-5), higher reflectance of NIR early in the morning (high sun zenith angles) often occurs. As sun zenith angle increases, the proportion of shaded area increases affecting visible BRF values; however, the shaded effect is less evident in NIR because this wavelength is multiply scattered by the vegetation, decreasing the contrast between sunlit and shaded areas within the canopy (Walter-Shea et al. 1992). Higher NIR reflectance was also observed when the sun zenith angles were high in the evening (higher than 75 degrees), but because our calibration factors exhibited less repeatability at these angles (data not shown) we did not consider these values in the analysis. However, based on the multiple scattering of NIR at high sun zenith angles we expected high NIR values in the evening. This behavior of high NIR values at high sun zenith angles was more significant in medusahead than in perennial grasses.

The strong reflectance anisotropy of perennial grasses relative to medusahead seen in this study was likely due to the more complex structure of perennial grasses. The native perennial grass species measured in this study are taller than medusahead, so the proportion of shaded areas in the field of view of the sensors was higher in perennial grasses than in medusahead at larger solar zenith angles (i.e. early in the morning and late in the afternoon). Thus, hotspots were expected at solar noon, especially with the lower shadowing in perennial

grasses at that time. This hotspot presence would allow separating medusahead from perennial grasses, especially when medusahead start to senesce (Table 3-3). This finding could be useful when scheduling multispectral or hyperspectral aerial image surveys, as the differences in reflectance between native and invasive grasses were more pronounced at solar noon. Middleton (1991) suggested that vegetation indices measured at high sun elevation angles (i.e. low SZA) could be good indicators of cover but not canopy attributes.

### **3.2 Seasonal reflectance changes between native perennial grasses and medusahead**

Seasonal reflectance, PAR and NDVIg variation for perennial grasses and medusahead are shown in Figure 3-6 and 3-7. Because of the effects of sun zenith angle on reflectance values especially early in the morning and late in the evening (Sellers 1985, Huete 1992) we set the analysis for PAR, NDVIg and reflectance values at 40° sun zenith angle (after Middleton 1991). Data recorded at this angle were mostly found around 10 a.m. and 3 p.m. between June 27<sup>th</sup> and August 16<sup>th</sup>. Values recorded at this angle are more consistent than values recorded at noon because of the variation in sun zenith angles at this time (Table 3-2). Sims et al. (2006) found that different conclusions could be drawn about NDVI seasonal changes comparing values at noon or at constant sun zenith angles between winter and summer. Conversely, Middleton (1991) suggested that a standard SZA could provide a good correspondence of vegetation indices and canopy characteristics such as LAI for values recorded during the summer

and early fall. In addition, medusahead started to show significant reflectance differences in PAR and reflectance values for NIR, 568 and 532 nm bandwidth relative to perennial grasses when medusahead started to senesce (Figures 3-6 and 3-7). However, these differences were not observed when we calculated NDVIg (Figure 3-6). Medusahead displayed slightly lower NDVIg values than perennial grasses when the former started to senesce. We expected much lower values of NDVIg for medusahead because most of the samples were already senescing by early July. In fact, medusahead NDVIg was similar to perennial grass NDVIg between the early senescent and mid senescent stage for medusahead (Table 3-2). A reason for high medusahead NDVIg values during senescence could be related to factors that cause simultaneous high increments in NIR and reduction of the green reflectance values (Epiphanio and Huete 1995). For example, NIR is more sensitive to changes in leaf orientation than is the visible region (Asner 2004). The other reason could be related with footprint composition of sensors pointing vertically at perennial grasses. Perennial grass NDVIg might be higher if bulbous bluegrass and soil background reflectance could be masked from the plot reflectance signal.

Green reflectance was not significantly different between the two plot types when both medusahead and perennial grasses were photosynthetically active (Figure 3-7). In addition, NIR reflectance for medusahead and perennial grasses showed similar trends to the green reflectance for these functional groups. Even though perennial grasses remain green for a longer period of time than medusahead, reflectance in the NIR is lower than the reflectance of

medusahead. After medusahead proceeded to senescence, there is a 100% increase in green reflectance due to changes not only in tissue content but also in leaf orientation. As mentioned above, as medusahead underwent senescence, its leaf orientation changed from erectophile to planophile. Reflectance comparisons between erectophile and planophile leaf orientation showed higher reflectance when leaf orientation was planophile (Aster 2004 Chapter 2). For instance, Jackson and Pinter (1986) found that wheat (*Triticum aestivum* L.) canopy with similar LAI and leaf optical properties showed nadir-viewed BRDF to be 20% higher in a planophile canopy compared to an erectophile canopy.

High PAR reflectance is indicative of low photosynthetic activity of chloroplast pigments when plants begin to senesce. PAR reflectance was 130% higher when medusahead was fully senesced (Julian Day 200) than during the pre-senescent stage. In contrast, the perennial grass PAR reflectance increased only 30% during this same phenological transition. The low variation of PAR reflectance in perennial grass could be related with presence of bulbous bluegrass (cover around 25% of the sensor field of view), which might mask or diminish the changes in perennial reflectance because bulbous bluegrass senesced early in the season. The increment in PAR reflectance follows the same trend as the green reflectance for both perennial grasses and medusahead. Middleton (1992) demonstrated that grassland PAR reflectance can be estimated from either green or red bidirectional reflectance using linear regression equations with an r-square higher than 0.9. In addition, Middleton (1992) suggested that green is preferable because “it provides the highest visible

flux, falls in the midrange of PAR, and a simple approximation for PAR reflectance is  $2/3$  (green)".

#### **4. Conclusions**

We conclude that sun zenith angles affect reflectance in the visible (PAR and green) and NIR wavebands. However, high sun zenith angles have a greater effect on NIR and small sun zenith angles have a greater effect on green bandwidth and PAR. The effects on visible light reflectance were amplified by the structure of perennial grasses, which demonstrated higher reflectance values near solar noon. These differences could be useful to detect medusahead from perennial grasses when scheduling multispectral or hyperspectral aerial image surveys. However, in order to detect seasonal changes in biomass, based on the relationship between vegetation indices and canopy properties such as LAI or absorbed PAR (APAR), we selected a fixed sun zenith angle to avoid variation of sun zenith angles at midday (Middleton 1991). Our results did not show differences between perennial grass and medusahead NDVIg along the season but differences in PAR, green and NIR reflectance were found. This could be interpreted as no differences in biomass changes when these vegetation groups start to senesce. However, further research to measure variation in biomass along the season would request assessment of red reflectance and other vegetation indices.

## 5. References

- Asner, G.P., Wessman, C.A. and Schimel, D.S. 1998a. Heterogeneity of savanna canopy structure and function from imaging spectrometry and inverse modeling. *Ecological Applications* 8:1002-1036
- Asner, G.P., Wessman, C.A. and Archer, S. 1998b. Scale dependence of absorption of photosynthetically active radiation in terrestrial ecosystems. *Ecological Applications* 8: 1003-1021
- Asner, G.P, Braswell, B.H., Schimel, D.S., and Wessman, C.A. 1998c. Ecological research needs from multiangle remote sensing data. *Remote Sensing of Environment*. 63:155-165
- Asner, G.P. 2004. Biophysical remote sensing signatures of Arid and Semiarid ecosystems. In: Susan Ustin (Ed). *Remote Sensing for Natural Resource Management and Environmental Monitoring: Manual of Remote Sensing*. Vol 4. 3 Ed.: John Wiley & Sons, Hoboken, New Jersey. p 53-109
- Asner, G.P. and Wessman, C.A. 1997. Scaling PAR absorption from the leaf to landscape level in spatially heterogeneous ecosystems. *Ecological Modeling* 103: 81-97
- Bonham, C.D. 1989. Measurements for terrestrial vegetation. Chapter 6. Wiley-Interscience Publication. John Wiley & Sons, Inc USA. p.199-264
- Bradley, B.A., and Mustard, J.F. 2005. Identifying land cover variability distinct from land cover change: Cheatgrass in the Great Basin. *Remote Sensing of Environment* 94: 204-213
- Caldwell, M.M., Dean, T.J., Nowak, R.S, Dzurec R.S., and Richards J.H. 1983. Bunchgrass architecture, light interception, and water use efficiency: assessment by fiber optic point quadrats and gas exchange. *Oecologia* 59: 178-184
- Chopping, M.J., Rango, A., Havstad, K.M., Schiebe, F.R., Ritchie, J.C., Schmutge, T.J., French, A.N., Su L., Mckee L. and Davis M.R. 2003. Canopy attributes of desert grassland and transition communities derived from multiangle airborne imagery. *Remote Sensing of Environment* 85: 339-354
- Dahl, B.E., and Tisdale, E.W., 1975. Environmental factors related to medusahead distribution. *Journal of Range Management* 28:463-468
- Davies, K.W. 2008. Medusahead dispersal and establishment in sagebrush steppe plant communities. *Rangeland Ecology and Management* 61:110-115

- Davies, K.W., and Svejcar, T.J. 2008. Comparison of medusahead –invaded and non-invaded Wyoming Big Sagebrush Steppe in Southeastern Oregon. *Rangeland Ecology and Management* 61:623-629
- Epiphanio, J.C.N, and Huete, A.R.1995. Dependence of NDVI and SAVI on sun/sensor geometry and its effect on fAPAR relationships in alfalfa. *Remote Sensing of Environment* 51:351-360
- Gamon, J.A., Serrano, L., Surfus, J.S. 1997. The photochemical reflectance index: an optical indicator of photosynthetic radiation use efficiency across species, functional types, and nutrient levels. *Oecologia* 112: 492-501
- Gamon, J.A., Cheng, Y., Claudio, H., MacKinney, L., and Sims, D.A. 2006. A mobile tram system for systematic sampling of ecosystem optical properties. *Remote Sensing of Environment* 103: 246-254
- Garrity, S.R., Vierling, L.A. and Bickford, K. 2010. A simple filtered photodiode instrument for continuous measurement of narrowband NDVI and PRI over vegetated canopies. *Agricultural and Forest Meteorology* 150: 489-496
- Gitelson, A.A., Kaufman, Y.J., and Merzlyak, M.N. 1996 Use of a green channel in remote sensing of global vegetation from EOS-MODIS. *Remote Sensing of Environment* 58: 289-298
- Gold, W.G., and Caldwell, M.M. 1990. The effects of the spatial pattern of defoliation on regrowth of a tussock grass. III Photosynthesis, canopy structure and light interception. *Oecologia* 82: 12-17
- Goodin, D.G., Gao, J., and Henebry, G.M. 2004. The effect of solar illumination angle and sensor view angle on observed patterns of spatial structure in tallgrass prairie. *IEEE Transactions on Geoscience and Remote Sensing* 42:154-165
- Gutschick, V.P., Barron, M.H., Waechter, D.A. and Wolf, M.A. 1985. Portable monitor for solar-radiation that accumulates irradiance histograms for 32 leaf-mounted sensors. *Agricultural and Forest Meteorology* 33: 281-290
- Harris, G.A. 1977. Root phenology as a factor of competition among grass seedlings. *Journal of Range Management* 30: 172-177
- Hironaka, M. 1961. The relative rate of root development of cheatgrass and medusahead. *Journal of Range Management* 14:263-267
- Huete, A.R., Hua, G., Qi, J., Chechbouni, A. and van Leeuwen, W.J.D. 1992. Normalization of multidirectional red and NIR reflectances with the SAVI. *Remote Sensing of the Environment* 40:1-20

- Hunt, E.R. Jr., Daughtry, C.S.T., Moon, S.K., and Parker Williams, A.E. 2007. Using canopy reflectance models and spectral angles to assess potential of remote sensing to detect invasive weeds. *Journal of Applied Remote Sensing* 1: 1-19
- Jackson, R.D., and Pinter, Jr. P.J. 1986. Spectral response of architecturally different wheat canopies. *Remote Sensing of Environment* 20:43-56
- Lass, L.W., Prather, T.S., Glenn, N.F., Weber, K.T., Mundt, J.T., and Pettingill, J. 2005. A review of remote sensing of invasive weeds and example of the early detection of spotted knapweed (*Centaurea maculosa*) and babysbreath (*Gypsophila paniculata*) with a hyperspectral sensor. *Weed Science* 53:242-251
- Middleton, E.M. 1991. Solar zenith angle effects on vegetation indexes in tallgrass prairie. *Remote Sensing of Environment* 38:45-62
- Middleton, E.M. 1992. Quantifying reflectance anisotropy of photosynthetically active radiation in grasslands. *Journal of Geophysical Research* 97:18935-18946
- Noujdina, N.V., and Ustin, S.L. 2008. Mapping downy brome (*Bromus tectorum*) using multivariate AVIRIS data. *Weed Science* 56:173-179
- Rahman, A.F. and Gamon, J.A. 2004. Detecting biophysical properties of a semi-arid grassland and distinguishing burned from unburned areas with hyperspectral reflectance. *Journal of Arid Environments* 58:597-610
- Ross, J. 1981. The radiation regime and architecture of plant stands. The Hague, The Netherlands: Dr. W. Junk Publishers. 391 p
- Ryel, R.J., and Beyschlag, W. 1995. Benefits associated with steep foliage orientation in 2 tussock grasses of the American intermountain west – a look at water-use-efficiency and photoinhibition. *Flora* 190:251-260
- Sellers, P.J. 1985. Canopy reflectance, photosynthesis and transpiration. *International Journal of Remote Sensing* 8:1335-1372
- Sharp, L.A., Hironaka M., and Tisdale E.W. 1957. Viability of medusahead seed collected in Idaho. *Journal of Range Management* 10:123-126
- Sims, D.A., Hongyan, L., Hastings, S., Oechel, W.C., Rahman, A.F., and Gamon, J.A. 2006. Parallel adjustments in vegetation greenness and ecosystem CO<sub>2</sub> exchange in response to drought in a southern California chaparral ecosystem. *Remote Sensing of Environment* 103:289-303

- USDA, NRCS. 2007. Web Soil Survey. Available online at <http://websoilsurvey.nrcs.usda.gov/>. Accessed March/03/2007
- Vierling, L.A., Deering D.W., and Eck T.F. 1997. Differences in arctic tundra vegetation type and phenology as seen using bidirectional radiometry in the early growing season. *Remote Sensing of Environment* 60:71-82
- Walter-Shea, E.A., Blad, B.L., Hays, C.J., and Mesarch, M.A. 1992. Biophysical properties affecting vegetative canopy reflectance and absorbed photosynthetically active radiation at the FIFE site. *Journal of Geophysical Research* 97:18925-18934
- US Naval Oceanography, Astronomical Applications Department. Available at <http://aa.usno.navy.mil/data/docs/AltAz.php>. Accessed June/03/2008

Table 3-1. Canopy cover classification of vegetation under light sensor field of view (Footprint 1-m radius).

Sensor	Bunchgrass	Bulbous bluegrass	Medusahead	Forbs	Litter	Green:dead dry matter ratio
1		32	68			1:0
5	79	18			3	3:1
8	69	28			3	2:1
11			97		3	1:0
12		10	90			1:0
16			98	2		1:0

Table 3-2. Collection dates samples and sun zenith angles (SZA) for full day reflectance measurement at four different phenological stages.

Vegetation group	Pre senescent	Early senescent	Mid senescent	Late senescent
Perennial grass				
Date	26 – 27 Jun	24 – 25 Jul	15 – 16 Aug	6 – 7 Sept
SZA *	72 – 21 – 54	75 – 25 – 56	79 – 30 – 60	83 – 38 – 67
Medusahead				
Date	27 – 28 Jun	9 – 10 Jul	24 – 25 Jul	14 – 15 Aug
SZA *	72 – 21 – 54	73 – 22 – 55	75 – 25 – 56	79 – 30 – 60

\* SZA values for three different times of the day; 7 a.m., noon, and 5 p.m.

Table 3-3. Results for T-test analysis between perennial grass and medusahead for full day reflectance comparisons ( $p < 0.05$ ).

Reflectance	Pre senescent	Early senescent	Mid senescent	Late senescent
NDVIg	<0.01	0.19	0.08	<0.01
PAR	<0.01	<0.01	<0.01	<0.01
NIR	<0.01	<0.01	<0.01	<0.01
Green (568nm)	0.39	<0.01	<0.01	<0.01
Green (532nm)	0.38	<0.01	<0.01	<0.01

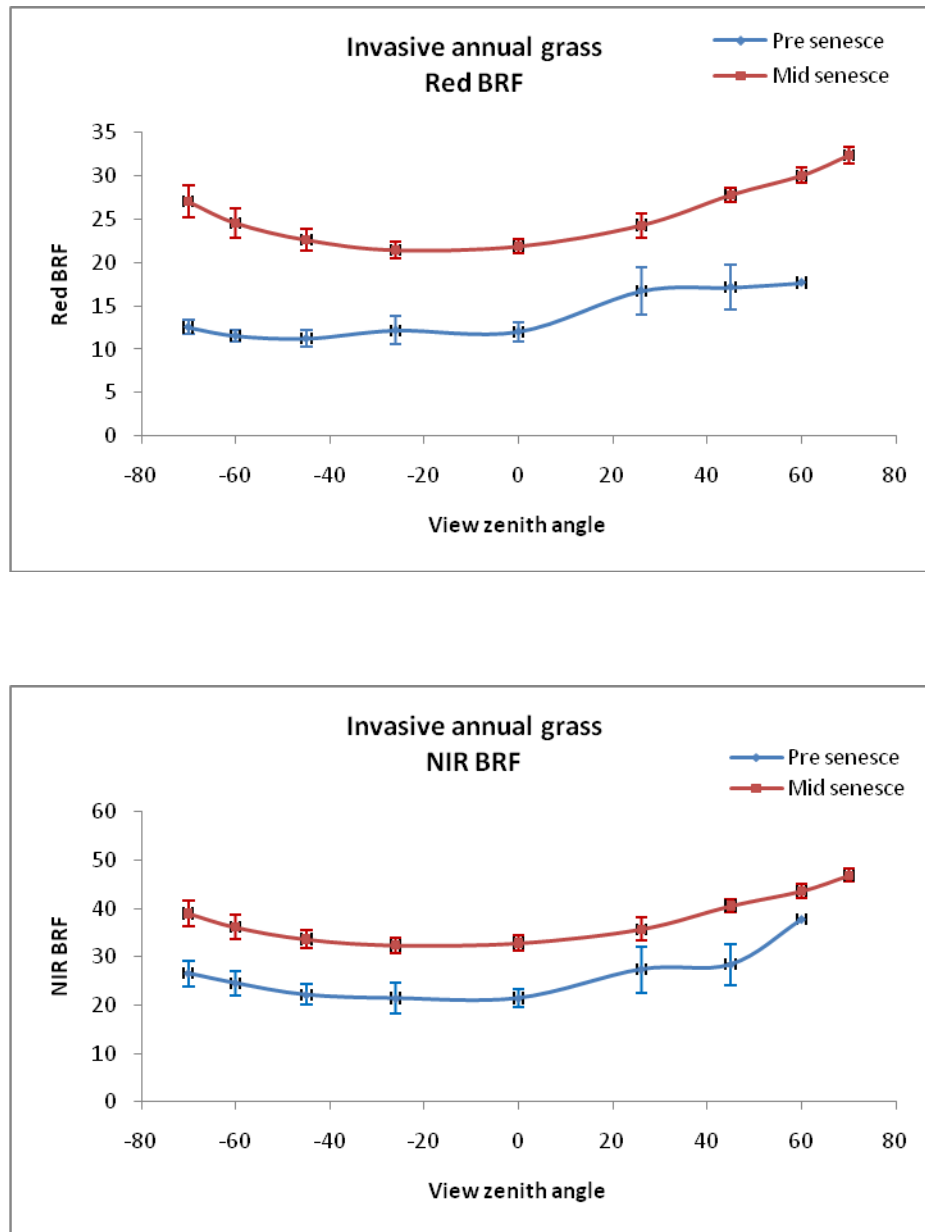


Figure 3-1. Near infrared (NIR) and Red bidirectional reflectance factor (BRF) for annual grasses for two different phenology periods. Changes in leaf orientation from erectophile to planophile affects reflectance values especially in the NIR region. Standard errors are depicted with vertical bars. Results from Chapter 2.

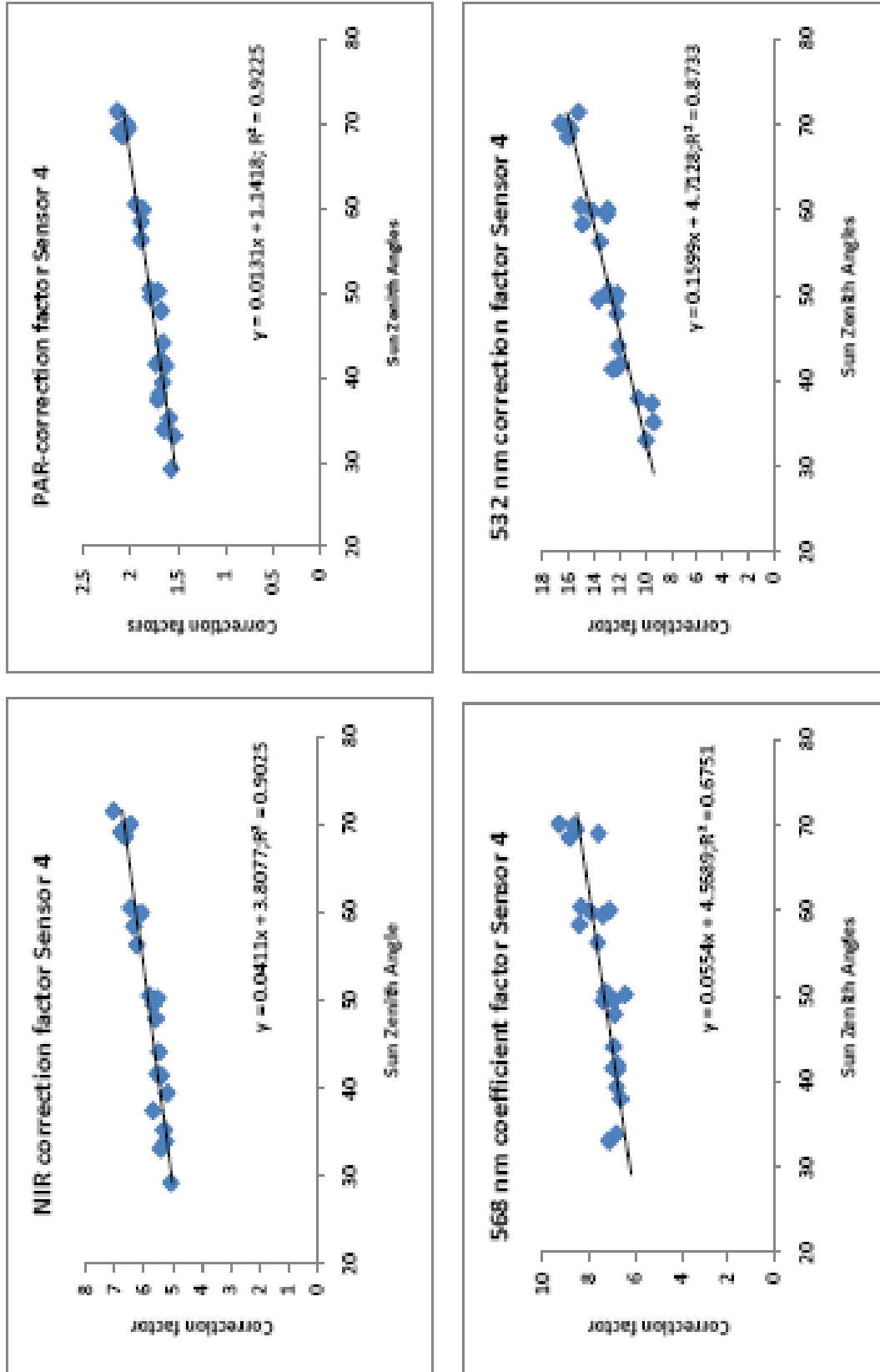


Figure 3-2. Correction factors for reflectance measurements at different sun zenith angles.

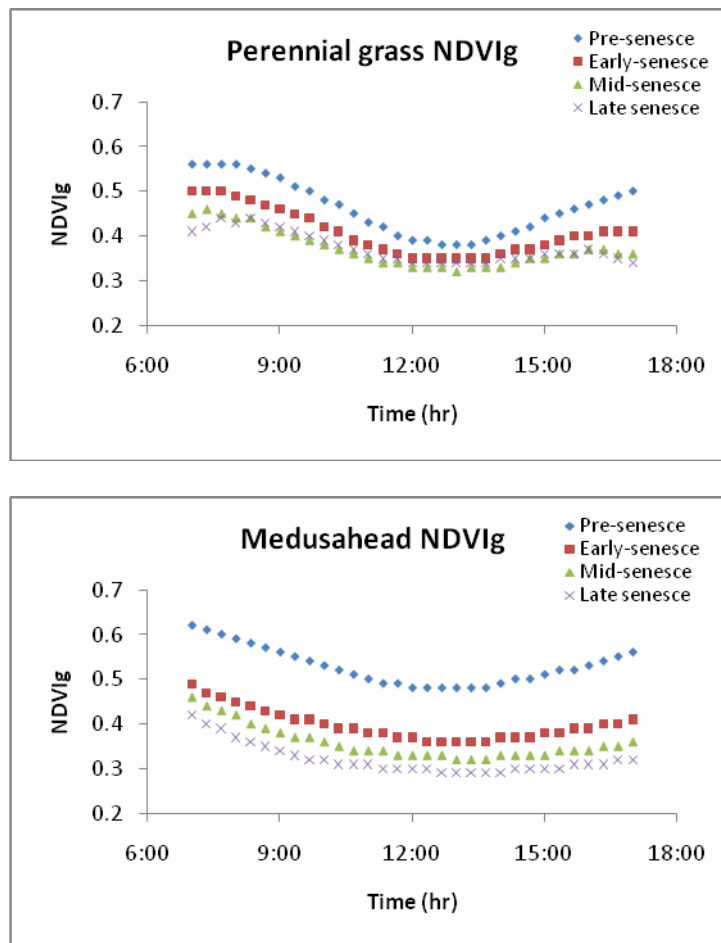


Figure 3-3. Green NDVI (NDVIg) of perennial and medusahead at four phenological stages.

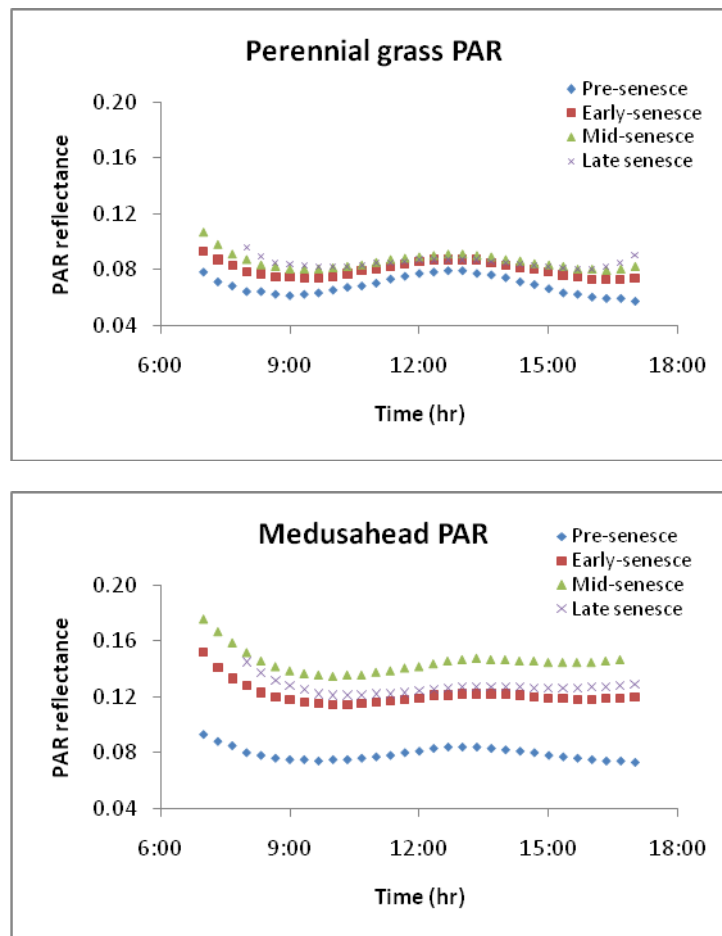


Figure 3-4. Photosynthetically active radiation (PAR) reflectance of perennial grass and medusahead for four phenology periods.

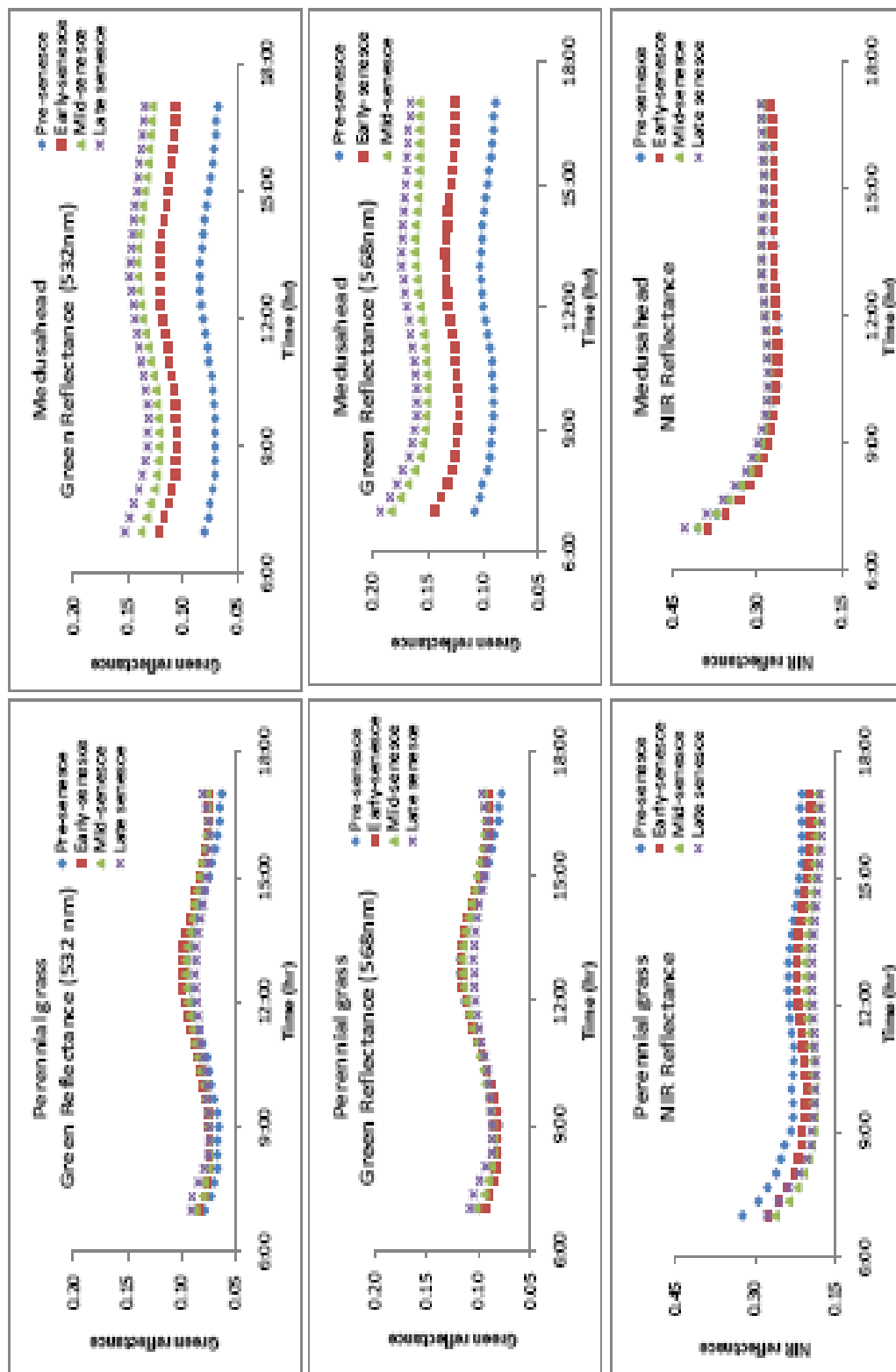


Figure 3-5. Green (568 and 532 nm) and NIR (800 nm) reflectance of perennial grass and medusahead at four different phenological stages.

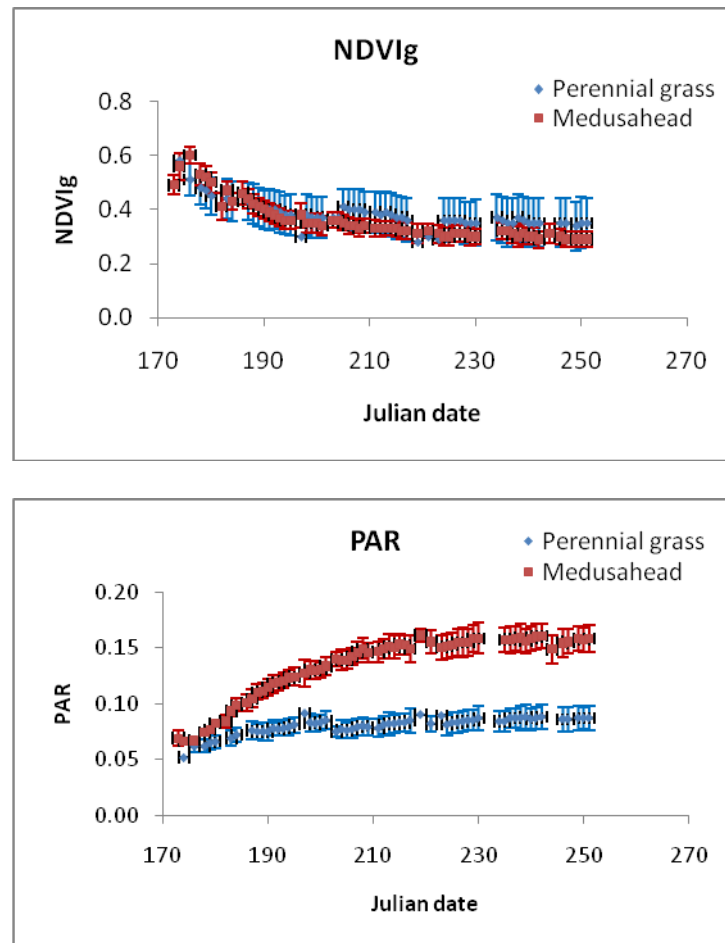


Figure 3-6. Green NDVI (NDVIg) and PAR reflectance variation of perennial grass and medusahead throughout the observational period. Standard errors are depicted with vertical bars.

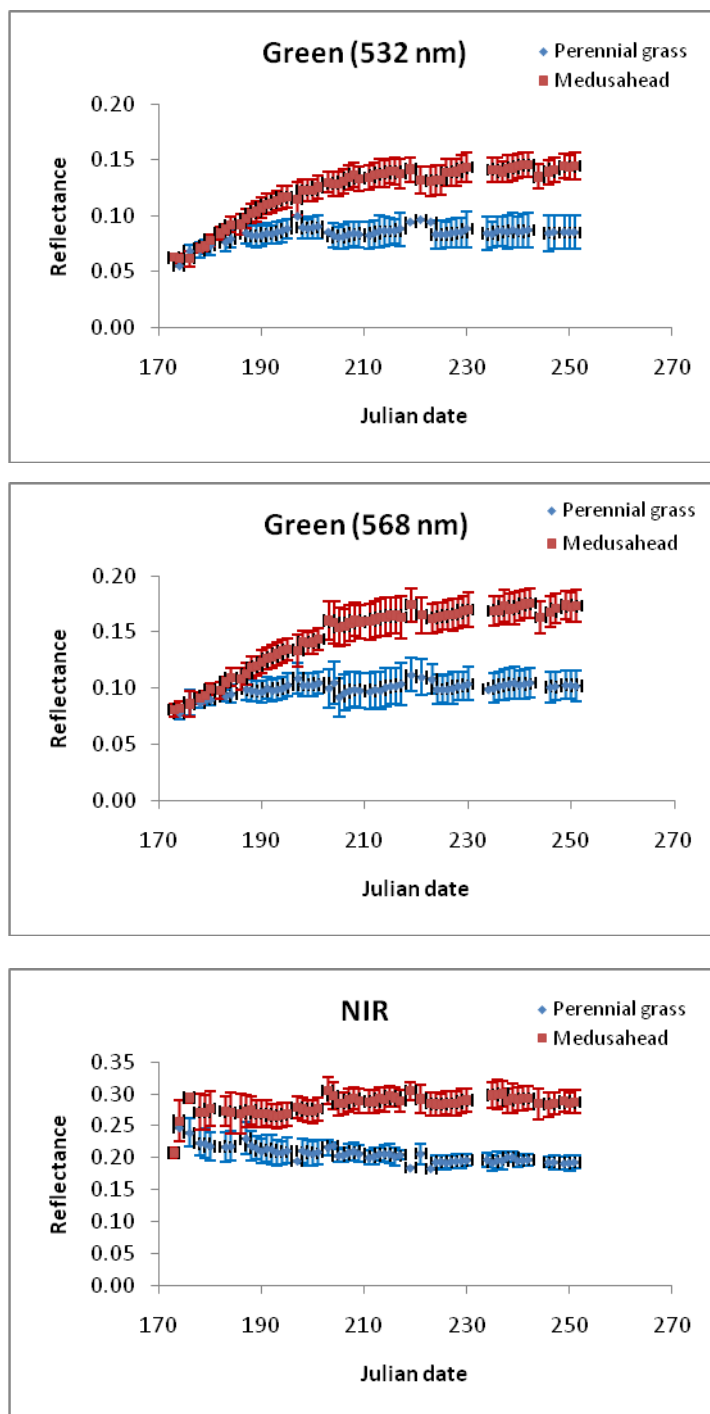


Figure 3-7. Green and NIR reflectance variation of perennial grasses and medusahead throughout the observational period. Standard errors are depicted with vertical bars.

## **CHAPTER 4. Bidirectional reflectance of shrub-steppe vegetation: towards MISR-based GPP partitioning**

### **Abstract**

Quantifying the cover fractions of various plant functional groups existing within the MODIS Gross Primary Productivity (GPP) model grid cells would be of great advantage for monitoring biomass changes within shrub steppe vegetation. We conducted shrub-steppe vegetation classification based on field data and remote sensing imagery collected at two different spatial resolutions (Landsat, 30 m; and Multi-angle Imaging Spectro Radiometer (MISR) local mode, 275 m) in order to obtain a fractional cover index to weight MODIS GPP product according to plant functional types. We hypothesized that: 1) multiangular data from MISR local mode data can improve plant functional type accuracy assessments relative to Landsat image classification at the end of the growing season and 2) vegetation classes generated from multiangular data can be used to produce GPP estimates using the MODIS GPP (1 x 1 Km) product. Maximum likelihood supervised classification was used to identify three classes based on field transect data: shrub, non-shrub and crop vegetation types. These classes were used to generate a fractional cover for MODIS GPP 1-km grid cells at different periods throughout the growing season. The overall classification accuracy was high for Landsat and the nadir MISR camera (An) images (88% and 98%, respectively). We additionally plotted the bidirectional reflectance factor (BRF) values for each of the MISR bands and cameras to evaluate whether the differences between shrub and non-shrub groups could be better discriminated

using the other cameras. Our results show that we could separate shrub and non-shrub for image classification because of the absolute difference between these two vegetation groups. Although we could separate all three cover types, the relationship between MODIS GPP and shrub cover variation was not significant ( $R^2 < 0.06$ ), likely because of the 'mixed' pixels that increased the variance and thus confounded the response within each MODIS GPP grid cell. However, a relationship between MODIS GPP and crop fractional cover was observed. Further studies that span longer time periods may be necessary to derive the productivity of individual plant functional groups using the MODIS GPP product.

## 1. Introduction and background

Rangeland inventory and mapping is used to characterize aspects of ecosystem structure that can be later linked to ecological processes. Classifying and mapping large areas of these heterogeneous ecosystems have relied mostly in the availability of remotely sensed imagery at various spatial and temporal resolutions (McGraw and Tueller 1983, Tueller 1989, Wylie et al. 2002, Cingolani et al. 2004).

The study of plant functional types provides new insights into the dynamics of shrub-steppe vegetation change in the western North America. Plant functional types such as shrubs greatly affect ecosystem properties such as carbon and water budgets (Gilmanov et al. 2003, 2004) and productivity (Wylie et al. 2003). Moreover, shrubs tend to be the dominant overstory species that can be distinguished by most nadir viewing remote sensing measurements, which generally extract information of the upper canopy without including information of the understory vegetation (Ustin and Gamon 2010). Although there is not a universal system in place to classify vegetation functional types, shrubs combine different functional attributes that can be used to predict relationships between characteristic plant physiological patterns and structural responses detectable by remote sensing (Ustin and Gamon 2010). These functional attributes include a distinctive growth form, perennial life history and evergreen leaf duration (DeFries et al. 1999). In addition, differences in plant functional types can affect interrelationships among plants, between plants and animals, and between plants and the environment. It is therefore helpful to estimate vegetation

production of shrubs versus other vegetation groups across the landscape. Although differentiating plant functional types using coarse scale remote sensing data can be challenging in semi-arid ecosystems, a fractional cover index to weight remote sensing products, such as the MODIS Gross Primary Productivity (MODIS GPP) product, may be useful to monitor ecosystem change as a function of plant functional types.

The principal application of the MODIS GPP product (MOD17) is to document and monitor global biospheric health (Running et al. 2000). In order to measure vegetation productivity, MODIS GPP is based on the productivity efficiency model proposed by Monteith (1972) or light use efficiency approach (Running et al. 2000):

$$\text{GPP} = \text{PAR} * \text{fPAR} * \epsilon \quad (1)$$

Where PAR is the photosynthetically active radiation incident on a plant canopy, fPAR is the fraction of PAR absorbed by a canopy and  $\epsilon$  is the radiation use efficiency (RUE), in terms of  $\text{g C MJ}^{-1}$ . In this model, GPP is a function of absorbed photosynthetic radiation ( $\text{APAR} = \text{PAR} * \text{fPAR}$ ) and RUE. fPAR for each MODIS GPP 1-km cell is measured using NDVI calculated from reflectance detected by the MODIS sensor (Sellers 1985, Myneni et al. 2002). The maximum radiation use efficiency ( $\epsilon_{\text{max}}$ ) to produce the final ( $\epsilon$ ) is derived from a lookup table and modified by scalars (0-1) associated with daily minimum temperature (TMIN) and vapor pressure deficit (VPD). PAR, TMIN and VPD are obtained from the meteorological data provided by the NASA Data Assimilation Office (DAO) at a resolution of  $1 \times 1.25^\circ$  in contrast to the 1-Km gridded MOD17 outputs. Thus,

the entries of this model are subject to uncertainties and assumptions (Heinsch et al. 2003). For instance, comparison of meteorological data recorded by MODIS DAO and flux tower in hardwood and boreal forest sites showed good agreement for VPD and TMIN, while the DAO PAR resulted in high bias (Turner et al. 2003).

One drawback of MODIS GPP products is that the scale of land cover variation is usually smaller than the ~ 1-km resolution. Classifying coarse resolution pixels as a unique type of land cover generally results in poor accuracy (Nelson and Holben 1986). Thus, quantifying fractional cover within MODIS GPP pixels would be of great advantage for monitoring biomass changes within shrub steppe vegetation. Building upon findings from Chapters 2 and 3, we therefore hypothesized that: 1) multiangular data from MISR local mode data (pixel size: 275 x 275m) can improve plant functional group accuracy assessments relative to Landsat image classification at the end of the growing season and that 2) vegetation classes generated from multiangular data can be used to produce GPP estimates using the MODIS GPP (1 x 1 Km) product. Our objectives were to: 1) detect differences in land cover types using bidirectional reflectance factor values at the landscape scale and 2) estimate non-shrub and shrub fractional cover using MISR and Landsat-based classification in order to refine plant GPP estimates using MODIS.

## 2. Methods

### 2.1 Study area.

Four square macroplots measuring 5 by 5 km, and separated from each other by 5 to 12 km, were delineated to include multiple MODIS 1 km GPP product grid cells (after Turner et al. 2003). These areas were emplaced on ecological site classes (USDA-NRCS; <http://websoilsurvey.nrcs.usda.gov/>) on lands managed by the Soulen Livestock Co., near Weiser, Idaho (Figure 2-2). Consequently, the macroplots included the dominant Loamy 12-16 ARTRX-PSSP6 ecological site, which extends over 28.4% of the overall study area shown in Fig. 2-2. This ecological site represents loamy soils with 12-16 inches (304-406 mm) of precipitation and it is cover predominantly by foothill big sagebrush (*Artemisia tridentata Nutt ssp. xericensis* Winward ex R. Rosentreter & R. Kelsey) and bluebunch wheatgrass (*Pseudoroegneria spicata* (Pursh) A. Love) (<http://websoilsurvey.nrcs.usda.gov/>). Other ecological sites that are dominant in the area include the Very shallow 12-20 ARRI2-POSE (20.8%) and the South slope loamy 12-16 ARTRX-PSSP6 (12.1%). Additional information relating to the study area was described in the previous chapters.

### 2.2 Field data collection

Training sites for remote imagery classification were chosen based on canopy cover measurements collected in 2007 and 2008. Canopy cover was estimated using permanent transects established within each of the macroplots. In 2007, cover was estimated in 36 225-m line transects with readings in 5-m

sections; thus a total of 115 readings were obtained per transect. In an attempt to capture variability caused by wind and terrain effects, in 2008 the number of transects were increased to 72, while reducing their length to 30 m each.

Transects were located within each macroplot in representative areas at different elevation levels (from 1000 to 1200 m) and close to the measurement enclosures described in Chapter 3. In addition, transects were located on areas with slope less than 15% to facilitate calibration and comparison with remotely sensed data.

Canopy cover of four vegetation types was derived using the line intercept method. Shrubs, native grasses (sparse and bunch types), perennial forbs, and invasive annual grass canopy cover were measured in these transects. These four plant functional types represented a range of canopy structure, phenology, and biomass, and grew on a variety of soil types. The shrub group was comprised of foothill big sagebrush (*Artemisia tridentata* Nutt ssp. *xericensis* Winward ex R. Rosentreter & R. Kelsey) and bitterbrush (*Purshia tridentata* [Pursh] DC.). Bunchgrasses were mainly comprised of bluebunch wheatgrass (*Pseudoroegneria spicata* [Pursh] A. Love) and squirreltail (*Elymus elymoides* [Raf.] Swezey). The sparse grass group included bulbous bluegrass (*Poa bulbosa* L), which exhibits different structure and phenology than the bunch type perennial grasses. The perennial forbs group included lupine (*Lupinus* spp.), curlycup gumweed (*Grindelia squarrosa* [Pursh] Dunal) and western yarrow (*Achillea millefolium* L.). Annual grasses were represented mainly by medusahead (*Taeniatherum caput-medusae* [L.] Nevski) and some scattered samples of cheatgrass (*Bromus tectorum* L.).

Cover readings were measured for two periods: growth (late spring) and senescent period (transition summer-fall). Because the line intercept method is more suitable for reading shrub and bunch grass cover, cover of annuals grasses, forbs and sparse vegetation was visually estimated (Canfield 1941). Therefore, we clustered annual and forbs as a non-shrub vegetation group for the supervised classification. The non-shrub vegetation group included also senesced crop areas and pasture/hay land.

### **2.3 Imagery acquisition**

Vegetation cover classification can be improved in some areas when nadir-based remote sensing imagery are supplemented by reflectance information collected from multiple sun and viewing geometries (Martonchik et al. 1998, Schaepman-Strub et al. 2006). As with most land surfaces, rangelands possess complex structures that result in highly anisotropic reflectance characteristics (Figure 2-1). We quantified the anisotropic nature of the vegetation canopies within our study area through the measurement of the bidirectional reflectance factor (BRF). The BRF is the ratio of the reflected radiant flux from a sample surface to the radiant flux reflected from an ideal and diffuse standard surface under identical view geometry and single direction illumination (Nicodemus et al. 1977, Diner et al. 1999, Schaepman-Strub et al. 2006).

MISR Level 1B2 Local Mode Terrain Radiance Data (Version F03\_0024) were acquired for the Crane Creek ID Site on July and August 2008 (Table 4-1). The local mode imagery was requested and granted by the MISR Local Mode

Science Coordinator (Figure 4.2). The local mode imagery corresponded to the nine pushbroom MISR cameras described as Df, Cf, Bf, Af, An, Aa, Ba, Ca and Da where A, B, C and D describe increasing viewing angles (26.1, 45, 60 and 70.5 degrees, respectively) and where the letters f, n, and a describe forward, nadir and aftward viewing cameras, respectively (Diner et al. 1999).

We downloaded Landsat 5 TM imagery from the USGS Global Visualization Viewer (<http://glovis.usgs.gov/>) for the July and August 2008 periods. We also downloaded and utilized Landsat 5 TM data to locate the training sites using the geolocated transect data.

MODIS products (MODIS GPP 8-Day L4 Global 1 Km (MOD17A2) and MODIS Vegetation Index 16-Day L3 Global 1 Km (MOD13A2)) were downloaded from the NASA Warehouse Inventory Search Tool (WIST) (<https://wist.echo.nasa.gov/>). MOD17A2 images were downloaded for the growing season from Julian date (DOY) 177 to 241. According to the MODIS science team, the L3 and L4 products are ready for use in scientific analysis and publication.

## **2.4 Imagery pre-processing**

We used the band minimum subtraction method to atmospherically correct Landsat and MISR local mode data (Chavez 1988). Prior to this step, and in order to get minimum values in the MISR image, zero values of bad pixels were change to NaN (Not a Number) values in the Environment for Visualizing Images (ENVI) software package. In addition, all the images were spatially resized using

ENVI nearest neighbor resampling to a rectangular area set to UL corner 44.5 N, -116.8 W and LR corner 44.0 N, -116.4 W geographic coordinates. MISR local mode and MODIS GPP images were re-projected using ENVI nearest neighbor resampling to Landsat UTM projection and WGS 84 datum.

## **2.5 Data analysis**

### **BRF calculation**

BRF values for each of the MISR images were obtained using the MISR Toolkit (Mtk) provided by the NASA Atmospheric Science Data Center (ASDC). The Mtk is a programming that involves different routines to extract and utilize MISR data sets like MISR level L1B2 and Level 2 (Rheingans et al. 2006). Among these routines the MtkFileToGridList, MtkFileGridToFieldList and MtkMisrToEnvi utilities were used. The MtkFileToGridList utility lists the following grids: BlueBand, GreenBand, RedBand, NIRBand, BRF conversion factors, and geometric parameters. Then, given a file and a grid, MtkFileGridToFieldList utility retrieves the 7 different fields of a file/grid. For instance for the red band the following fields are available: RedBand, Red Radiance/Radiometric data quality indicator (RDQI), Red Radiance, Red RDQI, Red DN, Red Equivalent Reflectance, Red Brf. From this list only the Red Radiance/RDQI is a real field. The others are derived by unscaling and unpacking or otherwise using the Brf conversion factors. The MtkMisrToEnvi utility imports MISR data into ENVI, preserving the projection parameters that are stored in a header (.hdr) file (Rheingans et al. 2006).

### **Image classification and accuracy assessment**

Maximum likelihood supervised classification was used because it is a standard classification algorithm based on Gaussian distribution of pixels from each class (Foody et al. 1992). Hence, data samples for training sites should be representative of each class (Prenzel and Treitz 2005, Su et al. 2009). Two classes were selected based on transects information: shrub and non-shrub vegetation. Since Landsat image pixels have a unique coordinate system located in the center of the pixel, it was possible to extrapolate the information provided by the line intersects onto the 30 x 30-m Landsat pixel size (Figure 4-1).

Therefore, based upon the field data, 39 shrub and 53 non-shrub pixels were randomly selected as a training set and the other pixels (37 shrub and 49 non-shrub) were retained for accuracy assessment for maximum likelihood classification. The minimum coverage for each pixel for quantifying an area as shrub or non-shrub was 70%. Furthermore, because there are irrigated crop areas in the study area that can be distinguished in the imagery, we used this vegetation type as an additional class because of the differences in biomass production compared to shrubs and non shrub vegetation groups. Therefore, 40 crop-training sites were selected to classify the Landsat image and the other 36 pixels were used for accuracy assessment. Pixels having a slope greater than 5% were eliminated to reduce interference due to complex terrain.

Using the three classes obtained using the Landsat classification; we selected training sites for the MISR image classification. All MISR pixels that had more than 70% cover of any of these three Landsat classes were selected as

training sites. First, we classified the MISR nadir camera image ( $A_n$ ) so we could compare this classification with a classification using the MISR cameras positioned at the other viewing angles because MISR off-nadir cameras would enhance the overall accuracy of nadir image (Armston et al. 2007, Su et al. 2007, Su et al. 2009). In addition, we also tested if all MISR cameras could distinguish the three classes in all bands. After the supervised classification was completed for both Landsat and MISR images, we built error matrices and calculated a  $K_{\text{hat}}$  statistic to gauge the level of agreement that cannot be attributed to random chance (Jensen 1986).

#### **Scaling up from Landsat (30 x 30 m) to MISR local mode (275 x 275 m) to MODIS GPP product (1 km)**

Each MISR pixel, after being reprojected in UTM projection, contains coordinate values set at the center of the pixel in ENVI. Using these coordinates and the location of each pixel edge we could estimate that each MISR local mode pixel (275 x 275 m) corresponded to approximately 9 x 9 Landsat pixels (Table 4-2). This analysis was similar to when trying to integrate MODIS GPP 1-km pixels, which output pixel size measures 926.6 m (LPDAAC 2008), to Landsat and MISR local mode pixels. However, because the MODIS GPP product coordinates correspond with the upper left corner of each pixel and proceeds right and downward (Table 4-2), additional considerations had to be made to spatially match the various datasets.

### **GPP Fractional cover**

MODIS GPP 1-Km pixels were classified using aggregations of Landsat-based class data. Because each MODIS pixel was comprised of approximately 90 and sometimes 120 pixels (Table 4-2) we selected the MODIS pixels that included at least 65% of the Landsat and MISR pixels located in flat areas (Table 4-3). After this evaluation we were able to choose 16 pixels with different percentages of shrub cover and we evaluate the relationship between cover and GPP via regression analysis. We did the same analysis with GPP and crop areas. In addition, we display the MODIS Enhanced Vegetation Index (EVI) 1-Km pixels to validate relationships between shrub and crop cover with MODIS GPP at the same spatial resolution.

### 3. Results and Discussion

#### 3.1 Vegetation type classification

The classification accuracies are shown in Table 4.4. The overall accuracy was high for both image classifications. In addition, the  $K_{\text{hat}}$  statistic shows excellent or full agreement for Landsat and MISR classification (Table 4-4). We inferred that the low number of classes (3) was likely to affect the accuracy classification. Even at the finer Landsat spatial resolution, we were unable to locate enough training sites with the cover of a particular plant functional group higher than 70% to split the non-shrub vegetation type into at least perennial grasses and invasive annual grasses. For instance, training sites of invasive annual grasses with a canopy cover higher than 70% were difficult to estimate; because of the complex variability of the community there were few areas dominated by this vegetation group. In addition, areas covered with squirreltail were also covered with sparse grass, which made it difficult to select a training site for perennial grasses. Furthermore, the crop areas were so few that the validation of these areas was almost 100%. However, commission errors occurred with riparian areas southwest of the Crane Creek Reservoir that were classified as crop areas in both image classifications (Figure 4-3).

To achieve better estimates of shrub fractional cover, we selected the MISR image from August 18<sup>th</sup> for the supervised classification because most of the non-shrub vegetation was senescent during this time. In addition, some croplands were still green because of irrigation, but those that were senesced during this time were classified as non-shrub to avoid problems in the relation

between MODIS GPP and crop cover. We first classified the MISR-nadir (An) because it has the same vertical observation angle that the Landsat sensor uses (Chapter 1, Table 4-4). We had originally planned to classify the images collected by the other MISR cameras to attempt to improve the nadir-based classification, but because the overall accuracy and  $K_{\text{hat}}$  statistic of the MISR-An image classification was 98.3% and 97.1% respectively, we did not try any further refinement of the classification for each of the other cameras because we expected to achieve the same or better accuracy (Su et al. 2007, 2009, Braswell et al. 2003, Armston et al. 2007, Liu and Kafatos 2007). However to test this hypothesis we plotted the BRF values for each of the MISR bands and cameras to evaluate differences between shrub and non-shrub groups (Figure 4-4 and Figure 4-5).

Before analyzing each MISR band at each off-nadir camera, we examined differences among these three classes based on ratio-based vegetation indices like the NDVI (Figure 4-4). It is clear that crop NDVI at all MISR cameras was substantially different from shrubs and non-shrub NDVI values. Most crop areas have irrigation systems that allow the farmers harvest barley (*Hordeum vulgare* L.) and alfalfa (*Medicago sativa* L.) during the summer season for storing hay during the winter season. On the other hand, there were small differences between shrub and non-shrub NDVI values. Even though shrub and non-shrub NDVI followed the same pattern along all MISR cameras, small differences between these two groups did occur.

NDVI is affected by the view angle, especially at the farthest forward and aftward MISR cameras (Figure 4-4). At the ground level less soil or litter background and greener canopy can be observed with large off-nadir view angles (Middleton 1991, Goodin et al. 2004). However, even with the determination of vegetation indices, variations in reflectance introduced by sun and view angle effects are not completely removed because these directional effects are dependent upon both the target anisotropy as well as spectral band region of interest (Middleton 1991, Epiphanio and Huete 1995, Walter-Shea et al. 1997, Galvao et al. 2004). Topographic effects can also increase NDVI values. Goodin et al. (2004) suggested that ratio-based vegetation indices do not entirely compensate for surface terrain effects (Goodin et al. 2004). Even though we selected flat areas for our training set, occlusion by some geological forms could affect NDVI values, especially in the area near the Crane Creek reservoir where steep terrain existed. In order to avoid high BRF values at off-nadir view angles, Walthall et al. (1985) showed that most bidirectional information of vegetated and soil surfaces are found in the principal solar plane within viewing angles approx  $50^\circ$  either side of nadir. In addition, Pinty et al. (2009) recommended that NDVI is not optimal for deriving one single and unique vegetation attribute for large spatial domains because it generally translates into an increasing set of constraints to be satisfied (Woodcock and Strahler 1987, Verstraete and Pinty 1996).

Shrub and non-shrub BRF at each band and camera are shown in Figure 4-5. The shape of the angular BRF signature for each band showed similar

shapes for shrub and non-shrub vegetation, with low BRF values at forward-viewing cameras and high BRF values at the aftwards cameras. Even though non-shrub vegetation is mostly senesced by this period, this exhibited higher green and NIR BRF values than 'evergreen' shrub vegetation. This behavior may be explained by data presented in Table 4-4. The selection of MISR 'pure' pixels was designed to include pixels with a minimum cover of 70% of either shrub or non-shrub vegetation. However, non-shrub 'pure' pixels still included approximately 16% of shrub vegetation that may affect the BRF response in all MISR bands (Table 4-4).

Vegetation structure and shadowing within pixels have been related to the shapes of BRF signatures (Nolin 2004, Pinty et al. 2002, Widlowski et al. 2004) where the presence of vertically elongated foliage clumps of moderate to high densities can exhibit a bell-shaped angular signature in the red BRF across the solar principal plane, while compact vegetation canopies exhibit bowl-shaped reflectance patterns (Pinty et al. 2002, Widlowski et al. 2004). In addition, a bowl-shaped NDVI pattern was described by Deering et al. (1994, 1999) in studies of spruce-hemlock forest and boreal forest ecosystems. In our study, the average height of sagebrush was 1.01 m while the average height for perennial grasses was approximately 0.5 m. These two dominant species grow surrounded by native annual grasses like bulbous bluegrass which senesce at the end of the spring remain as standing dead vegetation throughout the growing season. We considered that the physiognomy of the vegetation in the study area would not allow distinguishing differences in the shape of BRF signatures at moderate

resolution like the MISR local mode images. In addition, it is difficult to define a regular 'bowl shape' or 'bell shape' BRF shape for all the bands. Because these shapes did not occur in our BRF curves, we tried to distinguish these two vegetation types at the landscape scale using the anisotropy index (ANIX) as we did at the plant scale in Chapter 2 (Figure 4-6).

We observed that shrub ANIX was higher than non-shrub ANIX at the spatial resolution of MISR (Figure 4-6). However, this difference was not as high as the difference observed at the fine plant-scale resolution where shrubs showed high anisotropic reflectance behavior compared to other plant functional types (Chapter 2). Asner (2004) suggested that remote sensing observations in dryland ecosystems tend to integrate plant-to-plant variations in canopy structure when the spatial resolution is greater than 10 to 20 m. The exception to this observation takes place when a major change in vegetation structure occurs (Asner, 2004). Thus, the height difference between shrubs and perennial grasses were likely not great enough to represent a major structural change at MISR resolution; that the effect of anisotropic behavior recorded by ANIX at fine resolution may be smoothed at MISR resolution (Woodcock and Strahler 1987).

Although the shapes of BRF signatures for shrubs and non shrub vegetation were found to be similar, we were still able to use these values for image classification because of the absolute difference between these two vegetation groups (Figure 4-3). Therefore, we expected similar accuracy classification for each MISR off-nadir image compared to the MISR An image classification (Figure 4-3, Table 4-3). This is a different finding from other studies

such as Su et al. (2007, 2009) who demonstrated that multi-angular reflectances raised overall classification accuracy in 15% compared to nadir-only analyses in New Mexican arid and semi-arid grasslands. In addition, parameters derived from MISR data products have been found to improve the accuracy of moderate resolution mapping of semi-arid vegetation (Su et al. 2009).

### **3.2 MODIS GPP fractional cover**

Increments in shrub cover estimates using MODIS GPP pixel size show low R-square value (Figure 4-7). Logarithmic regression fit the curves with  $R^2 < 0.06$ . In fact, based on the figure we can establish that there was no relationship between GPP and shrub cover for our study area. The shrub fractional cover for GPP pixels was estimated using the Landsat image classes because this image provided more detail compared to the MISR An image. For instance, we observed that there were more clumped shrub areas in the MISR-based map than the Landsat-based map (Figure 4-3). In addition, we compared MODIS GPP with variation in crop cover to verify that this product pixel size responded to changes in coverage (Figure 4-7). We observed a slightly positive trend between crop cover increments and GPP ( $R^2 = 0.22-0.54$ , Figure 4-7). Based on the MOD17 model assumption, it seems that TMIN and VPD for this area may work fine for the crop areas. This is also supported by the trends in vegetation indices such EVI (Figure 4-7), which displays an upward-trending relationship with fractional crop cover at higher (>25%) crop cover values ( $R^2 = 0.5-0.7$ ). Thus, the lack of relationship between shrub cover and GPP may

be due to other factors such as smaller relative changes in biomass and leaf area index, and effects of non-shrub vegetation.

Pixels that represent areas comprising a mixture of two or more features (i.e. 'Mixed pixels'), present a common problem, confounding the classifier, in identifying vegetation types in imagery of low spatial resolution (Strahler et al. 1986, Ustin and Gamon 2010). Poor classification accuracy and overall underestimation of non dominant classes represent some common problems when classifying coarse resolution pixels as a unique type of land cover (Nelson and Holben, 1986). We surmise that the heterogeneity of the vegetation types and that the selection of shrub and non-shrub 'pure' pixels may affect the estimation of MOD17A2 sub-pixel land cover fractions (Table 4-4). Thus, it is possible that the classification of the three 'pure' classes in Landsat 5TM and MISR An may be affected by mixed pixel effects (Figure 4-7). Other sources of misclassification would be misregistration of the pixels and mapping errors and technical differences in sensor design and calibration (Foody 2002, Ustin and Gamon 2010)

Even though there is no relationship between MOD17A2 and shrub cover we could observe changes in GPP from high values to low values along the growing season, but at the end of the summer: GPP at DOY 233 was higher than GPP at DOY 217 (Figure 4-7). This fluctuation can be related to changes in VPD or TMIN. Reeves et al. (2006) found that GPP estimates for monitoring grassland biomass fluctuations improved when plant growth conditions, for instance

precipitation, were more favorable. Thus, it may also be helpful to have data from earlier in the growing season to assess these fluctuations.

#### **4. Conclusions**

We conclude that the overall accuracy of the Landsat and MISR An local mode supervised classification for our three class types was excellent. This high accuracy could have been related to the low number of classes set at moderate and coarse spatial resolution (MISR local mode and MODIS GPP, respectively). In addition, we conclude that this high accuracy classification could be obtained at different MISR off-nadir cameras because of the absolute differences between the spectral reflectance of shrub and non-shrub vegetation types. However, no distinction was observed between the shape of shrub and non-shrub BRF. In addition, anisotropic behavior that was recorded by ANIX at fine resolution was smoothed at MISR resolution, likely because the height difference between shrubs and perennial grasses were not great enough to represent a major structural change at the coarse scale. However, we were still able to use BRF signatures for image classification because of the absolute difference between these two vegetation groups. Even with the high accuracy classification of shrubs, non-shrubs and crop land cover types, we did not observe a significant relationship between MODIS GPP values and GPP pixel shrub fractional cover. Presence of 'mixed pixels' as well as other sources of misclassification such as misregistration of the pixels and mapping errors, as well as possible technical differences in sensor design and calibration would affect this relationship in low spatial resolution imagery.

Although classification of heterogeneous shrub-steppe vegetation is challenging, further studies to derive MODIS GPP fractional cover may be needed. However, the new approaches not only should consider the structural characteristic of vegetation functional types but also the spatial distribution of these in the landscape. For instance, biomass would be different for shrubs in clustered and dispersed spatial distribution. Selecting a significant number of transects for training sites at different shrub cover could increase the opportunities to obtain significant relationships between MODIS GPP values and shrub cover variation. In addition, further validation of classification of green cropland at earlier periods during the growing season would be needed to validate the relationship between MODIS GPP and cropland cover variation.

## 5. References

- Armston, J.D., Scarth, P.F., Phinn, S.R., and Danaher, T.J. 2007. Analysis of multi-date MISR measurements for forest and woodland communities, Queensland, Australia. *Remote Sensing of Environment* 107:287-298
- Asner, G.P. 2004. Biophysical remote sensing signatures of Arid and Semiarid ecosystems. In: Susan Ustin (Ed). *Remote Sensing for Natural Resource Management and Environmental Monitoring: Manual of Remote Sensing*. Vol 4. 3 Ed.: John Wiley & Sons, Hoboken, New Jersey. p 53-109
- Braswell, B.H., Hagen, S.C., Froking, S.E. and Salas, W.A. 2003. A multivariable approach for mapping sub-pixel land cover distributions using MISR and MODIS: Application in the Brazilian Amazon region. *Remote Sensing of Environment* 87:243-256
- Canfield, R.H. 1941. Application of the line interception method in sampling range vegetation. *Journal Forestry* 39:388-394
- Chavez, P.S. 1988. An improved dark-object subtraction technique for atmospheric scattering correction of multispectral data. *Remote Sensing of Environment* 24:459-479
- Cingolani, A.M., Renison, D., Zak, M.R., and Cabido, M.R. 2004. Mapping vegetation in a heterogeneous mountain rangeland using Landsat data: an alternative method to define and classify land-cover units. *Remote Sensing of Environment* 92:84-97
- Deering, D.W., Eck, T.F., and Banerjee, B. 1999. Characterization of the reflectance anisotropy of three boreal forest canopies in spring-summer. *Remote Sensing of Environment* 67: 205-229
- Deering, D.W., Middleton, E.M., and Eck, T.F. 1994. Reflectance anisotropy for a spruce-hemlock forest canopy. *Remote Sensing of Environment* 47: 242-260
- DeFries, R.S., Townshend, J.R.G., and Hansen, M.C. 1999. Continuous fields of vegetation characteristics at the global scale at 1-Km resolution. *Journal of Geophysical Research* 104:16911-16923
- Diner, D.J., Asner, G.P., Davies, R., Knyazikhin, Y., Muller, J-P, Nolin, A.W., Pinty, B., Schaaf, C.B., and Stroeve, J. 1999. New directions in earth observing: scientific applications of multiangle remote sensing. *Bulleting of the American Meteorological Society* 80(11): 2209-2228

- Epiphanio, J.C.N, and Huete, A.R. 1995. Dependence of NDVI and SAVI on sun/sensor geometry and its effect on fAPAR relationships in alfalfa. *Remote Sensing Environment* 51:351-360
- Foody, G.M., Campbell, N.A., Trodd N.M., and Wood T.F. 1992. Derivation and applications of probabilistic measures of class membership from the maximum-likelihood classification. *Photogrammetric Engineering and Remote Sensing* 58:1315-1341
- Foody, G.M. 2002. Status of land cover classification accuracy assessment. *Remote Sensing of Environment* 80:185-201
- Galvao, L.S., Ponzoni, F.J., Epiphanio, J.C.N, Rudorff, B.F.T, and Formaggio, A.R. 2004. Sun and view angle effects on NDVI determination of land cover types in the Brazilian Amazon region with hyperspectral data. *International Journal of Remote Sensing* 25:1861-1879
- Gilmanov, T.G, Johnson, D.A. and Saliendra, N.Z. 2003. Growing season CO<sub>2</sub> in a sagebrush-steppe ecosystem in Idaho: bowen ratio/energy balance measurements and modeling. *Basic and Applied Ecology* 4:167-183.
- Gilmanov T.G, Johnson D.A., Saliendra N.Z., Svejcar T.J., Angell R.F. and Clawson K.L. 2004. Winter CO<sub>2</sub> fluxes above sagebrush-steppe ecosystem in Idaho and Oregon. *Agricultural and Forest Meteorology* 126:73-88
- Goodin, D.G., Gao, J and Henebry, G.M. 2004. The effect of solar illumination angle and sensor view angle on observed patterns of spatial structure in tallgrass prairie. *IEEE Transactions on Geoscience and Remote Sensing* 42:154-165
- Heinsch, F.A., Reeves, M., Votava, P., Kang, S., Milesi, C., Zhao M., Glassy, J., Jolly, W.M., Loehman, R., Bowker, C.F., Kimball, J.S., Nemani, R.R., and Running, S.W. 2003. User's guide GPP and NPP (MOD17 A2/A3) products NASA MODIS Land Algorithm. MODIS Land Team. Land Processes Distributed Active Archive Center. South Dakota. USA. p 57
- Jensen, J.R. 1986 *Introductory digital image processing. A remote sensing perspective.* Prentice Hall Series in Geographic Information Science. Second Edition. New Jersey USA
- [LPDAAC]. Land Processes DAAC and EROS Center 2008. MODIS Reprojection Tool User's Manual p. 62
- Liu, X., and Kafatos, M. 2007. MISR multi-abgular spectral remote sensing for temperate forest mapping at 1.1-Km resolution. *International Journal of Remote Sensing* 28:459-464

- Martonchik, J.V., Diner, D.J., Pinty B., Verstraete M.M., Myneni R.B., Knyazikhin, Y., and Gordon, H.R. 1998 Determination of land and ocean reflective, radiative, and biophysical properties using multiangle imaging. *IEEE Transactions on Geoscience and Remote Sensing* 36:1266-1281
- McGraw, J.F. and Tueller, P.T. 1983. Landsat computer-aided analysis techniques for range vegetation mapping. *Journal of Range Management* 36:627-631
- Middleton, E.M. 1991. Solar zenith angle effects on vegetation indexes in tallgrass prairie. *Remote Sensing of Environment* 38:45-62
- Monteith, J.L. 1972. Solar radiation and productivity in tropical ecosystems. *The Journal of Applied Ecology* 9:747-766
- Myneni, R., Hoffman, S., Knyazikhin, Y., Privette, J.L., Glassy, J., Tian, Y., Wang, Y., Song, X., Zhang, Y., Smith, G.R., Lotsch, A., Friedl, M., Morisette, J.T., Votava, P., Nemani, R.R., and Running, S.W. 2002. Global products of vegetation leaf area and fraction absorbed PAR from year one of MODIS data. *Remote Sensing of Environment* 83:214-231
- NASA. Warehouse Inventory Search Too (WIST). 2009. Available online at <https://wist.echo.nasa.gov/>. Accessed October/08/2009.
- Nelson, R. and Holben, B. 1986. Identifying deforestation in Brazil using multiresolution satellite data. *International Journal of Remote Sensing* 7:429-448.
- Nicodemus, F.E., Richmond, J.C., Hsia, J.J., Ginsberg, I.W. and Limperis, T. 1977. Geometrical considerations and nomenclature for reflectance. NBS Monograph 160. National Bureau of Standards. U.S. Department of Commerce, Washington D.C. 52 p
- Nolin, A.W. 2004. Towards retrieval of forest cover density over snow from the Multi-angle Imaging Spectroradiometer (MISR). *Hydrological Processes* 18:3623-3636
- Pinty, B., Widlowski, J.L, Gobron, N., Verstraete, M.M. and Diner, D.J. 2002. Uniqueness of multiangular measurements- Part I: An indicator of subpixel surface heterogeneity from MISR. *IEEE Transactions on Geoscience and Remote Sensing* 40:1560-1573.
- Pinty, B., Lavergne, T., Widlowski, J. L., Gobron, N., and Verstraete, M.M. 2009. On the need to observe vegetation canopies in the near-infrared to estimate visible light absorption. *Remote Sensing of Environment* 113:10-23.

- Prenzel, B., and Treitz, P. 2005. Comparison of function- and structure-based schemes for classification of remotely sensed data. *International Journal of Remote Sensing* 26:543-561
- Rheingans, B., Matthews, J. and Thompson, C. 2006. MISR Toolkit Users Guide. Jet Propulsion Laboratory, California Institute of Technology p 1-23
- Reeves, M.C., Zhao, M. and Running, S.W. 2006. Applying improved estimates of MODIS productivity to characterize grassland vegetation dynamics. *Rangeland Ecology and Management* 59:1-10
- Running, S.W., Thornton, P.E., Nemani, R., and Glassy, J.M. 2000. Global terrestrial gross and net primary productivity from the Earth observing system. In Sala O.E., Jackson, R.B., Mooney, H.A. and Howarth, R.W. (Eds), *Methods in Ecosystem Science*. New York: Springer-Verlag. p 44-57
- Sellers, P.J. 1985. Canopy reflectance, photosynthesis and transpiration. *International Journal of Remote Sensing* 6:1335-1372.
- Schaepman-Strub, G., Schaepman, M.E., Painter, T.H., Dangel, S. and Martonchik, J.V. 2006. Reflectance quantities in optical remote sensing – definitions and case studies. *Remote Sensing of Environment* 103:27-42
- Strahler, A.H., Woodcock, C.E., and Smith, J.A. 1986. On the nature of models in remote sensing. *Remote Sensing of Environment* 20:121-139
- Su, L., Chopping M.J., Rango A., Martonchik J.V. and Peters D.P.C. 2007. Differentiation of semi-arid vegetation types based on multi-angular observation from MISR and MODIS. *International Journal of Remote Sensing* 28:1419-1424
- Su, L., Huang Y., Chopping M.J., Rango A. and Martonchik J.V. 2009. An empirical study on the utility of BRDF model parameters and topographic parameters for mapping vegetation in a semi-arid region with MISR imagery. *International Journal of Remote Sensing* 30:3463-3483
- Tueller, P.T. 1989. Remote sensing technology for rangeland management applications. *Journal of Range Management* 42:442-453
- Turner, D.P., Ritts, W.D., Cohen, W.B., Gower, S.T., Zhao, M., Running, S.W., Wofsy, S.C., Urbanski, S., Dunn, A.L. Munger, J.W. 2003. Scaling gross primary production (GPP) over boreal and deciduous forest landscapes in support of MODIS GPP product validation. *Remote Sensing of Environment* 88:256-270

- USDA, NRCS. 2007. Web Soil Survey. Available online at <http://websoilsurvey.nrcs.usda.gov/> accessed March/03/2007
- USGS Global Visualization Viewer. Glovis. 2009. Available online at <http://glovis.usgs.gov/>. Accessed July/14/2009
- Ustin, S.L., and Gamon, J.A. 2010. Remote sensing of plant functional types. *New Phytologist* 186:795-816
- Verstraete, M.M., and Pinty, B. 1996. Designing optimal spectral indices for remote sensing applications. *IEEE Transaction on Geoscience and Remote Sensing*. 34:1254-1265
- Walter-Shea, E.A., Privette, J., Cornell, D., Mesarch, M.A. and Hays, C.J. 1997. Relations between directional spectral vegetation indices and leaf area and absorbed radiation in alfalfa. *Remote Sensing Environment* 61:162-177
- Walthall, C.L., Norman, J.M., Welles, J.M., Campbell, G. and Blad, B.L. 1985. Simple equation to approximate the bidirectional reflectance from vegetative canopies and bare soil surfaces. *Applied Optics* 24:383-387
- Widlowski, J.L., Pinty, B., Gobron, N., Verstraete, M.M., Diner, D.J. and Davis A.B. 2004. Canopy structure parameters derived from multi-angular remote sensing data for terrestrial carbon studies. *Climatic Change* 67:403-415
- Woodcock, C.E. and Strahler, A.H. 1987. The factor of scale in remote sensing. *Remote Sensing of Environment* 82: 311-332
- Wylie, B.K., Meyer, D.J., Tieszen, L.L., and Mannel, S. 2002. Satellite mapping of surface biophysical parameters at the biome scale over the North American grasslands A case study. *Remote Sensing of Environment* 79:266-278
- Wylie, B.K., Johnson, D.A., Laca, E., Saliendra, N.Z., Gilmanov, T.G., Reed, B.C., Tieszen, L.L., Worstell, B.B. 2003. Calibration of remotely sensed, coarse resolution NDVI to CO<sub>2</sub> fluxes in a sagebrush-steppe ecosystem. *Remote Sensing of Environment* 85:243-255

Table 4-1. Orbit number, acquisition date and time for two MISR local mode over passing the study site. \*

Site Name	Acquisition Date	Orbit #	GMT Day (Df)
Crane Creek ID	Jul 17, 2008	45645	2008/199/18:45:49
Crane Creek ID	Aug 18, 2008	46111	2008/231/18:46:00

\* Times are shown for the start of Local Mode acquisition for Df camera, duration of Local Mode is 7:35 minutes. The local time for study area was around 12:45 pm (including saving time). Both images correspond to Path 42 and Block 55.

Table 4-2. Scaling up Landsat pixels to MISR and MODIS pixels. Re-projection of MISR and MODIS to UTM projection and WGS 84-datum was performed before scaling up.

Landsat		MISR		MODIS	
Sample	Line	Sample	Line	Sample	Line
37-67	110-152	6-9	14-18	8	11
68-98	153-195	10-12	19-22	9	12
99-129	196-238	13-16	23-27	10	13
130-160	239-281	17-19	28-32	11	14

Table 4-3. Composition of MISR shrub and non-shrub vegetation 'pure' pixels located at different locations.

Macroplot	MISR Shrub 'pure' pixel				MISR Non-shrub 'pure' pixel			
	#	Shrub	Non-shrub	Crop	#	Shrub	Non-shrub	Crop
A	29	79.3±5.4	20.7±5.4	0.0±0.0	9	22.6±6.0	77.2±5.7	0.2±0.6
B	41	84.5±5.3	15.4±5.3	0.1±0.3	17	14.6±8.5	85.4±8.5	0.0±0.0
C	13	76.3±4.5	23.6±4.4	0.1±0.2	41	17.3±9.0	82.6±9.0	0.1±0.3
D	14	79.1±4.4	20.8±4.4	0.1±0.2	93	14.3±8.4	85.6±8.4	0.0±0.2

Table 4-4. Accuracy classification for shrub using Landsat and MISR nadir (An) images.

Image	Accuracy for shrub (%)			K <sub>hat</sub> (%)
	Overall	Producer	User	
Landsat-Set	87.7	72.9	94.6	81.6
MISR Nadir-Aug	98.3	96.2	98.1	97.1

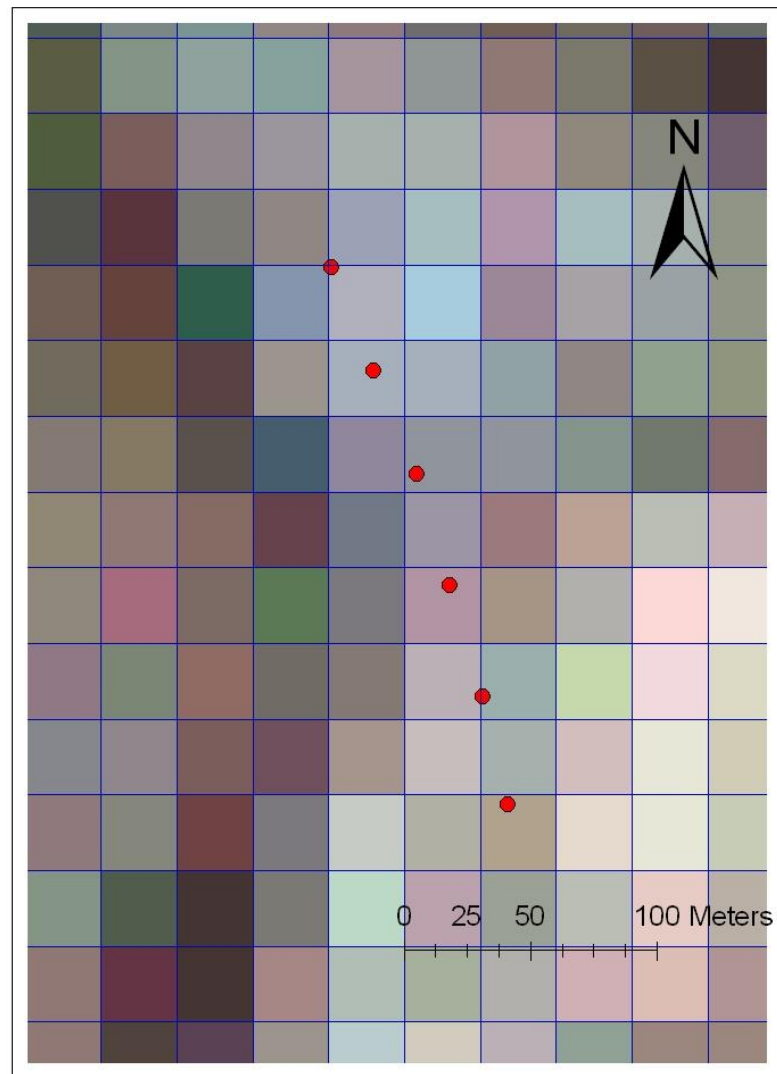


Figure 4-1. Line transect (225 m in length) overlain on Landsat pixels. Red dots represent stakes set at every 45 m. In 2008, 30-m transects were set at each end of the 225-m transect set in 2007.

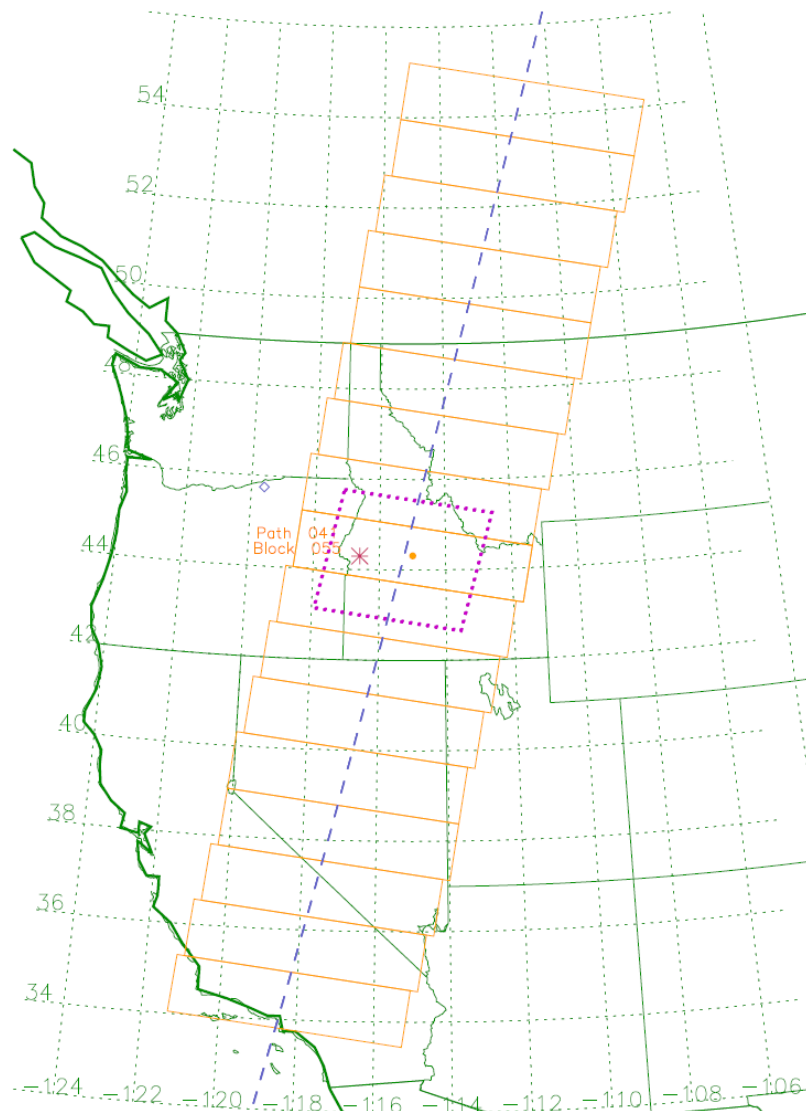


Figure 4-2. MISR paths over CraneCreekID, Local Mode Site # 313 (44.300, - 116.600). Path 042 and block 55 are shown with a dot (MISR Local Mode team)

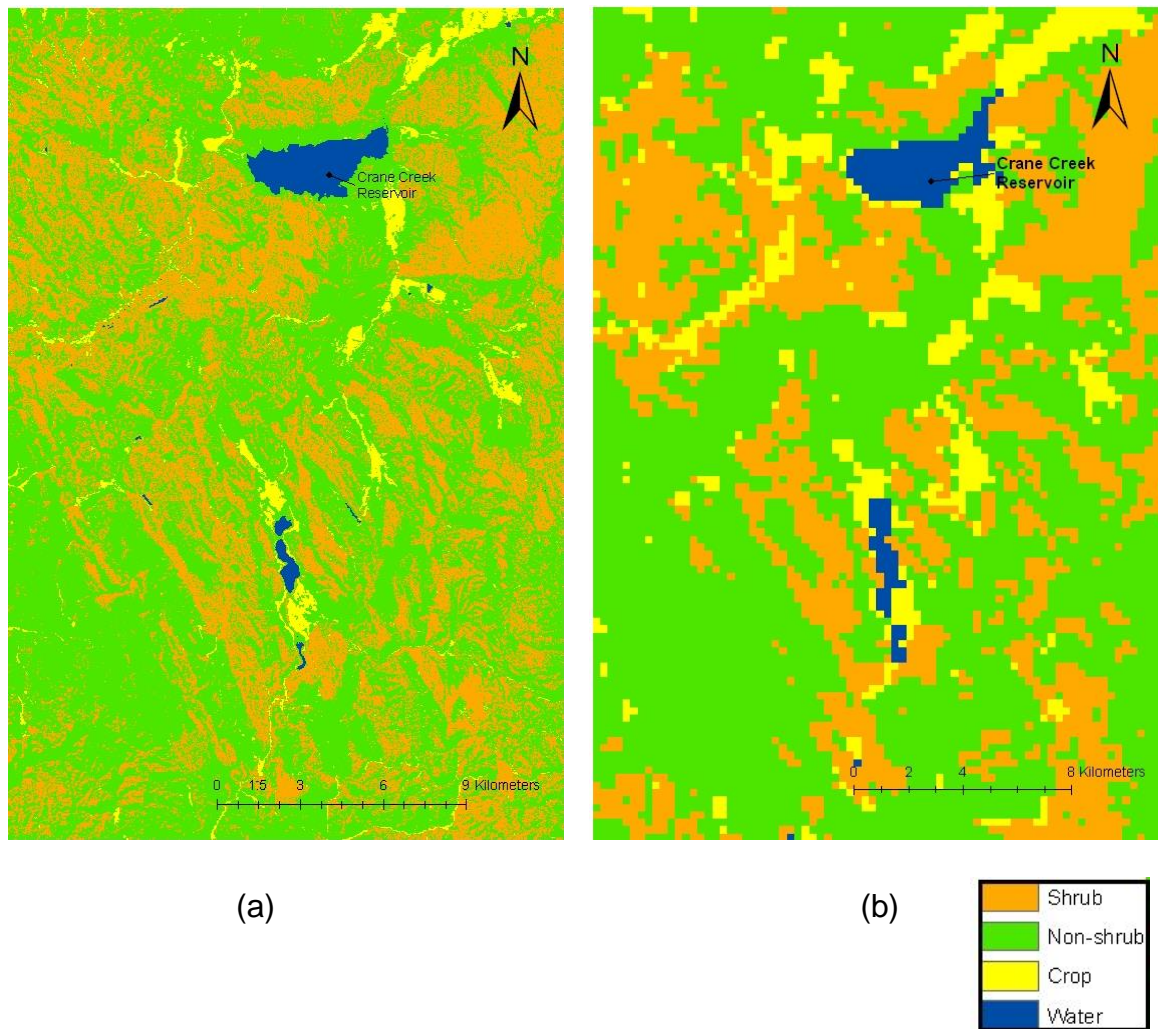


Figure 4-3. (a) Landsat and (b) MISR An image classification. Observe the aggregation of small patches into large cover types (clumpiness) when using a coarser spatial resolution.

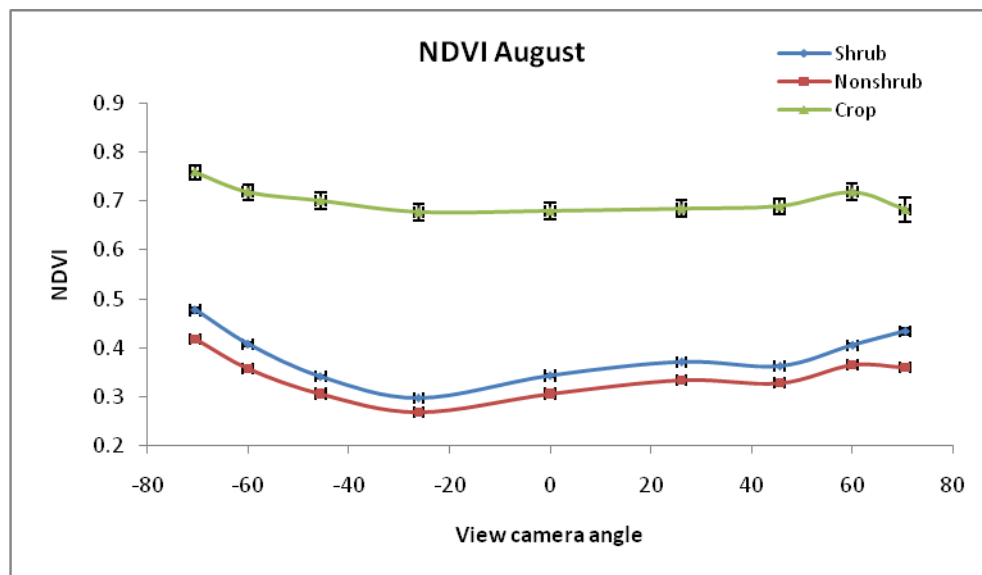


Figure 4-4. NDVI variation for MISR 9-view cameras. There are slight differences between shrub and non-shrub vegetation types while large substantial differences are detected between crop vegetation and the other two.

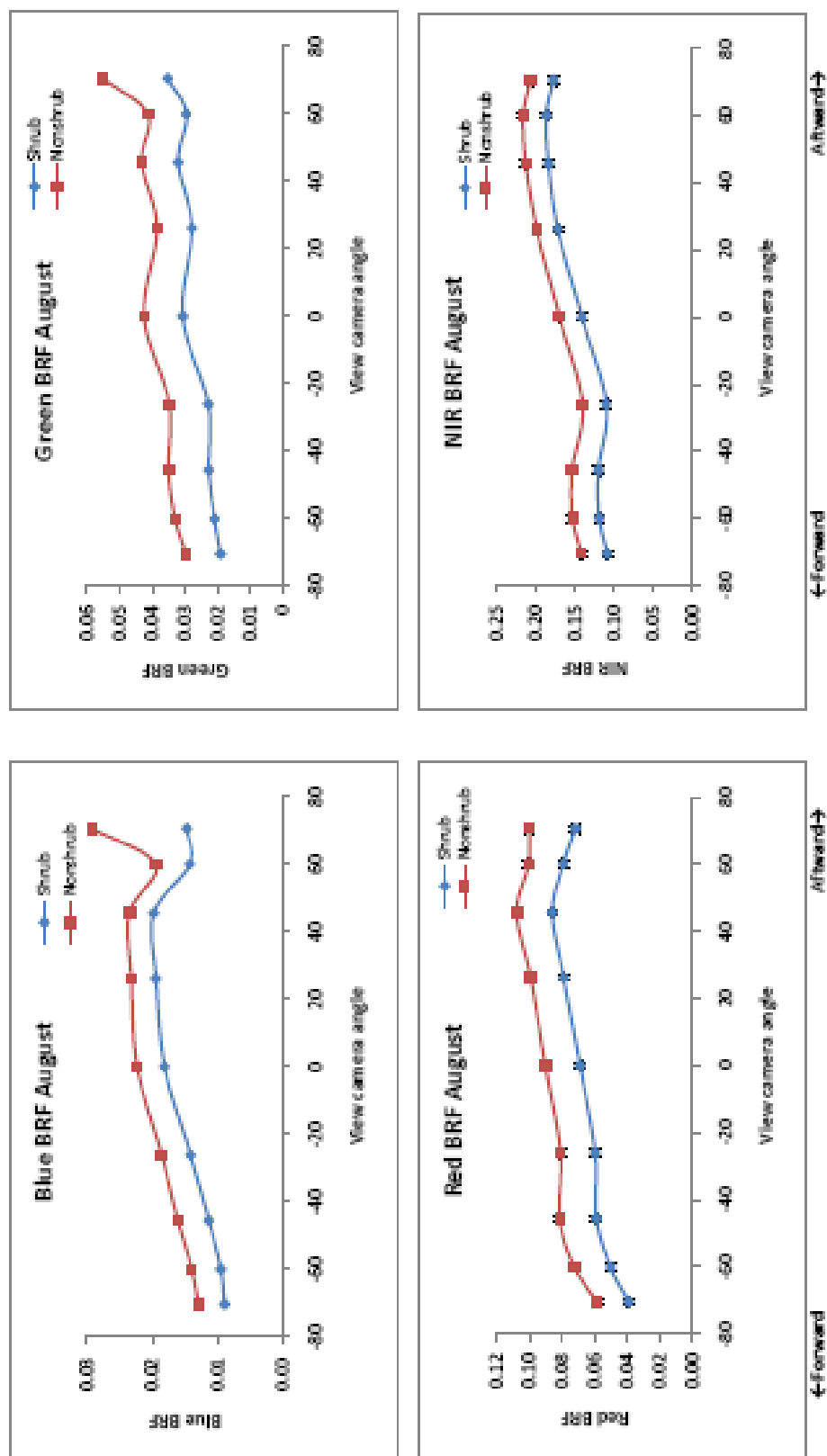


Figure 4-5. BRF variation for each band and each MISR viewing camera. At any view camera and band we can observe significant differences between shrub and non-shrub vegetation types. This means that using any camera for supervised classification would give us similar or better accuracy compare to the MISR An image classification.

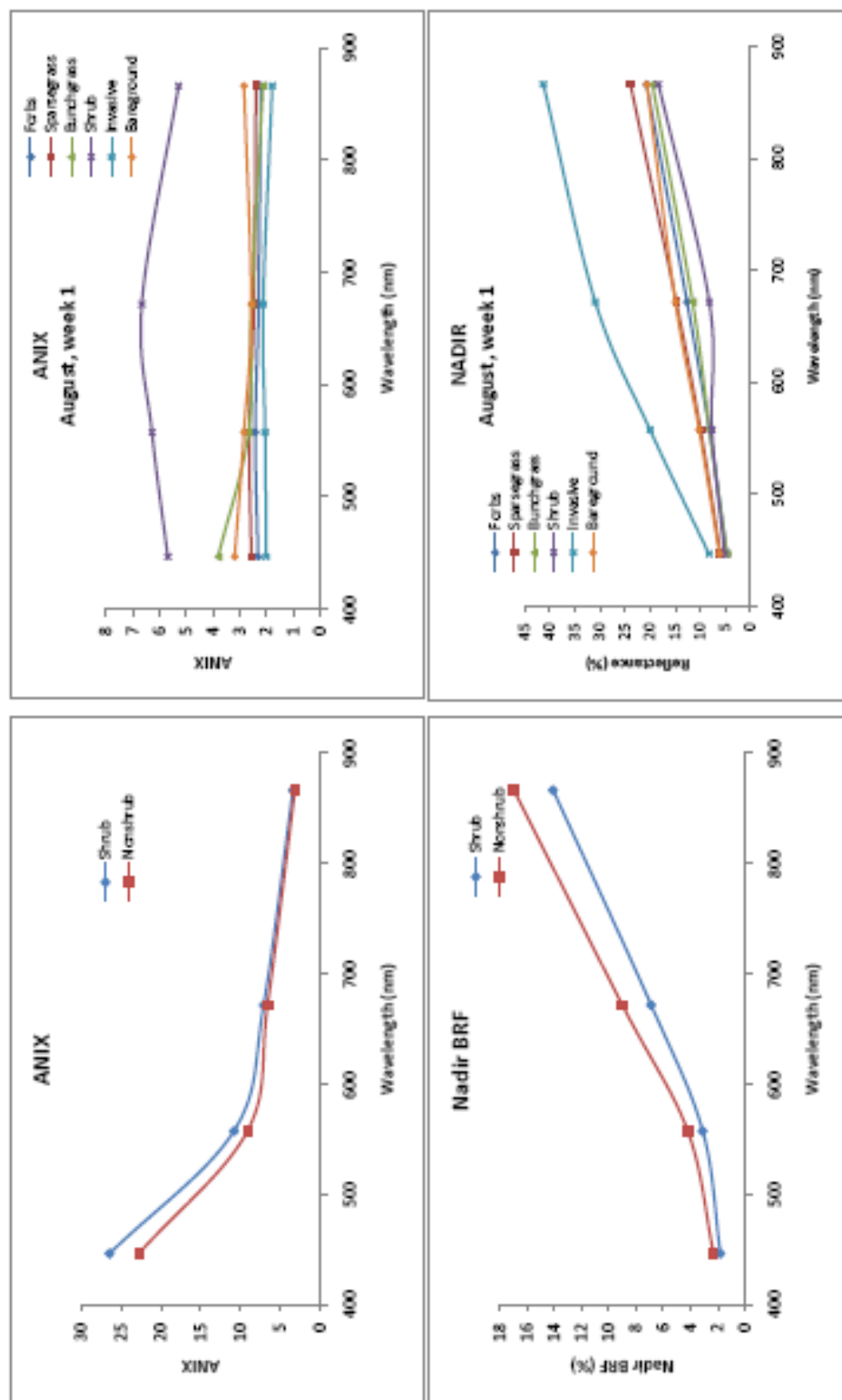


Figure 4-6. Comparison between ANIX at coarse scale (MISR local mode, left panels) and fine scale (field data, right panels).

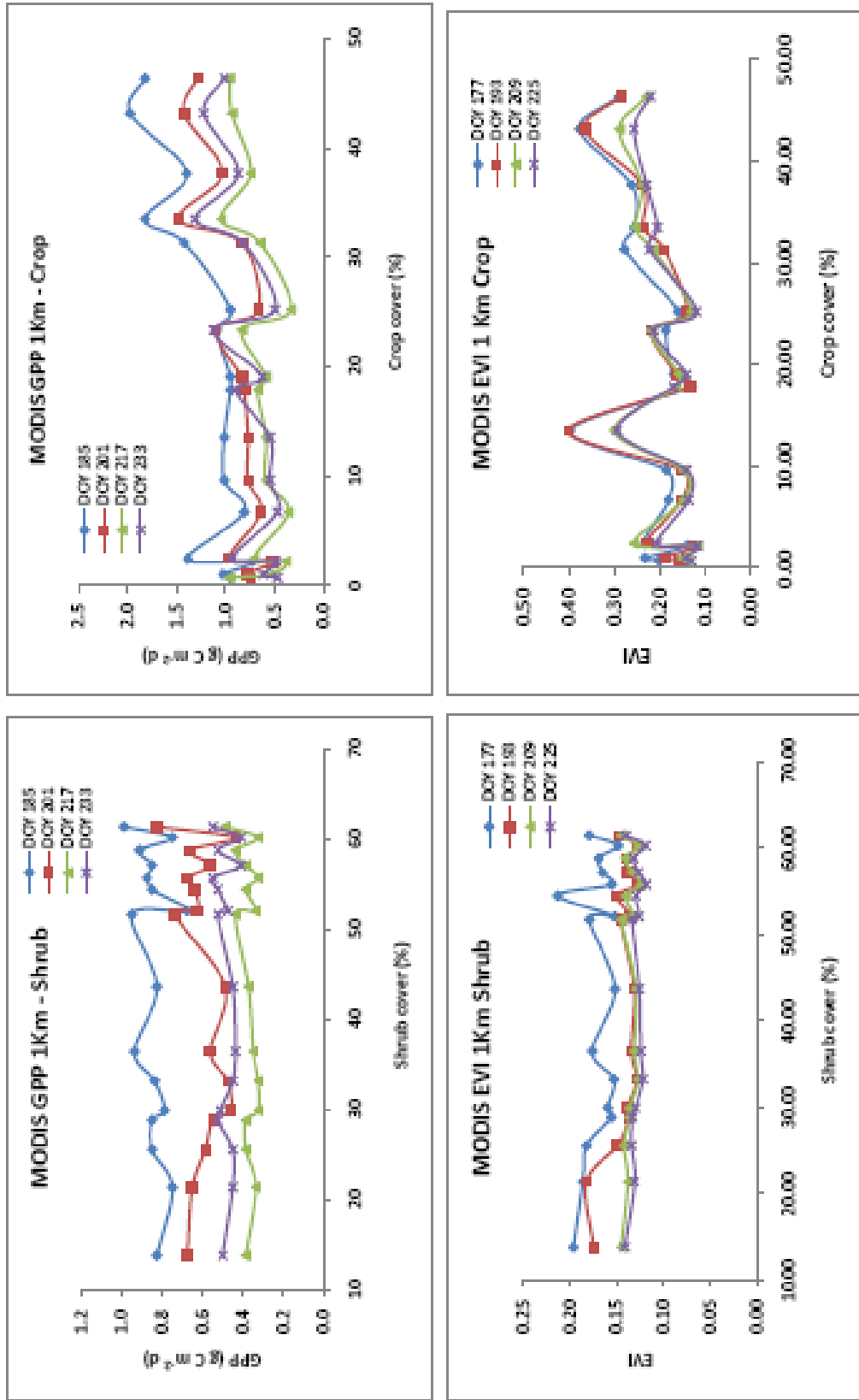


Figure 4- 7. MODIS GPP and EVI variation at different levels of shrub and crop cover in the study area. While there was not a certain relationship between GPP and shrub cover, there is a slightly positive trend between GPP and crop cover.

## CHAPTER 5. Conclusion

In pursuing research relating to the use of multi-angle remote sensing data to delineate plant functional types in a shrub-steppe rangeland ecosystem in west-central Idaho, three key questions formed the crux of the work. Each of these questions relate to future understanding of how these plant functional types can be mapped and monitored in the future across large spatial scales to better understand plant community responses in a highly changing environment (see review by Ustin and Gamon 2010). We discuss each of these questions below.

**Question 1.** How does the bidirectional reflectance factor (BRF) vary among the physiological and structural status of three different rangeland functional groups; shrubs, perennial native grasses, and annual invasive grasses?

We found that two of the plant functional types could be distinguished using different physiological and structural analyses. It was possible to distinguish medusahead (*Taeniatherum caput-medusae* [L.] Nevski) during the transition period from green to senescent phenological status (late July through early August). Changes in medusahead canopy structure from erectophile (green) to planophile (senesced) leaf orientation increased the reflectance in the visible light and the near infrared allowing us to detect it even at nadir view using these individual wavebands. However, the confounding effects of soil and litter reflectance did not allow this observation past the third week of medusahead

senescence. The other plant functional type that could be detected was shrubs. Because of their strong anisotropy behavior due to their complex structure, the anisotropy index (ANIX; Sandmeier and Itten 1999) provided additional information that allowed us to differentiate shrubs from other plant functional groups throughout the mid and late growing season.

In addition, NDVI calculated at the nine view angles (from  $-70^{\circ}$  forward to  $70^{\circ}$  backward scattered reflectance) in the principal plane revealed that the NDVI of senescent invasive annual grasses was significantly lower than that of the other vegetation groups over the  $70^{\circ}$  forward scatter to nadir view. The NDVI angular signatures of this functional type was a flatter shape than that of other functional groups because the 'hotspot' effect increases reflectance in the red band reducing the reflectance contrast between NIR and red (Myneni and Williams 1994). Confounding effects of bare ground BRDF values could also explain this shape. Finally, NDVI was affected by view zenith angle and the degree of change varied as a function of the phenological stage and the vegetation functional group (Goodin et al. 2004, Middleton 1991).

**Question 2.** What are the effects of sun zenith angle and view zenith angle on vegetation reflectance and vegetation indices?

We used filtered photodiodes to record data for two green wavelengths (centered upon 530 and 570 nm) as well as in the near infrared portion of the spectrum (centered upon 800 nm; after Garrity et al. 2010) and one unfiltered

GaAsP photodiode to record photosynthetically active radiation (PAR; 400-700 nm; Gutschick et al.1985) to record 1) diurnal reflectance variation at different phenological stages and 2) seasonal reflectance changes between native perennial grasses and medusahead. We found that high sun zenith angles (early in the morning and late in the afternoon) have bigger effects on NIR reflectance while small sun zenith angles (near solar noon) have bigger effects on green waveband and PAR reflectance. The anisotropy behavior of the bunchgrasses amplified the reflectance of the visible light (green and PAR sensors) that made its reflectance different from that of medusahead, especially near solar noon (Middleton 1991, 1992). These differences could be useful to detect medusahead from perennial grasses when scheduling multispectral or hyperspectral aerial image surveys.

**Question 3.** Using the BRF response for these plant functional types, can we generate a fractional cover index using MISR BRF values to partition MODIS gross primary production (GPP) and net primary production (NPP) products?

Because of the coarse scale of the MODIS GPP product, we only could find representative training sites for shrubs. These sites were the only ones distinguishable even at the spatial resolution of Landsat. The other plant functional types were aggregated as non-shrub vegetation type. Thus, we shifted our goal to detect shrub fractional cover for MODIS GPP. Hence, we first classified Landsat TM images for these two groups (shrubs and non-shrubs) plus

crop areas that were detectable at moderate spatial resolution (MISR local mode images). We found that high accuracy classification (overall accuracy and  $K_{\text{hat}}$  statistic) can be obtained with these three classes using Landsat and MISR nadir view ( $A_n$ ) imagery. We also inferred that the same accuracy may be obtained with the off-nadir MISR cameras because of the absolute differences between the spectral signature of shrub and non-shrub vegetation types.

Even through the high accuracy classification, we could not establish a substantial relationship between MODIS GPP and variation in shrub fractional cover. Presence of 'mixed pixel' as well as other sources of misclassification would affect this relationship in low spatial resolution imagery (Foody 2002, Woodcock and Strahler 1987). Further studies to derive MODIS GPP fractional cover would need larger number of training sites and validation of biomass production to develop a robust relationship among MODIS GPP, shrub and other plant functional types fractional cover in shrub-steppe ecosystems. In addition, it is possible that the algorithms used to derive the MODIS GPP product operate at too coarse a spatial resolution to be reconciled at the resolution of 1 km<sup>2</sup> grid cells.

## References

- Foody, G.M. 2002. Status of land cover classification accuracy assessment. *Remote Sensing of Environment* 80:185-201
- Garrity, S.R., Vierling, L.A., and Bickford, K. 2010. A simple filtered photodiode instrument for continuous measurement of narrowband NDVI and PRI over vegetated canopies. *Agricultural and Forest Meteorology* 150:489-496
- Goodin, D.G., Gao, J., and Henebry, G.M. 2004. The effect of solar illumination angle and sensor view angle on observed patterns of spatial structure in tallgrass prairie. *IEEE Transactions on Geoscience and Remote Sensing* 42:154-165
- Gutschick, V.P., Barron,, M.H., Waechter, D.A., and Wolf, M.A. 1985. Portable monitor for solar-radiation that accumulates irradiance histograms for 32 leaf-mounted sensors. *Agricultural and Forest Meteorology* 33: 281-290
- Middleton, E.M. 1991. Solar zenith angle effects on vegetation indexes in tallgrass prairie. *Remote Sensing of Environment* 38: 45-62
- Middleton, E.M. 1992. Quantifying reflectance anisotropy of photosynthetically active radiation in grasslands. *Journal of Geophysical Research* 97: 18935-18946
- Myneni, R.B., and Williams, D.L. 1994. On the relationship between fAPAR and NDVI. *Remote Sensing of Environment* 49:200-211
- Sandmeier, S.R., and Itten, K.I. 1999. A field goniometer system (FIGOS) for acquisition of hyperspectral BRDF data *IEEE Transactions on Geoscience and Remote Sensing* 37: 978-986
- Ustin, S.L. and Gamon, J.A. 2010. Remote sensing of plant functional types. *New Phytologist* 186:795-816
- Woodcock, C.E. and Strahler A.H. 1987. The factor of scale in remote sensing. *Remote Sensing of Environment* 82: 311-332